School of Chemical Science
Irish Separation Science Cluster (ISSC)
Dublin City University
Glasnevin, Dublin 9.

Fabrication and characterisation of nano-agglomerated monolithic stationary phases for separation science.

Ali Alwy, B.Sc.

Student No: 10118802

Under the supervision of:

Dr. Damian Connolly, Pharmaceutical and Molecular Biotechnology Research Centre (PMBRC), Department of Chemical and Life Sciences, Waterford Institute of Technology.

Dr. Blánaid White, School of Chemical Sciences, Irish Separation Science Cluster, Dublin City University, Glasnevin, Dublin 9, Ireland.

Prof. Brett Paull, Australian Centre for Research on Separation Science (ACROSS), Department of Chemistry, University of Tasmania, Hobart, Tasmania, Australia.

A thesis submitted to Dublin City University for consideration
for the degree of:
Master of Science.

Declaration

I hereby certify that this material, which I now submit for assessment on the programme of study leading to the award of *Masters in Science* is entirely my own work, that I have exercised reasonable care to ensure that the work is original, and does not to the best of my knowledge breach any law of copyright, and has not been taken from the work of others save and to the extent that such work has been cited and acknowledged within the text of my work.

Signed: Student No: 10118802 Date: 07/01/2013

Abstract

The following thesis provides an extensive study into the fabrication, surface modification and physical characterisation of polymer monoliths in capillary formats. These polymer monoliths were subsequently immobilised with metal oxide nanoparticles for separation of phosphorylated compounds. The fabricated monolithic columns in capillary format, in all instances, were modified with diethylamine and subsequently immobilised with citrate stabilised iron oxide nanoparticles. The monolithic stationary phases were characterised using back pressure and sC^4D measurements, which can provide information on the reproducibility and density of the stationary phase. Citrate stabilised iron oxide nanoparticles (Fe_3O_4 NP's) with a particle size of 15.8 nm were electrostatically immobilised on a poly(butylmethacrylate-*co*-ethylene dimethacrylate) monolith bearing grafted functional polymer chains with quaternary amine groups resulting in homogeneous and high density coverage of iron oxide nanoparticles on the monolithic column demonstrated by FE-SEM images. The monolithic column immobilised with Fe_3O_4 nanoparticles was connected to a HPLC instrument and used in the separation of phosphorylated compounds such as adenosine, adenosine monophosphate, adenosine diphosphate and adenosine triphosphate using gradient elution. In a related study, commercially available centrifugally driven solid-phase extraction silica monoliths were immobilised with 15.8 nm citrate stabilised iron oxide nanoparticles with a dense coverage without detrimental blockage of the flow-through macropores. Since Fe_3O_4 is known to form reversible complexes with phosphorylated species, the silica monoliths were subsequently used for the enrichment of selected nucleotides and phosphorylated peptides.

List of abbreviations

BuMA – Butyl methacrylate

CapLC – Capillary liquid chromatography

CEC – Capillary electrochromatography

DAP - 2,2-dimethoxy-2-phenacetophenone

EDMA – Ethylene dimethacrylate

EDX – Energy dispersive X-ray

Fe_3O_4 nanoparticles – Iron oxide nanoparticles

FE-SEM – Field emission scanning electron microscopy

GMA – Glycidyl methacrylate

VAL - 2-vinyl-4,4-dimethylazlactone

HETP – Height equivalent to a theoretical plate

HPLC – High Performance Liquid Chromatography

IMAC – Immobilised Metal Affinity Chromatography

MOAC – Metal Oxide Affinity Chromatography

sC^4D – Scanning capacitively coupled contactless conductivity detection

SEM – Scanning electron microscope

SPE – Solid phase extraction

UV - Ultraviolet

List of poster presentations

- Conference on Analytical Science Ireland (CASi) – 6^{th} CASi on the 21-22 February 2011, The Helix, DCU.
- Conference at the European Lab Automation congress (ELA 2011) in Hamburg, Germany, from 30 June to 1 July 2011.
- Conference on Functional Nanomaterials in DCU on the 6-7 September 2011.

Table of Contents

List of Figures

Acknowledgements

I would like to thank Prof. Brett Paull (ACROSS) and Dr. Damian Connolly (WIT), firstly for the opportunity to undertake this Masters and also for all the guidance and advice over the duration of this Masters.

I would like to thank my family, especially my beloved mother Manthura Ahmed Athman and dad Alwy Khalifa, for all the support and guidance in this road we call life. I would also like to thank my schartz Sameea without which I would not have completed this Masters.

Many thanks also go to all the technical staff and postgraduates of the School of Chemical Sciences, for the many answered questions.

Chapter 1: Introduction to monolithic stationary phases, their preparation and characterisation.

1.1. Monolithic Stationary Phases

Liquid chromatography is a versatile analytical technique used to separate and determine chemical species depending on their interactions between two phases. The two phases are chosen such that rapid equilibration of sample components occurs in both and the degree of interaction will affect the speed and efficiency of a separation. The mobile phase is a liquid solvent containing a mixture of solutes which percolates through the solid stationary phase and is separated depending on the relative affinity of the solutes for the stationary phase. Michael Tswett [1] developed chromatography over a century ago, and since then, chromatography has advanced and diversified rapidly.

Monolithic stationary phases are relatively new materials that emerged in the late 1980's and were first used for HPLC in the early 1990s [2]. A monolith is a single rigid piece of porous polymer through which all the mobile phase percolates. It conforms to the shape of the mould and can therefore be covalently bonded to the walls of a UV transparent fused silica capillary column [3]. The mobile phase travels through the void spaces between adjacent globular clusters known as pores. Monolithic stationary phases can be divided into two main groups; silica based monoliths also known as inorganic polymer monoliths prepared using sol-gel technology, and organic polymer monoliths prepared by a polymerisation reaction. Svec described polymer monoliths as poorly organised microglobule structured materials with only large pores present whereas silica monoliths are characterised by a well organised distribution of through-pores and meso-pores [4]. In silica monoliths the pores are divided into three groups. The most substantial contribution to the overall surface area are the micropores [5] with sizes smaller than 2 nm followed by mesopores [6] ranging from 2-50 nm. Macropores and gigapores (also known as through-pores) are the largest pores (~ 1-2 µm) and have minimal contribution to the overall surface area of the column. Figure 1.1 (a), (b) and (c) are FE-SEM images that illustrate the housing, macropores and mesopores respectively. In the case of Figure 1.1 (a), it illustrates a monolith prepared in 100 µm fused silica capillary. Figure 1.1 (b) shows large flow through pores known as macropores. These through-

pores are essential in allowing the mobile phase to flow through at a reasonable pressure which facilitates high linear velocity and thus rapid separations. Figure 1.1 (c) shows mesopores which range from 2 – 50 nm in size.

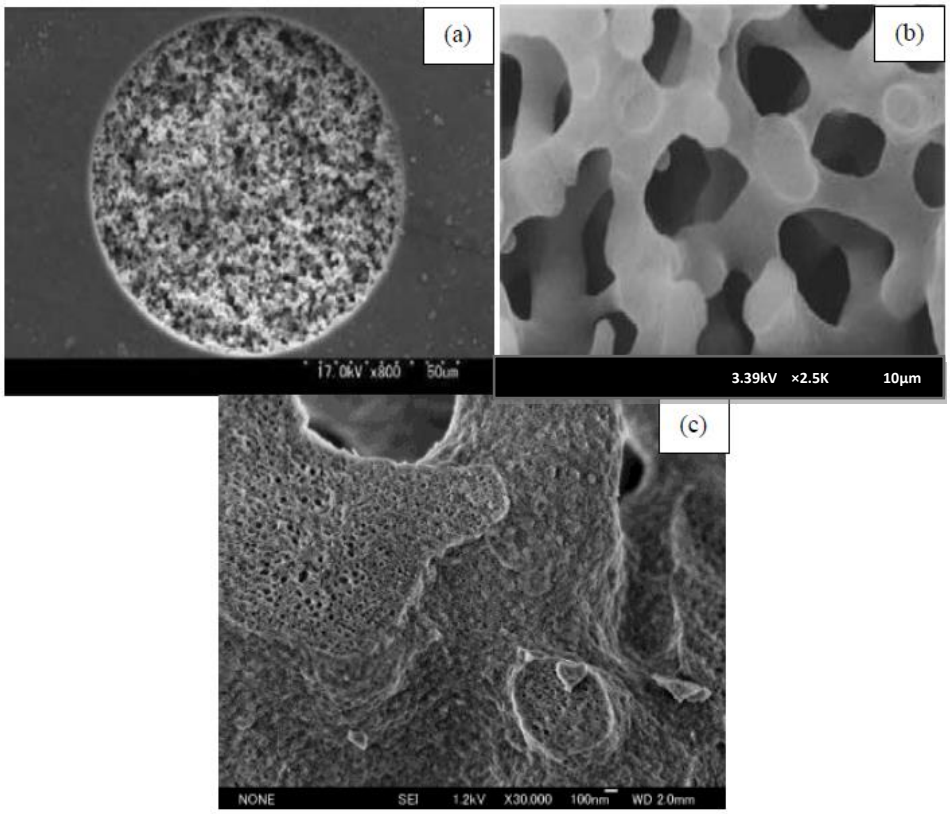

Figure 1.1: *SEM images of monolithic stationary phases. (a) Polymer monolith. (b,c) silica monolith [7,8].*

Capillary scale liquid chromatography (capLC) is a type of chromatography performed in columns of inner diameters (i.d) of less than 300 µm. Generally, monolithic columns are prepared in capillaries of less than 250 µm in i.d due to the difficulty in bonding the monolith to the walls of larger diameter columns [9].

1.2. Advantages of monolithic stationary phases over particulate columns

The advantages of capillary scale liquid chromatography (capLC) relative to microbore or standard bore chromatography have been well documented and capLC is increasingly becoming more routine and practical [4]. Certainly the relatively recent availability in the market of reliable liquid chromatographs for capillary scale chromatography is a welcome advance [6]. Most of the main vendors now offer instruments with pumps capable of producing stable, accurate gradients at flow rates

from 100 nL/min to 20 µL/min with suitably small delay volumes. These instruments have autosamplers that can accurately deliver injection volumes as low as 20 nL and contain low-volume flow cell (3 nL) detectors which in turn minimise extra-column band broadening. However, the availability of columns with a wide range of selectivities for capillary scale chromatography lags behind somewhat. The advantages of polymeric monolithic stationary phases compared to columns packed with particles is that they have lower operating back pressure relative to packed columns of similar dimension and require no frits since the stationary phase is covalently bonded to the column walls. They also exhibit excellent chromatographic efficiency for the separation of large bio-molecules. In the case of organic polymer monoliths, they are easy to fabricate and functionalise and can be modified with a wide range of chemistries. These monoliths are formed *in-situ* within the mould and thus can be adapted to any shape i.e. columns, pipette tips [10], micro-fluidic channels [11] and so on. However, the surface area of porous polymer monoliths is significantly lower than their silica-based counterparts such that they are largely unsuited to the separation of small molecules (< 500 Da) with any degree of efficiency [12].

The van Deemter equation describes band broadening on the chromatographic column. Plate height (H), also known as height equivalent to a theoretical plate (HETP), was redefined by Giddings [13] as the rate at which the variance of the chromatographic band increases with increasing migration distance. The smaller the plate height, the narrower the bandwidth, thus the ability of a column to separate components of a mixture is significantly improved [4]. In chromatography, the efficiency (N), also called plate number, is indicative of column performance and is determined by measuring the retention time (t_R) of the analyte and the width of the peak at half the height ($W_{50\%}$). Using the column length (L), the plate height (H) can be determined. Ideally, the smaller the plate height (H), the shorter the distance the solute particles move for a single mobile phase/stationary phase equilibration and therefore, the greater the efficiency of separation, represented by a sharp Gaussian peak shape. The main contributions to band broadening from the column are multilayer diffusion also known as eddy diffusion (A), longitudinal (molecular) diffusion (B) and resistance to mass transfer (C). The

van Deemter equation defines the physical processes occurring in the column with respect to the solute and the linear mobile phase velocity (linear flow rate).

The A-term represents eddy diffusion (the multi-path effect) which are the different paths taken by the analyte as it percolates through the separation column. The B-term represents longitudinal diffusion which refers to the movement of analyte from a region of high concentration i.e. the centre of the band to a region of low concentration i.e. more dilute regions. However, this phenomenon has little significance in HPLC as diffusion rates are much smaller than in gas chromatography. The C-term represents resistance to mass transfer and is the main cause of band broadening. It depends on how fast the analyte distributes between the stationary phase and mobile phase. This term can be reduced by increasing the surface area to volume ratio in the case of monolithic stationary phases [14]. Figure 1.2 is a graphical expression of a van Deemter equation showing the contributions of terms A, B and C. It is expressed in the H-u curve which is a plot of plate height (H) as a function of mobile phase velocity (u). The graph shows that the A-term is independent of u and does not contribute to the shape of the H-u curve. The contribution of the B-term is negligible at normal operating conditions. This is due to the fact that the molecular diffusion coefficient in a liquid medium is very small. The C-term increases linearly with mobile phase velocity and therefore, its contribution to the H-u curve is considerable [15].

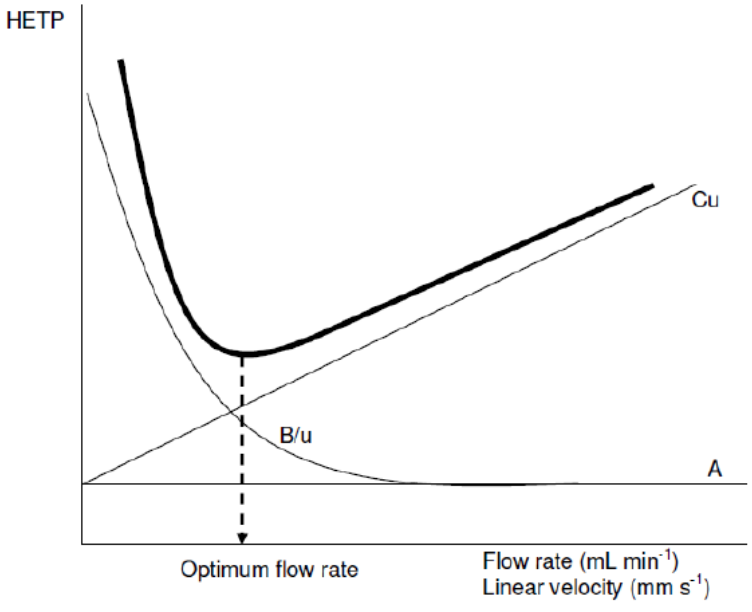

Figure 1.2: *Van Deemteer plot showing contributions of terms A, B and C.*

Monolithic stationary phases however, have a number of advantages compared to particulate based materials. Polymer monolithic columns do not have the limitation of poor mass transfer of larger molecules (such as proteins) due to the macroporous structure available in polymer monolithic columns. The efficiency of silica monolithic columns was discussed in an excellent review by Guiochon [3]. Silica monoliths exhibit similar efficiencies to particles of 5 µm diameter. The permeability of these columns is comparable to columns packed with ~10 µm particles. Silica monoliths, in terms of height equivalent to theoretical plate (HETP) plots, exhibit superior properties such as reduced resistance to mass transfer (C-term), and a reduction in eddy diffusion (A-term), at higher linear velocities when compared to particulate columns due to convective flow rather than diffusive flow. The change in slope for a packed and a monolithic column for plate height vs. increasing linear velocity can be seen in Figure 1.3. For a particulate column with increasing linear velocity the slope of the curve beyond the optimum linear velocity increases dramatically, indicating an increase in resistance to mass transfer. The slope for the monolithic column is not as steep indicating a much smaller change in resistance to mass transfer with an increase in linear velocity.

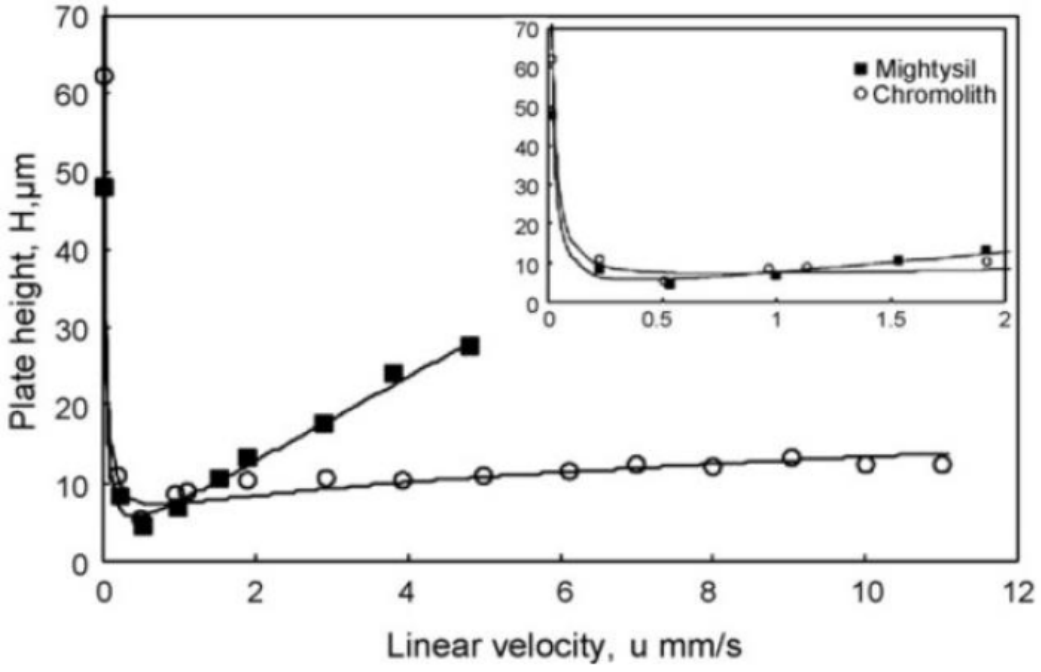

Figure 1.3: *Van Deemter plot of a particulate stationary phase (Mightysil) and a silica monolith (Chromolith). The inlay is a magnification of the main image. Mightysil (■) and Chromolith (o). Reproduced from [16].*

The improved mass transfer kinetics of monolithic stationary phases can be attributed to convective rather than diffusive mass transfer. This is due to the mobile phase being forced to flow through the pores of the monolith whereas in a particle column the majority of the mobile phase flows between the particles [4].

1.3 Silica based monoliths (inorganic monoliths)

Silica based monoliths have been extensively studied and applied to the separation of small (< 500 Da) and large molecules (> 500 Da) over the last 15 years [4]. Most silica based monolithic columns originate from sol-gel synthesis described by Nakanishi *et al.* [17]. Silica monoliths are formed through the mixing of reactants, the production of a colloidal solution (sol), the transition to a gel, aging, drying, surface modification (if any), and finally the column is clad [18]. It should be noted that the use of PEEK cladding on silica monoliths is a limiting factor of the linear velocities applied due to the low back pressure capabilities of PEEK which cannot achieve pressures of 200 bar or above. With the production of silica monoliths in a mould, the entire volume of silica is reduced and as a result the structure must be encased in PTFE or a PEEK resin to be suitable for use in HPLC. These monoliths possess a spongy non-compressible structure characterised by round pores [19] and a skeletal-like network structure which has been described as agglomerated silica particles with varying sizes and through-pore distribution. Silica based monoliths can only operate between pH 2-8 since at pH<2, the bonded phase is lost due to hydrolysis and at pH > 8 the silica begins to dissolve. The first generation of inorganic monolithic columns were made in long silica capillary tubes with 50 µm i.d. and were developed by Nakanishi *et al.* [20].

Monolithic columns have been studied for the past two decades, however, very few columns have been commercialised due the complex nature of monolith fabrication and only a few companies have successfully prepared commercial silica monoliths. Chromolith™ from Merck KGaA, Darmstadt, Germany and Onyx [21] from Phenomenex are two examples [3]. According to Merck [22], the surface area of the Chromolith™ columns is ~ 300 m^2/g, made available by the mesopores. Since the overall porosity of the monolithic silica matrix is greater than 80 %, due to this, the user is able to perform chromatography with a significantly lower backpressure than with conventional particle-packed silica HPLC columns, which exhibit total porosity of

just 65 %. MonotipTiO$_2$™ [23] and Monospin™ [24] are another type of silica monoliths produced by GL Science. MonoTip TiO$_2$ is designed for the purification and enrichment of phosphopeptides prior to MALDI-MS and LC-MS analyses. The unique monolith structure leads to low pressure-drop and strong analyte-to-surface interactions [25].

1.4 Organic polymer monoliths

Organic polymer monoliths were first prepared in the early 1990's and demonstrated as stationary phases in liquid chromatography [2]. These polymers were prepared from methacrylates, acrylates, styrene, acrylamide, or cyclic monomers and in vast majority of cases, were formed in fused silica capillaries [4]. Generally, the first step of process is the silanisation of capillary. This process is performed to ensure that the resulting monolith covalently adheres to the walls of the fused silica capillary [26]. The next step is the preparation of the monomer mixture. This mixture consists of a selected functional monomer, cross-linking monomer, a porogen and a free radical initiator (catalyst). Nitrogen purging also known as degassing is performed to remove dissolved oxygen from the monomer solution to prevent the interference of oxygen radicals with the polymerisation reaction. The column housing i.e. fused-silica capillary is filled with the monomer mixture by capillary action; sealed at both ends and subjected to either UV (photo-initiated polymerisation) or thermal energy (thermally initiated polymerisation) to form the polymer monolith *in-situ*. The polymer monolith is washed to remove the porogen and any un-polymerised monomer with an appropriate solvent e.g. methanol or acetonitrile [27].

1.4.1 Types of monomers used in the preparation of polymer monoliths

The pioneering work in the preparation of monolithic columns with polymers was performed by Hjerten *et al.* [28] and later by Frechet and Svec who published studies on *in-situ* co-polymerisation of glycidyl methacrylate and ethylene dimethacrylate [29]. Poly(glycidyl methacrylate-co-ethylenedimethacrylate) (GMA-*co*-EDMA) polymer monoliths have a neutral hydrophilic surface and surface epoxide groups. Epoxide groups on the polymer surface are then generally converted to amino groups using simple modification steps [30]. A number of monomers and monomer mixtures may be used to fabricate polymer monoliths for various

applications. This increase in the variety of surface chemistries can be advantageous and limiting at the same time. It can be advantageous as new and unique chemistries can be developed. However, it is a limitation, because of the fact that the new monomer mixtures require complete re-optimisation of polymerisation conditions in order to obtain sufficient permeability of the resulting monolith [31]. Generally, the total monomer concentration is usually 40 % wt (with 24 % wt functional monomer(s) and 16 % wt cross-linker). Figure 1.4 shows a few examples of monomers (1-9) and cross-linkers (10-13) that have been used to fabricate monolithic stationary phases. Desired surface chemistry and the potential applications of the monolith are crucial factors in choosing the functional monomer (and to a lesser extent, the cross-linker). The examples below range in chemistries from hydrophobic compounds such as butyl methacrylate (4) required for reversed phase chromatography, to reactive compounds such as glycidyl methacrylate (5) for affinity chromatography, and hydrophilic compounds such as acrylamide (8). The chemical modification of reactive monoliths will be discussed later in Section 1.6.

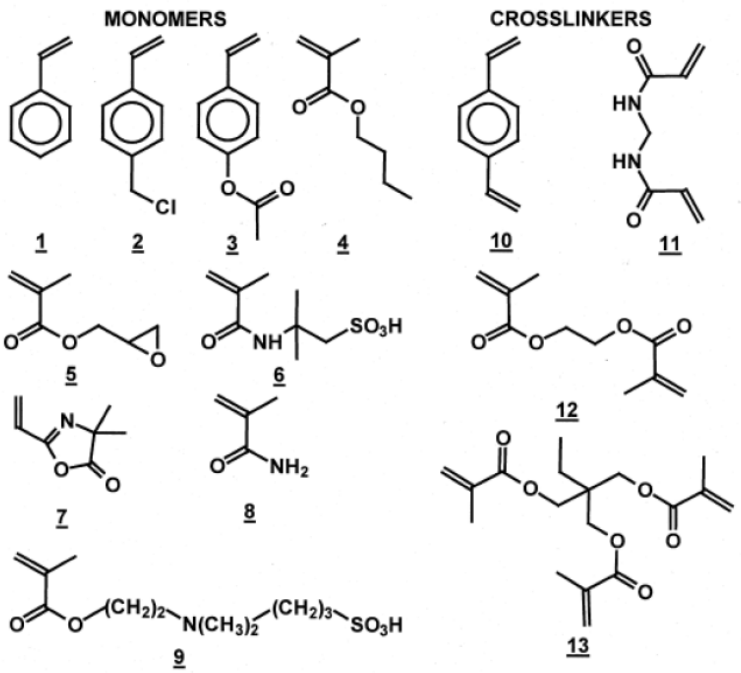

Figure 1.4: *Some examples of monomers used for the preparation of polymer monoliths. Reproduced from [4].*

1.4.2 Effect of cross-linker on porous structure

The choice of cross-linker and the concentration of cross-linker used in a co-polymerisation mixture affect the final composition of the polymer monolith. Most cross-linkers are divinyl monomers which translate to more cross-linking of the polymers in the early stages of the co-polymerisation process and leads to earlier phase separation. More cross-linking affects the final morphology with the resulting macroporous structure consisting of smaller globules with smaller voids and relatively large surface areas [32]. The number of cross-linkers used is limited due to the limited availability of these compounds commercially. Figure 1.4 (10-13) shows examples of cross-linking monomers used in the preparation of porous polymer monoliths. The most commonly used cross-linkers are ethylene dimethacrylate (12), divinyl benzene (10) used with styrenic monomers and N,N'-methylenebisacrylamide (11) used in aqueous systems [33]. Trimethylpropanetrimethacrylate (13) is another cross-linker that is often used in the preparation of porous polymer monoliths.

1.4.3 Effect of porogen on porous structure

The choice of porogen(s) used and their concentration (percentages w.r.t. monomer) plays a crucial role in controlling the porous properties of the monolith and therefore optimising its final morphological composition. The porogen concentration is usually 60 % wt with respect to monomer concentration. There is a fine balance between obtaining a large number of small pores i.e. micropores and mesopores and larger pores i.e. macropores and gigapores. The small pores significantly increase the overall surface area of the monoliths, and even though the macropores do not contribute significantly to the overall surface area, they are essential in providing flow through pores which allow the mobile phase to percolate at a reasonable pressure. It is therefore important to prepare a generic monolithic column that provides good separation efficiency and a low resistance to mobile phase flow [34]. There are a range of porogens that can be used as part of the co-polymerisation mixture. These can be used singly (one porogen in a co-polymerisation mixture) or as a mixture of 2 - 3 porogenic solvents. Porogens such as 1-propanol, 1,4-butandiol, cyclohexanol, 1-decanol, dodecanol, dimethylsulfoxide and benzene are commonly used as part of a co-polymerisation mixture. Another rather interesting porogen is supercritical CO_2. Copper *et al.* [35] pioneered the use of this porogen which is attractive because it is non-toxic, inexpensive, non-flammable and interestingly, the morphology of the final

monolith can be tuned by varying the pressure during polymerisation and thus the CO_2 solvating power. Viklund *et al.* [32] reported the preparation and characterisation of monolithic stationary phases and more importantly reported the effect of varying the percentage porogen in a co-polymerisation mixture. They used varying percentages of dodecanol and cyclohexanol and measured pore size using mercury-intrusion porosimetry. The results are shown in Figure 1.5.

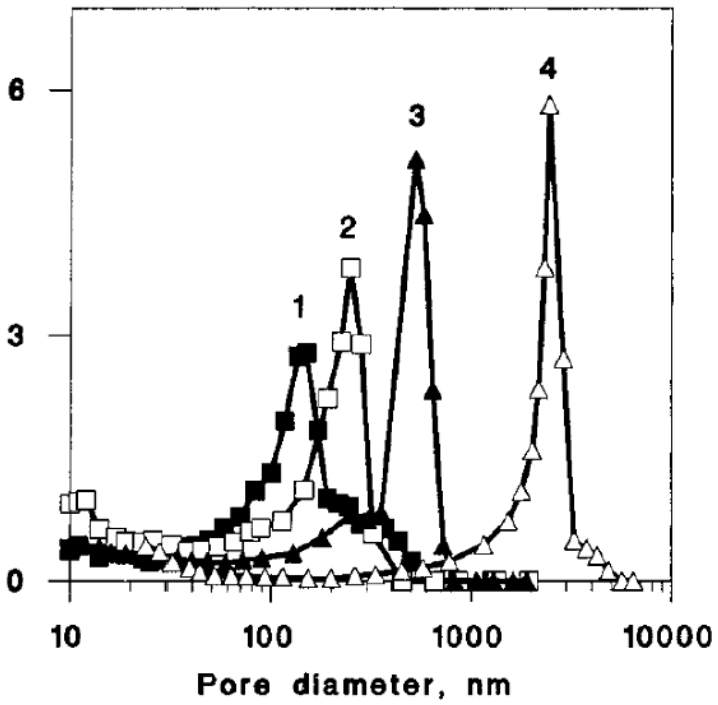

Figure 1.5: *Effect of dodecanol in the porogenic solvent on differential pore size distribution curves of a poly(GMA-co-EDMA) monoliths. GMA 24 %, EDMA 16 %, cyclohexanol and dodecanol contents in mixtures 60:0 (1), 57:3 (2), 54:6 (3), and 45: 15 % (4). Reproduced from [32].*

Figure 1.5 shows the effect of dodecanol in the porogenic solvent on differential pore size distribution curves of moulded poly(GMA-co-EDMA) monoliths. The average pore size can be controlled by at least an order of magnitude by controlling the porogen ratio in a binary mixture.

1.5 Polymerisation initiation strategies for polymer monoliths.

There are various methods used for the *in-situ* polymerisation of monomer mixtures. High energy sources used for polymerisation include thermal [36], UV [37] and γ-rays [38]. Different initiators decompose at different rates to produce free

radicals, and therefore possess different half lifes. Half-life ($t_{½}$) is a measure of the time taken for a substance to reduce to half its original quantity. Therefore, half-life affects the number of radicals produced, the polymerisation rate and most importantly the pore size. Generally, the concentration of free radical is 1% wt relative to the monomer.

1.5.1 Thermally initiated polymerisation

This type of free radical polymerisation was the first method used in the preparation of polymer monoliths [39]. It involves filling a fused silica capillary with the monomer mixture, end-capping the capillary and placing it in a water-bath at a polymerisation temperature ranging from 60 °C to 70 °C for 16 - 24 hours. Temperature selection can also influence the final pore structure. Figure 1.6 shows the pore size distribution of GMA-*co*-EDMA prepared at 55 (1) 60 (2), 65 (3), 70 (4), 80 (5) and 90 ºC (6). An increase in temperature increases the rate of polymerisation and rate of nuclei formation which in turn leads to faster consumption of GMA producing smaller pores. This phenomenon is due to the temperature dependant free radical initiator which affects the decomposition rate [40]. Therefore by controlling the temperature, monoliths of the desired structural properties can be obtained. The most commonly used free radical initiator is 2,2′-azobis(2-methylpropionitrile) abbreviated as AIBN [41].

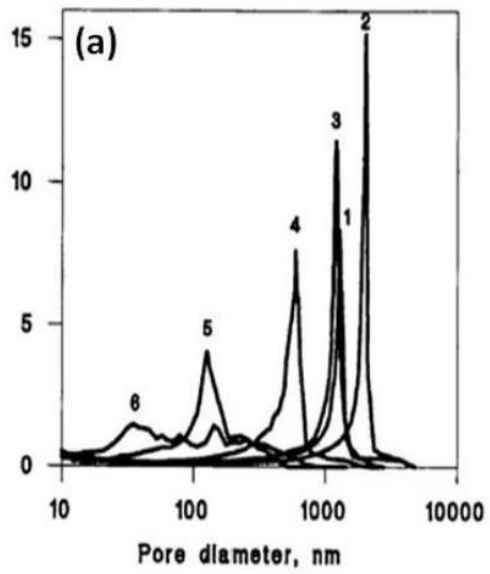

Figure 1.6: *Pore size distribution of GMA-co-EDMA monoliths prepared at 55 (1) 60 (2), 65 (3), 70 (4), 80 (5) and 90 ºC (6). Reproduced from [32].*

1.5.2 Photo-initiated polymerisation

This type of polymerisation originated in late 1990's [6]. This is a simple and significantly faster method compared to thermally initiated polymerisation. It usually requires a few minutes instead of hours to complete the polymerisation process and is conducted at room temperature. The limitation to this type of polymerisation is (i) the requirement for UV transparent monomers and (ii) difficulty in producing very long (> 25 cm) columns. Photo-initiated polymerisation also produces columns which exhibit higher back pressure compared to thermally initiated polymerisation because of the generally smaller pore sizes. Connolly *et al.* [27] produced a photo-initiated methacrylate polymer monolith using an aromatic ketone such as 2,2-dimethoxy-2-phenacetophenone (DAP) as the free radical initiator and irradiated the capillary with 2 $J.cm^{-2}$ UV energy at 254 nm. They subsequently functionalised and covalently attached 20 nm gold nanoparticles with high capacity coverage via grafted polymer chains terminated with amine groups.

1.6 Post-polymerisation modification of monoliths

1.6.1 Chemical modification of reactive monoliths

Monoliths can exhibit a wide range of functionalities depending of the desired application. The modification of stationary phase chemistries is generally carried out to change the selectivity of the phase as it increases the number of available chemistries to afford stationary phases for a variety of separation modes. For permanent modification of stationary phase chemistry, the formation of chemical bonds is required. The modification is generally carried out on-column in a flowing system. Glycidyl methacrylate (GMA) is extensively used as a reactive monomer to achieve a wide range of functionalities as it contains highly reactive epoxy rings which can be reacted with a range of nucleophiles [42,43]. Svec *et al.* [29] was the first to incorporate GMA which contained an epoxy moiety. Applying this chemistry, diol functional groups could be formed on the surface of the monolith, resulting from a ring opening reaction of epoxy group with sulphuric acid. Similarly, amine based functionalities can be added following the ring opening reaction of the epoxy group with a base such as ethylenediamine or diethylamine. Figure 1.7 illustrates application of epoxy chemistry to create a wide range of functionality on the surface of the GMA monolith.

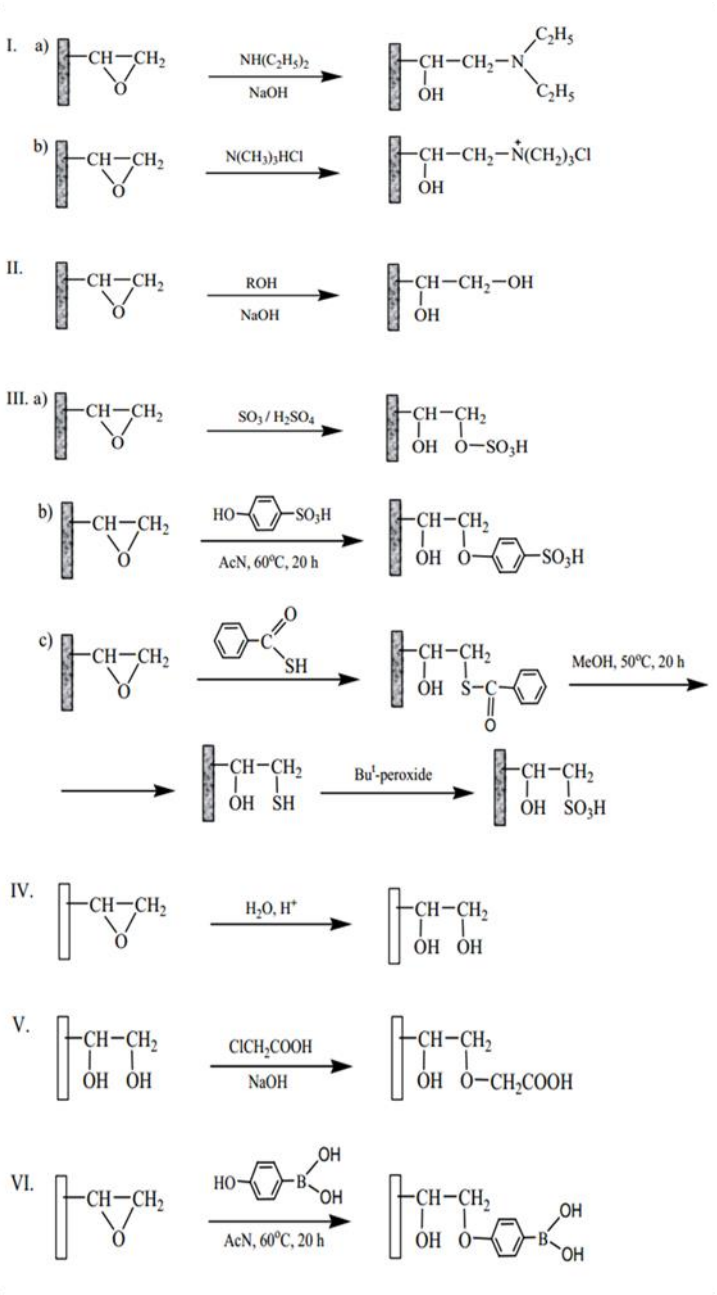

Figure 1.7: *Chemical conversion of epoxy groups by means of various reagents.I. amination; II.alkylation; III. sulfonation; IV. hydrolysis; V. carboxymethylation; VI. modification with p-hydroxyphenylboronic acid. Reproduced from [44].*

Svec *et al.* [6] used the chemical modification approach shown on Figure 1.8 to lead to a widely used anion exchanger by reacting the monolith with diethylamine.

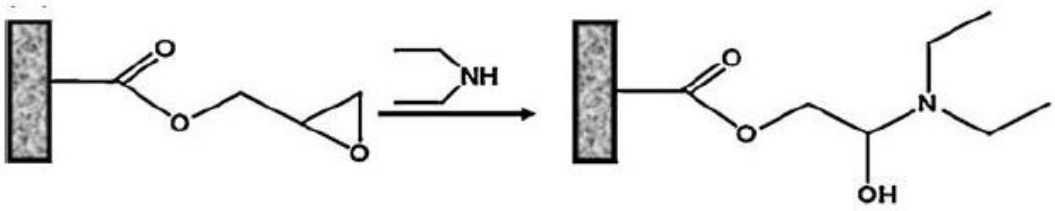

Figure 1.8: *Chemical modification of porous polymer monoliths with glycidyl methacrylate and subsequently with diethylamine to produce an anion exchanger. Reproduced from [6].*

Alternatively, a reaction between the epoxy group of GMA and sodium sulphide (Na_2S) was used to achieve cation exchange functionality. Ueki *et al.* [45] modified a glycidyl methacrylate/ethylene dimethacrylate monolith (250 µm i.d.) to create a strong cation exchange phase. It was found that by controlling the pH, time and temperature of the sulfonation reaction the capacity of the monolith could be controlled (capacities of 90 and 300 µeq/mL were produced using pH 7 and 11, respectively). The separation of inorganic cations using a 150 µeq/mL column was found to have efficiencies of 20,000 N/m. As the monolith had a hydrophilic nature, it was subjected to injections of proteins (e.g. bovine serum albumin) and the proteins were found to elute at nearly the void volume. This showed the monolith to be protein resistant and was then applied to the direct analysis of inorganic cations in human saliva. Potter *et al.* [46] previously reported covalent bonding of phenylboronic acid to a GMA-*co*-EDMA monolith using nucleophilic attack of the epoxide with p-hydroxyphenylboronic acid. In an effort to increase the surface coverage of boronic acid groups on the monolith, the authors also grafted chains of glycidyl methacrylate groups onto the surface of the monolith prior to reaction with the p-hydroxyphenylboronic acid and demonstrated the column for the separation of compounds containing cis-diol groups.

Another reactive monomer that can be chemically modified on the surface of the monolith is 2-vinyl-4,4-dimethylazlactone (VAL) [47]. VAL can be used to subsequently covalently attach amine groups on the surface. This is due to the fact the azlactone ring is susceptible to nucleophilic attack from the incoming amines, resulting in the covalent attachment of the amine containing group [48].

1.6.2 Disadvantages of using co-polymerisation methods to produce reactive monoliths.

Usually, reactive monoliths are produced using co-polymerisation methods, where the reactive monomer is co-polymerised with a cross-linker (and sometimes an additional functional monomer). Incorporating reactive monomers via co-polymerisation has certain fundamental limitations. Firstly the amount of available reactive functional groups on the surface of the porous monolith is often relatively small (compared with photografting method described later). Secondly, it often requires constant re-optimisation of the polymerisation mixture since a slight adjustment to concentration of functional monomer (in order to modify the functional ligand density) would lead to a completely different pore morphology [49]. Figure 1.9 shows a schematic of a monolith co-polymerised with a reactive functional monomer represented by (R) illustrating the sporadic distribution of reactive groups throughout the entire porous structure. It illustrates that not all the functional groups are present on the surface of the monolith, resulting in a lower surface ligand density after subsequent chemical reaction/s.

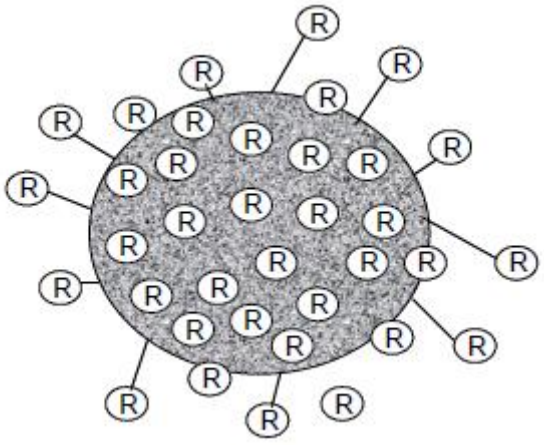

Figure 1.9: *Schematic of co-polymerisation of a monolith with a functional monomer, expressing a functional group (R). Not all the reactive groups are present on the surface.*

The next section which discusses photografting methods, it is an alternative method which ensures a more dense coverage of functional groups directly on the monolith surface.

1.6.3 Mechanism of photografting using benzophenone

Photografting is a post-modification procedure for polymer monoliths and involves surface-initiated grafting of polymer chains based on pioneering work by Bengt Ranby [50]. Ranby described the experimental processes of surface photografting and discussed the photochemical mechanism of a grafting reactions using benzophenone. Benzophenone acts as a free radical initiator and absorbs UV light at 254 nm as shown in Figure 1.10.

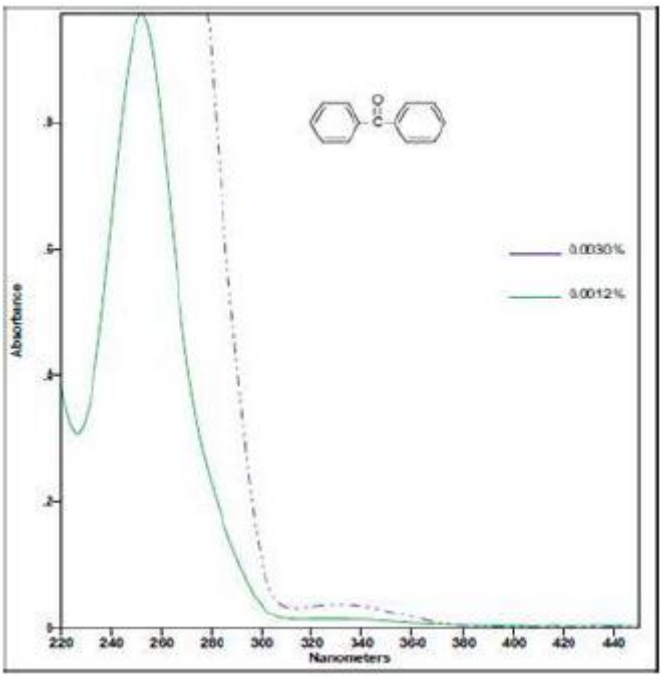

Figure 1.10: *UV-Vis absorbance spectrum of benzophenone. Reproduced from [51].*

The surface photografting reaction begins by the excitation of benzophenone to an excited singlet state (S_0 to S_1) which is a short lived species (~10-12 seconds). This is transformed to a triplet state through inter-system crossing which causes hydrogen abstraction from the monolith surface, thus initiating grafting. This energy rich surface radical formed, adds a reactive monomer which causes the growth of grafted chains. Figure 1.11 shows the surface photografting reaction using benzophenone.

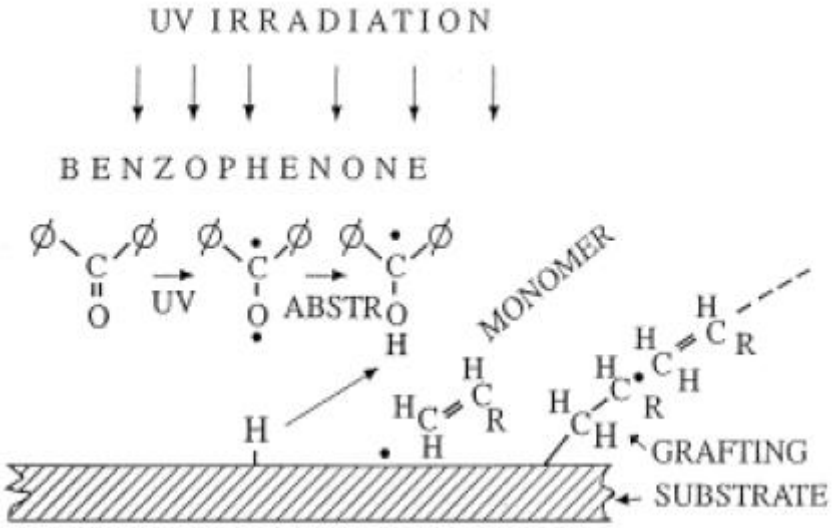

Figure 1.11: *Schematic shows surface photografting reaction using benzophenone. Reproduced from [52].*

In Ranby's pioneering works, he studied the surface modification of filaments, yarn and commercially available polymer films [52]. It involved grafting of reactive monomers such as glycidyl acrylate using 5 % benzophenone thus making the surface reactive to stabilizers, hydrophilic polymers and bio-active agents which give a range of functionalisation properties [53]. This is advantageous in post fabrication of monolithic columns as this can be used to photograft reactive monomers such as vinyl azlactone and glycidyl methacrylate which allow subsequent functionalisation. Photografting can be either a single or a two-step process. The single step process however limits the efficiency of the grafting, often leaving ungrafted polymer filling the pores of the monolith which is often difficult to remove and could potentially lead to blocking. In order to counteract these limitations, two-step processes have been developed which aim at improving the grafting efficiency. The first step involves covalent immobilisation of the initiator to the monolith surface which is followed by a step in which the graftable monomer is introduced into the pore volume in the presence of initiator. Figure 1.12 shows the two-step sequential photografting procedure for a selected monomer i.e. GMA using benzophenone as the initiator.

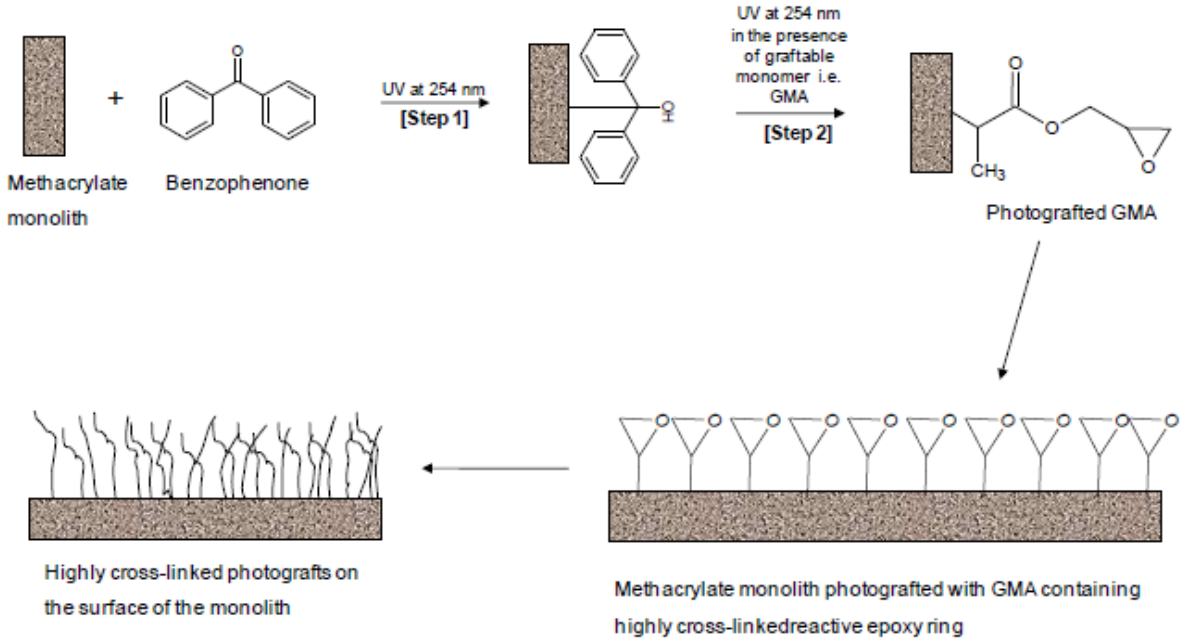

Figure 1.12: *Schematic showing the two-step sequential photografting procedure for selected monomer i.e. GMA using benzophenone as the initiator.*

Eeltink *et al.* [54] photografted methacryloyloxyethyltrimethylammonium chloride (META) on a BuMA-*co*-EDMA monolith and subsequently used the resulting monolith for a CEC separation of a test mixture consisting of thiourea, benzene, methylbenzene, ethylbenzene, propylbenzene, and butylbenzene. Baseline resolution, good peak symmetry, and column efficiencies up to 85,000 plates/m were reported for this column as shown in Figure 1.13.

Stachowiak *et al.* [55] also adopted the sequential two-step strategy to modify a BuMA-*co*-EDMA monolith with discrete site-specific zones of a hydrophilic monomer (poly ethyleneglycol methacrylate) in order to obtain a monolith with alternating hydrophilic and hydrophobic zones along its length. Photografted regions of the polymer monoliths were tested for their ability to resist protein adsorption by subjecting the monolith to a solution of fluorescein-labelled bovine serum albumin (BSA), which served as the model protein for the study. The extent of adsorption of protein was characterised using the value of the maximum intensity in the fluorescence intensity profile using fluorescence microscopy.

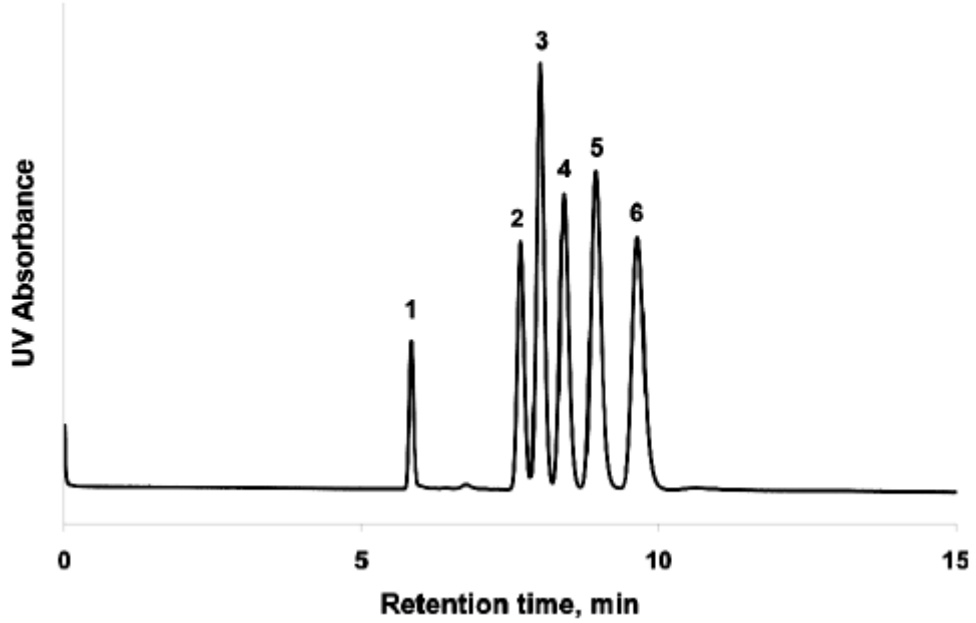

Figure 1.13. *CEC separation of a mixture of alkylbenzenes obtained a photografted methacrylate-ester-based monolithic column. Peaks: thiourea (1), benzene (2), toluene (3), ethylbenzene (4), propylbenzene (5), and butylbenzene (6). Reproduced from [56].*

Rohr *et al.* [56] photografted porous monoliths with 2-acryloamido-2-methyl-1-propanesulfonic acid (AMPS) for CEC studies and used electro-osmotic flow (EOF) to monitor the extent of grafting. Furthermore, Rohr *et al.* also successfully grafted 4,4-dimethyl-2-vinylazlactone on a porous polymer monolith and visually monitored the grafted chains which were fluorescently labelled with Rhodamine 6G using fluorescence measurements. Figure 1.14 is a reaction schematic showing the photografting of azlactone moieties on the surface of a monolithic column.

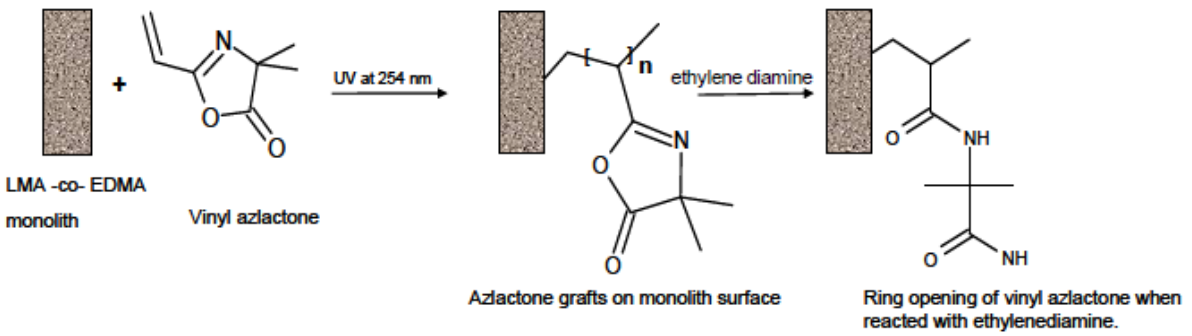

Figure 1.14: *Reaction schematic showing photografting of azlactone moiety on a monolithic column followed by subsequent reaction with ethylenediamine.*

1.6.4 Modification of capillary polymer monoliths with selected nanoparticles.

Nanotechnology is a unique and complex field of science that has evolved and revolutionised the development of new materials and technologies. A particle is considered a nanoparticle if it is between 0.1 ≤ 100 nm in size. As the size of these nanoparticles grow smaller, their physio-chemical properties such as surface area to volume ratio and surface charge significantly change. These properties are not mirrored in fine or bulk materials. The principal properties of nanoparticles are their shape, size, and the morphological sub-structure of the substance. Nanoparticles are exhibited as an aerosol (mostly solid or liquid phase in air), a suspension (mostly solid in liquids) or an emulsion (two liquid phases). The potential of nanoparticles such as silica, carbon nanotubes, fullerenes, magnetic and non-magnetic metal oxides, and gold nanoparticles has been acknowledged and utilised in chromatographic and electrophoretic methods [57].

Polymer monoliths have been modified with selected nanoparticles in order to increase their surface area in order to facilitate the chromatographic separation of small molecules. Surface attachment of nanoparticles to a polymer monolith also results in significant selectivity differences depending upon the nature of the nanoparticle under investigation. Polymer monoliths have been modified with a wide range of nanomaterials including latex nanoparticles, fullerenes, carbon nanotubes, gold, silica nanoparticles and a range of metal oxide nanoparticles. For the sake of clarity, a discussion of metal oxide nanoparticle-modified monoliths is reserved for Chapter 2.

1.6.4.1 Latex nanoparticles

The first report of latex-modified monoliths was in 2004 when Hilder *et al.* formed a poly(butyl methacrylate–*co*-ethylene dimethacrylate–*co*-2-acrylamido-2-methyl-1-propanesulfonic acid) monolith (BuMA-co-EDMA-co-AMPS) within fused silica capillary and subsequently coated with oppositely charged quaternary latex nanoparticles bearing quaternary ammonium functional groups [58]. The latex was immobilised by electrostatic interactions and the nano-structured monolith was subsequently used to separate seven monosaccharides in less than 10 minutes. The monolith before and after immobilisation of the nanoparticles is shown in Figure 1.15 along with the optimised separation. The coverage of latex on polymer monoliths

was improved relative to this earlier work by Hutchinson *et al.*[59] who chemically modified the surface of a glycidyl methacrylate monolith by reacting the pendant epoxy groups with sodium sulphite resulting in a sulphonated surface for subsequent latex attachment. The monolith was subsequently used for the separation of a range of small inorganic anions.

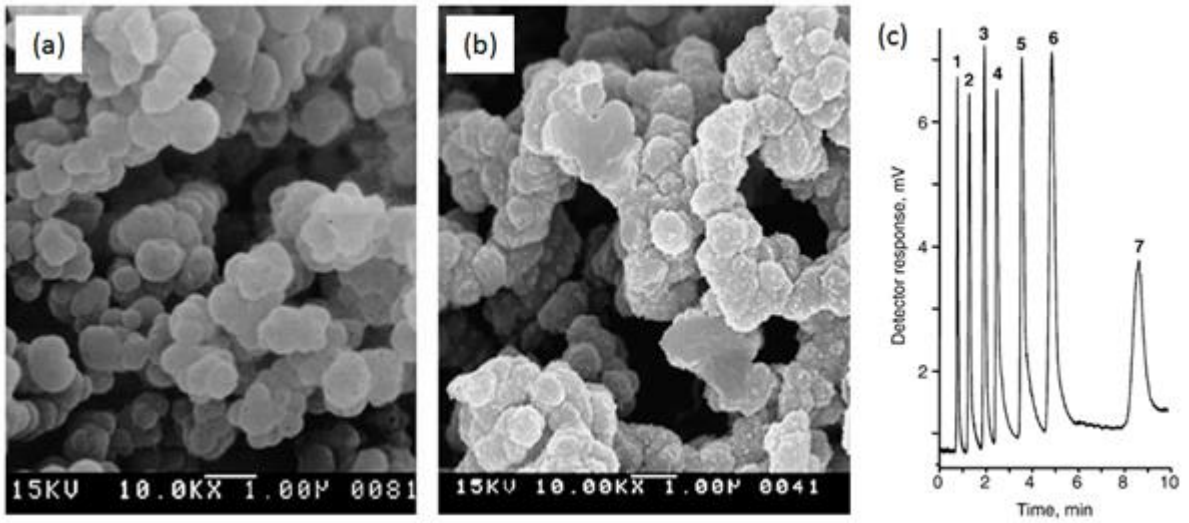

Figure 1.15: *Scanning electron micrograph (SEM) images of (a) BuMA-co-EDMA-co-AMPS monolith, (b) a latex nano-particle coated version of the same monolith and (c) the separation of a mixture of carbohydrates using a 100 x 0.25 mm I.D. capillary housing. Reproduced from [60].*

1.6.4.2. Carbon-based nanomaterials

Li *et al.* reported the incorporation of single-walled carbon nanotubes (SWCNTs) within a poly(vinylbenzyl chloride-*co*-ethylene dimethacrylate) (VBC-EDMA) monolith by admixing the SWCNTs into the monomer mixture prior to polymerisation [61]. The SWCNTs were first oxidised in acid to improve their dispersion in the monomer mixture and the resulting monolith was used in HPLC and in CEC for the separation of small neutral molecules. Interestingly the monolith exhibited enhanced hydrophobicity (manifesting as increased retention) relative to an unmodified VBC-EDMA monolith. This demonstrated that a significant amount of the SWCNTs were presented at the monolith surface. The authors also demonstrated the CEC separation of a number of selected peptides in which there was a very obvious improvement in separation efficiency relative to the unmodified monolith.

Chambers *et al.* incorporated multi-walled carbon nanotubes (MWCNTs) into a GMA-*co*-EDMA monolith by admixing 0.25 % MWCNTs into the monomer mixture

and reported improved retention and efficiency for a range of small molecules separated in reversed phase mode [62]. However, the authors also reported that the monoliths were difficult to prepare due to aggregation of the MWCNTs during polymerisation, and there were limitations on the maximum loading of nanomaterials in the monolith for this reason. Therefore the authors adopted an alternative approach in which the MWCNTs were oxidised such that they exhibited carboxyl groups on the ends of the nanostructures (130 nm ± 30 nm long). This allowed the electrostatic attachment of the carboxylated MWCNTs upon an aminated polymer monolith such that the MWCNTs were confined to the surface of the monolith. This resulted in separation efficiency of 44,000 N/m for a number of small neutral molecules separated in reversed phase mode.

Chambers *et al.* also reported the use of a C_{60}-fullerene containing methacrylate monomer namely: [6,6]-phenyl-C_{61}-butyric acid 2-hydroxyethyl methacrylate ester ($PC_{61}B$-HEM) which was copolymerised with GMA resulting in monoliths which demonstrated excellent separation efficiencies up to 85,000 N/m in reversed phase mode. When the co-monomer was butyl methacrylate instead of glycidyl methacrylate the separation efficiency was as high as 100,000 N/m [63].

Graphene oxide (GO) is the latest carbonaceous nano-material to be incorporated into polymeric monoliths. In a recent article by Wang and Yan [64], GO containing polymer monoliths were utilised in the CEC of small molecules, such as anilines and substituted aromatics. The poly(methacrylate-*co*-ethylene dimethacrylate) (MA-EDMA) monolith containing GO nano-sheets was prepared using a one-step room temperature 24 hr polymerisation, with the resultant phase ultimately providing considerably greater retention of small organic neutral molecules than the same monolithic phase minus the GO.

1.6.4.3. Gold nanoparticles

A significant number of reports have appeared in the literature regarding the incorporation of gold nanoparticles in polymer monolith due in part to their bio-compatibility, but mainly due to the ease with which the gold nanoparticles, once immobilised, can be readily functionalised. This is due to the strong covalent bonds which can be formed between gold and thiol-containing compounds and to a lesser extent with amines and cyano groups.

In 2010, Xu *et al.* reported the surface attachement of gold nanoparticles on a GMA-*co*-EDMA monolith which had previously been reacted with either sodium hydrogen sulphide or cysteamine resulting in pendant thiol groups or amine groups [65]. Gold nanoparticles were then prepared "*in-situ*" by connecting the monolith to a T-piece and flushing the monolith with gold chloride and sodium citrate. By holding the monolith at 100 ^{o}C, gold nanoparticles were reduced by citrate directly on-column, and were simultaneously immobilised upon the thiol or amine functionalities. Although it was not possible to control the size or size distribution of the nanoparticles thus formed, nevertheless the monolith could subsequently be used for the selective extraction of cysteine-containing peptides due to the reasonably dense surface coverage of nanoparticles. The authors used mercaptoethanol to desorb the peptides from the gold surface such that they could be separated and quantified using reversed phase chromatography. Interestingly, the authors also reported that the nanoparticles did not detach from the monolith surface but instead remained tightly bound even after flushing with hot water or high concentrations of mercaptoethanol. It was proposed that the gold nanoparticles were attached via multi-point interactions with the functional groups on the monolith surface by virtue of the nanoparticles relatively massive size. The stable attachment of the gold nanoparticles is clearly an advantage when the gold surface itself is acting as the stationary phase.

Also published in 2010, Connolly *et al.* used a different approach to attach gold nanoparticles and subsequently achieved a more dense coverage and much better control of the nanoparticle size [49]. This was possible by first preparing the nanoparticle suspension using classical citrate reduction methods in a stirred solution to ensure a narrow size distribution of the resulting nanoparticles. A butyl methacrylate-*co*-ethylenedimethacrylate monolith was photografted with an amine-reactive monomer (vinyl azlactone) and subsequently aminated with ethylenediamine. Flushing the monolith with gold nanoparticles resulted in excellent coverage of the monolith surface as shown in Figure 1.16 below. The bare patch on the surface of the monolith was due to cutting the monolith into cross-sections for imaging and shows that coverage of nanoparticles was confined to the monolith surface.

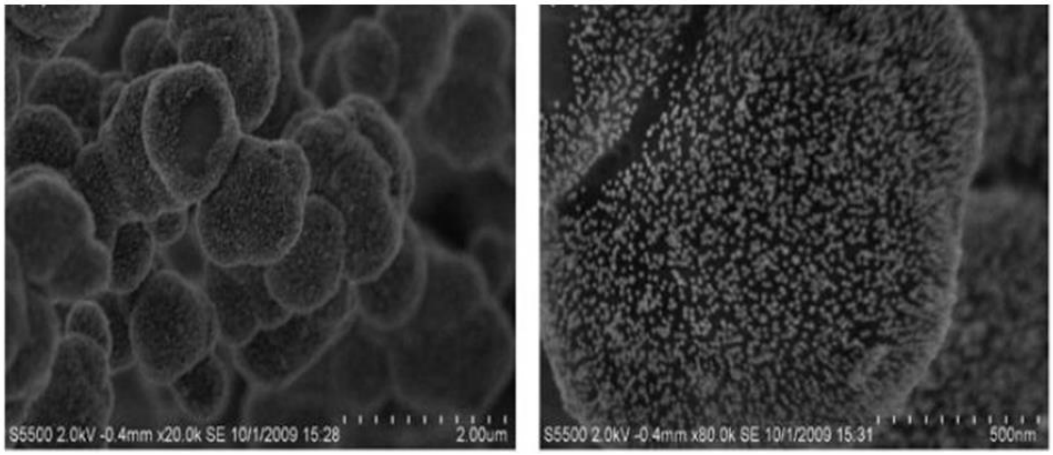

Figure 1.16: *SEM images of a polymer monolith agglomerated with 20 nm gold nano-particles. Reproduced from [49].*

By taking advantage of the affinity of gold surfaces for thiol compounds, Cao *et al.*[66] prepared a gold nanoparticle modified monolith using the same strategy as Xu *et al.*[65]. Using a simple ligand exchange reaction, the authors demonstrated that the monolith could be used in a number of different separation modes (ion-exchange, reversed phase) by replaced one adsorbed ligand with another on the gold surface. Specifically, the monolith was flushed with 3-thiopropionic acid after attachment of the gold nanoparticles and used for the ion-exchange separation of three peptides in CEC mode. Subsequently, the monolith was flushed with an excess of 2-mercaptoethanol or cysteamine to yield a hydroxylated surface or an aminated surface respectively, with a CEC separation of peptides demonstrated in each instance to show the difference in selectivity that could be obtained. Finally, the authors flushed the monolith with 1-octadecanethiol to permit the reversed phase separation of three proteins using liquid chromatography (i.e: with pressure-driven flow). Figure 1.17 below illustrates the various selectivities that were possible with the gold-modified monolith and the corresponding separations of peptides/proteins that resulted.

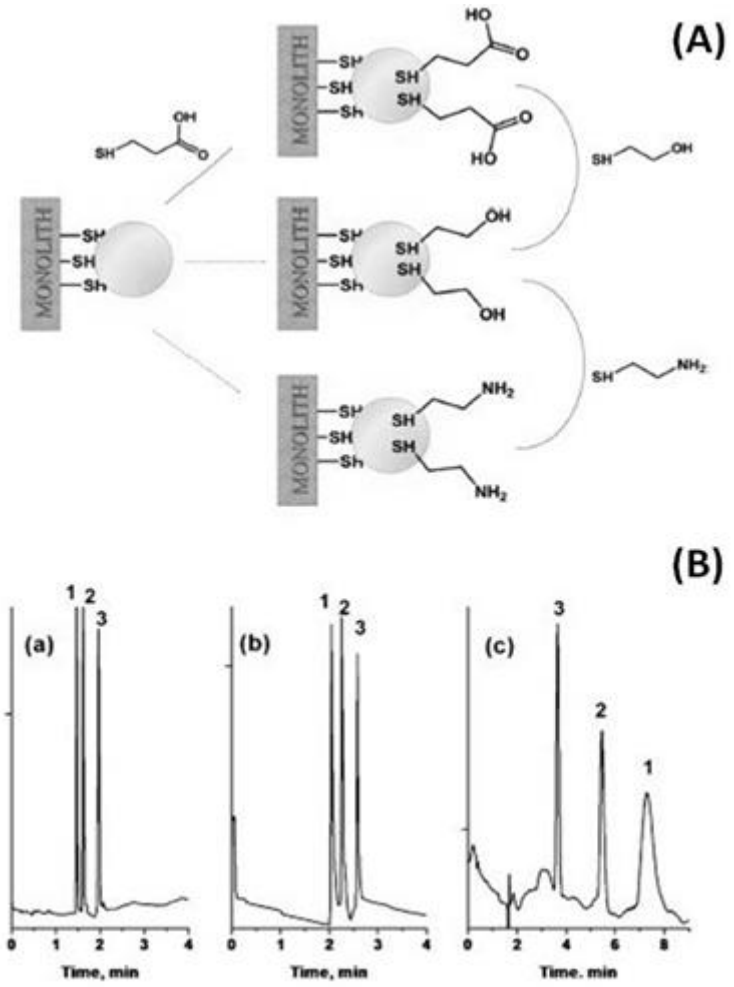

Figure 1.17: *Schematic diagram of the protocol used for modification of the surface chemistry of a GNP-modified monolith via ligand exchange with thiol compounds (upper). Electropherograms of three peptides using a GNP-modified monolith functionalised with 3-thiopropionic acid (a), mercaptoethanol (b) and cysteamine (c). Conditions: 100 µm i.d. monolith with total length 33 cm and effective length 8.5 cm, mobile phase: 10 mmol/L sodium phosphate with 50 % acetonitrile, pH 2.5; applied voltage -10 kV, UV detection at 214 nm. Peaks: (1): Tyr-Gly, (2): Tyr-Gly-Gly, (3): Tyr-Gly-Gly-Phe-Leu. Reproduced from [66]*

The same research group have most recently expanded upon this work using an alternative gold immobilisation strategy [67]. A GMA-*co*-EDMA monolith was reacted with cysteamine and the disulphide bonds were cleavage by flushing the monolith with tris(2-carboxylethyl)phosphine, providing available thiol groups for GNP attachment. The gold-modified monolith was then functionalised with either 1-

octanethiol or 1-octadecanethiol which allowed for the reversed phase separation of ribonuclease A, cytochrome C and myoglobin under gradient conditions.

Alwael *et al.* recently prepared a polymer monolith within a pipette-tip format and immobilised gold nanoparticles after grafting with vinyl azlactone and reacting the monolith with ethylenediamine [68]. A lectin (*Erythrinacristagalli,* ECL) was then covalently anchored to the gold using a bifunctional crosslinker which had a thiol group at one end (for attachment to the gold) and a succinimidyl group at the other end for immobilisation of the lectin via lysine residues on the protein surface. The authors successfully demonstrated that glycoproteins with terminal galactose could be enriched from a complex mixture of proteins because ECL is selective for glycans with terminal galactose. The authors also demonstrated that there was a 95 % increase in binding capacity for the target glycoproteins on the gold modified monolith relative to a monolith that had the ECL lectin bound directly to its surface, presumably due to the increased surface area afforded by the gold nanoparticles.

1.7 Characterisation of monolithic stationary phases

There are several commonly used techniques to characterise monolithic stationary phases. These methods include field emission scanning electron microscopy (FE-SEM) with electron dispersive X-ray (EDX), scanning capacitively coupled contactless conductivity (sC^4D), mercury intrusion porosimetry, Brunauer-Emmett-Teller (BET) and inverse size exclusion chromatography. Most of these methods are generally destructive and are used to measure morphology, porosity, surface area, surface chemistry and homogeneity of stationary phase density or surface charge.

1.7.1. Field Emission Scanning Electron Microscope/ Electron dispersive X-rays (FE-SEM/EDX)

This is one of the most important characterisation tools used in characterising the monolithic stationary phase. Most new FE-SEM instruments are coupled with EDX. FE-SEM is an ultra-high resolution electron spectroscopy technique used in visualising fine structures such as thin films and nanoparticles. Although this is a destructive method of characterisation, it is essential in the visualisation of both covalent bonding of monolithic stationary phase to the walls of the housing and immobilised nanoparticles on the surface of the stationary phase. It is also helpful in visually evaluating the pore size and morphology of the monolith. Samples are

imaged by irradiating the sample with a beam of electrons and detecting either the secondary electrons or the back-scattered electrons, depending on the information that is required. The source of electrons is either by thermionic or field emission which produces a high energy monochromatic beam of electrons. In order for samples to be imaged, they have to be electrically conductive and are rendered conductive by simply coating the sample (e.g. thin gold coat) using a sputter coater. FE-SEM contains a system of pumps in the column which pump the chamber to a high vacuum.

Secondary electrons are a beam of low energy electrons produced by inelastic scattering interactions and are the most common and standard detection mode used in FE-SEM analysis. The detector counts the electrons and sends the signals to an amplifier. They reveal a characteristic 3D image at high resolution of the surface. The secondary electron detector provides the topography of a sample. In general, the magnification ranges from 15x to 200,000x with a resolution of 5 nm and a penetration depth of 1 nm to 5 μm. EDX is applied in elemental analysis of the monolithic stationary phase as it identifies and measures the percentage of elements present. It relies on the principle that each element has a unique atomic structure which generates specific x-rays. In order to generate such x-rays, a high-energy beam of electrons irradiates the sample zone which contains the desired elements. A detector is used to convert the generated x-rays into a voltage which is sent to a pulse process and generates the data. This technique has proven to be particularly useful for the determination of atomic % of metals immobilised onto monolithic surfaces.

1.7.2. Scanning capacitively coupled contactless conductivity (sC^4D)

This conductivity detection method has gained significant interest especially for capillary electrophoresis and can be applied in liquid chromatography. The principles of this mode of detection are well understood and have been discussed in detail in the literature. [69,70,71,72,73]. The main difference between this conductivity detector relative to traditional conductivity detectors is that the sample solution does not flow across or past the electrodes and as such the electrodes are not in physical contact (i.e. they are not wetted) with the sample solution. An obvious advantage is that since the electrodes are not in physical contact with the sample, then they are not susceptible to electrode fouling. Instead, the electrodes comprise two cylindrical

ring electrodes approximately 1 mm long and separated approx. 1 mm apart such that there is a detection gap between the electrodes as shown in Figure 1.18. The fused silica capillary is passed through the bore of the electrode pair, and in capillary electrophoresis applications, or in LC, the detector head (comprising the electrode pair and associated amplifiers) is usually in a fixed position at one end (the detection end) of the capillary.

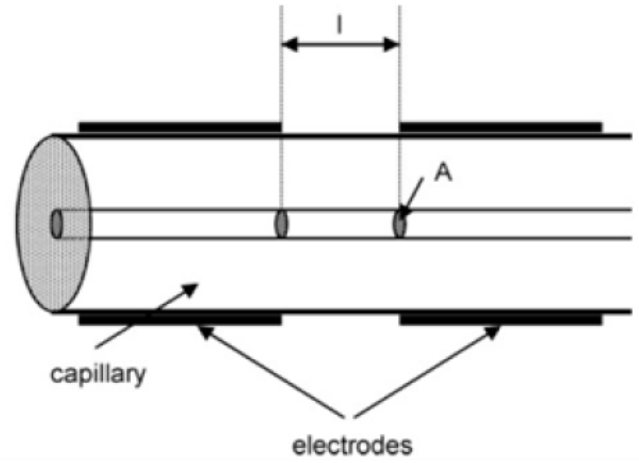

Figure 1.18: *Diagram of the cell model showing the basic configuration of the C^4D electrodes.*

A general definition of a capacitor is when two conductive materials are separated by an insulating material such as a vacuum. However in the case of a C^4D cell, the capacitors are not of two metallic plates but rather one plate is a metallic cylinder (labelled as an “electrode” in Figure 1.18) and the other is the fluid at the internal surface of the capillary tubing (e.g. fused silica capillary). The resistor between the two capacitors is the fluid inside the tubing between the two capacitors and therefore, capacitance is defined by:

$$C = \frac{2\pi\varepsilon_0\varepsilon_r l}{\ln D - \ln r}$$

Where C = the cell capacitance in Faradays, ε_0 = the relative permittivity of vacuum, ε_r = the relative permittivity of the silica capillary wall, l = the length of the electrodes in meters, D = the outer radius of the capillary in meters, r = the internal radius of the capillary in meters.

The measurement of conductivity is achieved by applying an alternating current (a.c) at a high frequency to the actuator electrode (left-hand electrode in Fig. 1.18) and measuring the resulting current at the pick-up electrode (right-hand electrode in Fig. 1.18). The current is converted to voltage using an operational amplifier and detector response is reported in millivolts (mV). If the AC voltage is kept constant, the passage of a charged species in the detection gap between the ring electrodes causes a decrease in resistance which increases the resulting current as described by Ohm's law. Usually the passage of a charged species through the detection gap represents the elution or migration of a charged analyte as it passes through the capillary (and thus the detector) from left to right in Figure 1.18.

Although typically operated in a fixed position upon the capillary, the detector cell can readily be moved to any location along the capillary length which lead researchers to explore the use of the detector in "scanning mode". When operated in "scanning" mode, it is an effective non-invasive technique that measures either the axial homogeneity of the stationary phase density or surface charge along the column. A scanning C^4D profile is acquired by moving the detector head at millimetre intervals along the length of the capillary, recording the detector response at each location. The resulting data is plotted as detector response on the y-axis and detector position (in millimetres) on the x-axis. Usually a ruler is used as a calibration guide to validate the position of the detector at any location along the column length as shown in Figure 1.19.

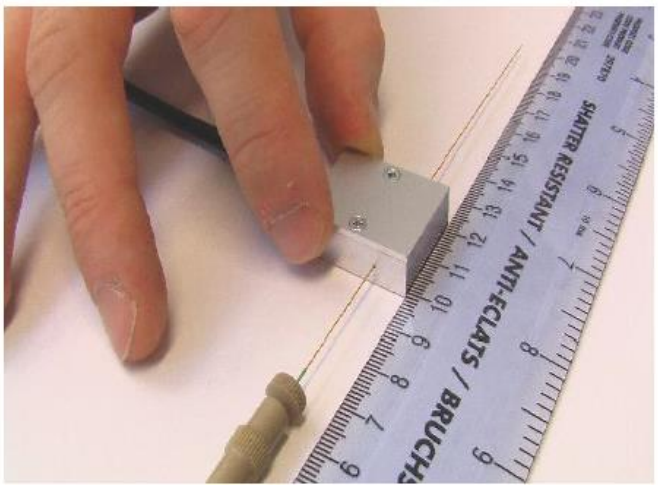

Figure 1.19: *Schematic above shows scanning of a capillary monolith in 1 mm increments using C^4D.*

The results obtained are used to plot a graph of conductive response (mV) against detector position along column length (mm) thus permitting axial evaluation of monolith quality such as monolith density or longitudinal distribution of charge density. An excellent review of applications of scanning C^4D was recently published by Connolly *et al.* [74] Indicative examples of the use of sC^4D include the evaluation of monolith density during the formation of monolithic porous layer open tubular (monoPLOT) columns by Nesterenko *et al.* [75] The technique was used as a quality control tool in order to profile the longitudinal homogeneity of the monolithic stationary phase which was fabricated by filling fused silica capillary with a monomer mixture and then scanning a UV light source at a fixed speed along the capillary length for photo-polymerisation of the monomer mix. Scanning C^4D was then used to evaluate the axial homogeneity of the resulting monolith. The authors demonstrated that by using the automated scanning polymerisation technique, the longitudinal stationary phase thickness and column reproducibility was within 5 % RSD (percentage relative standard deviation - % RSD). A separation of up to 8 proteins within 15 minutes was demonstrated using optimised gradient conditions.

Connolly *et al.* [76] used sC^4D evaluate homogeneity of packing density for 100 µm i.d. capillaries packed with silica stationary phase using polymer monoliths as retaining frits. Using C^4D in “scanning” mode, Connolly *et al.* identified gross column voids by deliberately positioning frits within the capillary column. The location of the column voids were confirmed by digital photography. The packing density was compared for two packed columns by measuring difference in conductive response per unit length as shown in Figure 1.20. The conductive response varied from 1.1 to 4.2 %.

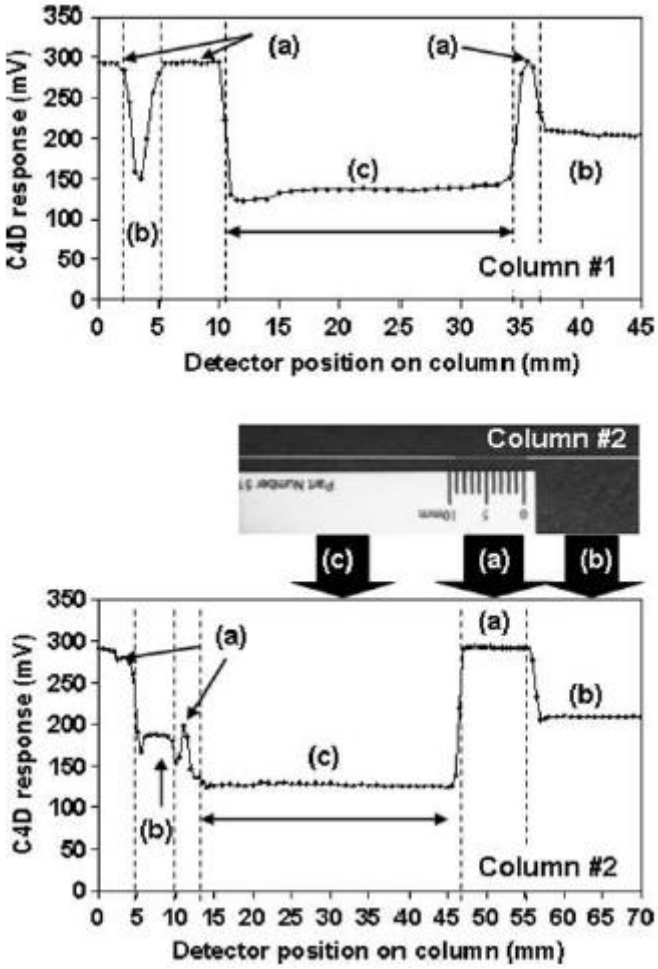

Figure 1.20: *sC^{4}D profiles of Column #1 and Column #2 with a digital photograph of Column #2 showing the 9 mm void between the monolithic frit and the packed resin. (a) Column void, (b) monolithic frit, (c) packed bed of Dionex PAX100 resin. Reproduced from [76]*

Walsh *et al.* [77] used sC^{4}D to characterise the axial homogeneity of monolith density of a range of poly(styrene-*co*-divinylbenzene) monoliths. Four poly(styrene-*co*-divinylbenzene) monoliths were synthesised in the channel of COC micro-fluidic chips from different batches of pre-polymer solutions using visible light-initiated polymerisation (light emitting diode at 470 nm as a light source). The results showed a similar degree of homogeneity along the length of the channel after characterisation using sC^{4}D. Calculation of the percentage relative standard deviation (% RSD) showed that the values for each of the four columns were 7.6 % (Z2), 3.8 % (Z3), 11.1 % (Z4) and 8.9 % (Z6) shown on Figure 1.21 which suggests a reasonably good overall consistency of the columns generated by the *in-situ* polymerisation procedure.

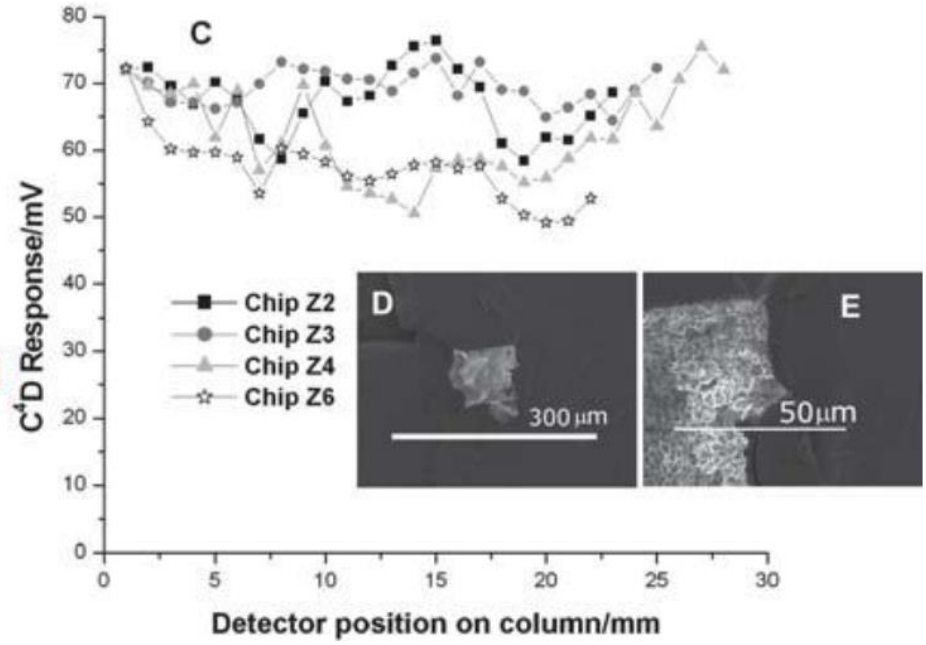

Figure 1.21: *(C) sC^{4}D profiles of poly(S-co-DVB) monoliths within the channels of the COC microfluidic chips, (D) a scanning electron micrograph of the poly(S-co-DVB) monolith in the channel and (E) ×6 magnification of (D) at the channel wall. Reproduced from [77]*

Gillespie *et al.* [78] evaluated neutral and charged surfactants and polyelectrolyte coatings on a silica monolith using sC^{4}D and observed that coating in one direction and subsequently reversing the column produced higher surfactant loadings with an even surface coverage. The column was coated for over 60 minutes with sodium dioctylsulfosuccinate (DOSS) solution (flow from the inlet to the outlet of the capillary), and a breakthrough curve was seen at 26 min (26 nM DOSS). The capillary was then reversed and was coated (flow from the outlet to the inlet of the capillary) for a further 60 min with the same coating solution, resulting in a second breakthrough curve seen at 30 min (30 nM DOSS). DOSS coating results are shown in Figure 1.22

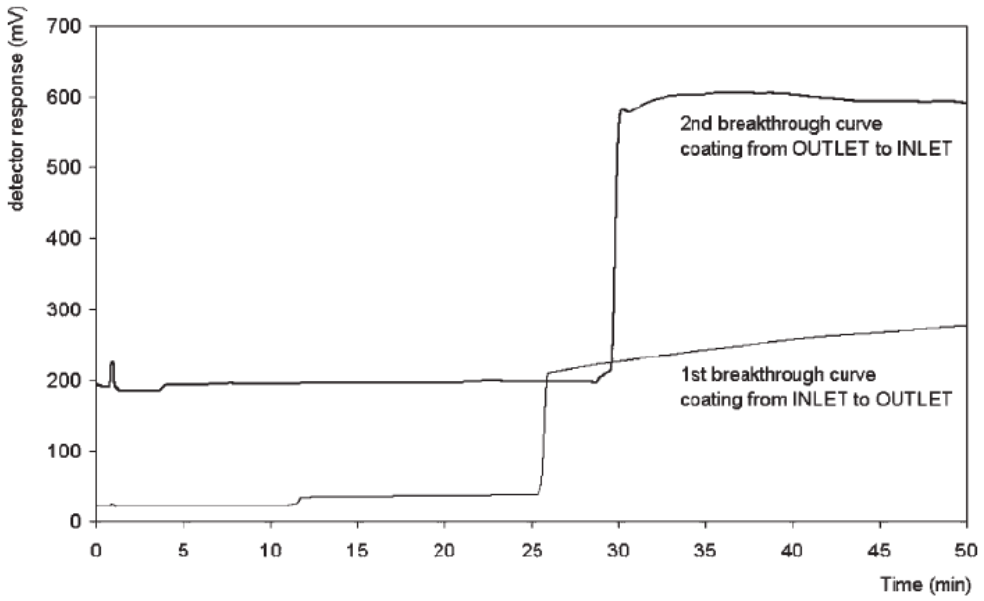

Figure 1.22: *Breakthrough curves for a coating solution of 1 mM DOSS used to modify the stationary phase within a monolithic capillary column.1st coating from the capillary INLET to the OUTLET, followed by a 2nd coating in the reverse direction OUTLET to the INLET. Reproduced from [78]*

The discussion above of the application of scanning C^4D is illustrative rather than exhaustive, and the reader is directed to the excellent review by Connolly *et al.* [74] for a more comprehensive discussion of this monolith evaluation method.

1.8 Overall aims of the presented thesis

The overall aim of this thesis is to examine various methods for the modification of monolithic stationary phases with nano-materials for enrichment or separation of phosphorylated compounds. Chapter 2 discusses the fabrication of polymer monoliths in capillary formats and the subsequent functionalisation using two-step photografting methods such that the monolith had pendant quaternary ammonium functional groups at the pore surface. Iron oxide nanoparticles were then immobilised via electrostatic interactions and the coverage of the nanoparticles evaluated using scanning C^4D profiling methods. Field emission scanning electron microscopy is also presented as an alternative (albeit destructive) method for evaluation of nanoparticle coverage. The monolith was finally used for separation of phosphorylated small molecules using a phosphate gradient.

Chapter 3 deals with the modification of monolithic silica centrifugal spin columns with iron oxide nanoparticles using a layer-by-layer approach. Field emission scanning electron microscopy and energy dispersive x-ray microscopy were used to characterise the coverage of nanoparticles on the surface. The nano-structured spin-columns were subsequently used for the extraction of phosphopeptides and the selectivity was compared with that of a commercially available titania monolithic spin column.

In both Chapter 2 and Chapter 3, the advantage of using a monolithic substrate for the immobilisation of nanoparticles is clearly demonstrated.

Chapter 2: Fabrication and characterisation of nano-structured capillary polymeric monoliths for separation of phosphorylated compounds

1. Introduction

1.1 Metal Oxide Affinity Chromatography (MOAC)

Protein phosphorylation is a post-translation modification step after protein synthesis and is a fundamental event in intracellular signalling and thus identification of protein phosphorylation is of significant importance [79]. Traditionally, protein phosphorylation is usually detected using antibodies and/or specific radioactive labelling methods. This method is challenging since immuno-labelling is often unspecific, causes waste disposal issues and most importantly may result in unwanted artificial phosphorylation events [80]. Phosphopeptide abundance in biological samples is generally significantly lower (by several orders of magnitude) relative to endogeneous proteins such as albumins and so accurate identification of phosphorylated proteins or peptides is further hampered [80]. Mass spectrometry (MS) is commonly used in characterisation of phosphorylated compound such as phosphoproteins. However, smaller phosphorylated species are difficult to detect and analyse using the MS due to their low ionisation efficiency in the company of non-phosphorylated species [81]. Therefore, a range of sample preparation, purification and isolation techniques have been developed to allow pre-concentration of a mixture of phosphopeptides or phosphoproteins and typically involves either magnetic nanoparticles, or chromatographic methods [82]. Figure 2.1 shows the common strategies used for enrichment of phosphorylated compounds [83].

For a long time, enrichment of phosphorylated compounds relied heavily on a well-established mode of chromatography known as immobilised metal affinity chromatography (IMAC) [84]. IMAC is a tool that has been developed to aid in the isolation and subsequent identification of phosphorylated molecules based on their affinity for metal ions. Traditional IMAC technologies consist of two components; an immobilised chelating group and a metal species such as Cu^{2+}, Ni^{2+}, Ga^{3+}, Al^{3+}, Zr^{4+} or Fe^{3+}. Chelating groups such as iminodiacetic acid (IDA) or nitrilotriacetic acid (NTA) groups are covalently attached to the stationary phase support particle and bind to the metal ion thus allowing interaction and separation of phosphorylated

compounds [85]. However, even though IMAC supports have been used for a long time, they are predisposed to metal leaching due to changing metal ion – organic chelator interactions, consequently column regeneration is essential after each usage. Furthermore, carboxylic groups of the phosphopeptides or phosphoproteins may also interact with the chelated metal cations resulting in non-specific binding [86].

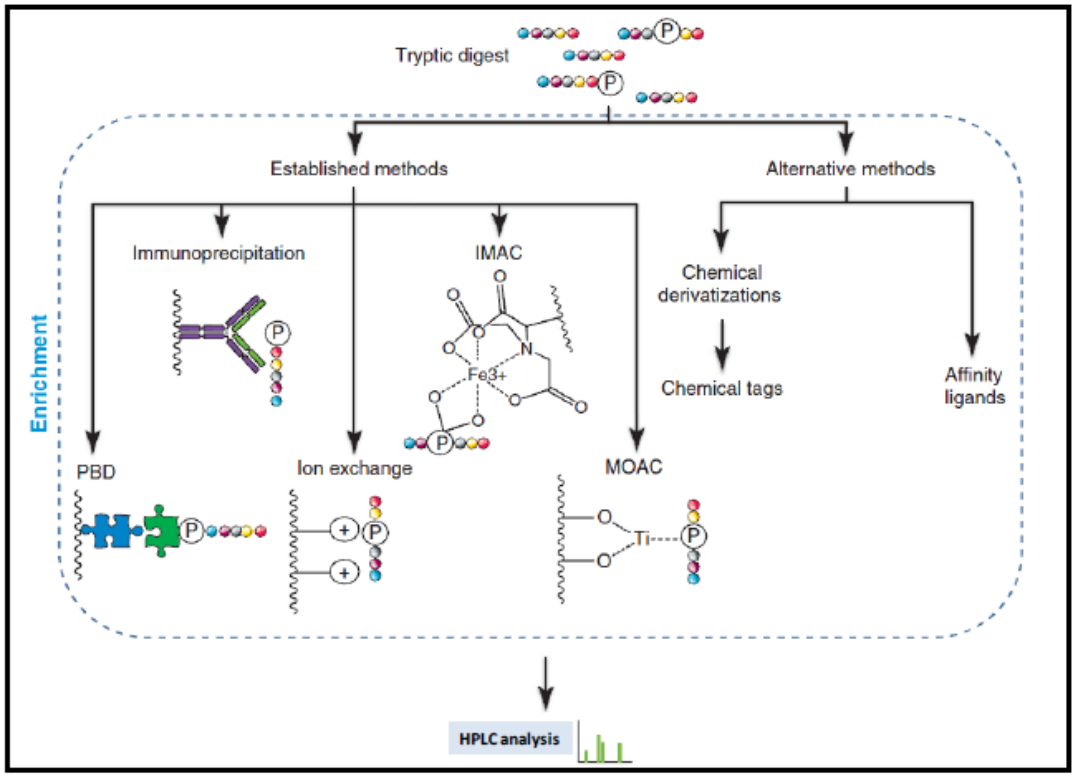

Figure 2.1: *Common strategies for enrichment of phosphorylated compounds including peptides. Reproduced from [83].*

In the last decade, pioneering scientists such as Nawrocki [87] have suggested using metal oxide materials such as TiO_2 and ZrO_2 as alternative stationary phases for liquid chromatography. Metal oxides tend to have higher selectivity for phosphopeptides, relative to IMAC methods [88]. The focus of this chapter is metal oxide affinity chromatography (MOAC) and this approach is the most powerful and promising strategy in recent years and takes advantage of the particular affinity of phosphate groups for metal oxides.

Connor *et al.* [89] used Fourier Transform Infrared spectroscopy (FTIR) to study the kinetics and pH properties of TiO_2 adsorption processes. From their

results, Connor *et al.* concluded that the governing binding mode of the phosphate anion and mono-substituted phosphates to the TiO_2 surface was “bidentate” in nature which is similar to many carboxylic acids. Interactions between metal oxides and phosphate groups can be also looked at from an ion exchange vantage point; where the metal oxide acts as a Lewis acid and the interaction with different types of Lewis bases is influenced by a variety of properties. For example, slight temperature changes during synthesis of metal oxide materials can affect the end product and significantly influence the binding characteristics [90]. As a consequence, while the “spatial” characteristics of phosphate binding are well established, limited knowledge is known of the factors that play a role in the overall recognition process driven by surface chemistry. However, it has been established that the predominant binding mode of phosphorylated species with metal oxide surface is considered a bidentate binding mode as illustrated in Figure 2.2 below.

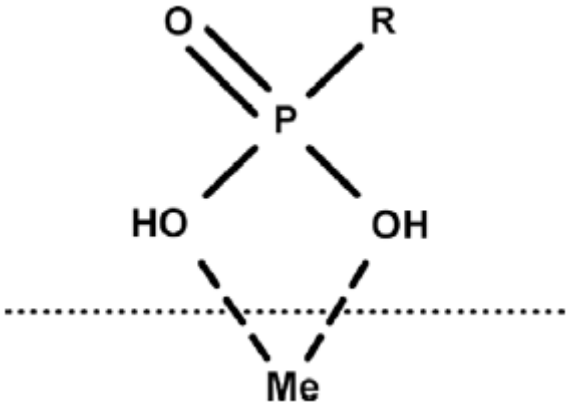

Figure 2.2: *Bidentate binding mode of phosphates to a metal oxide surface (Me = metal). Reproduced from [91].*

1.2 Nano-particle modified monoliths for enrichment of phosphorylated compounds

An increasing number of studies have described the use of various metal oxide nano-materials for the enrichment of phosphorylated compounds due in part to the affinity of such compounds to metal oxide surfaces and use to the relative ease with which nano-materials can be incorporated into stationary phases as discussed in Chapter 1 Section 1.6.4. For the sake of clarity, monolithic stationary phases

modified with metal oxide nanoparticles was not mentioned in Chapter 1, and is instead discussed hereafter in this chapter.

1.2.1 Hydroxyapatite.

The crystalline form of calcium phosphate is known as hydroxyapatite and has the general formula $Ca_{10}(PO_4)_6(OH)_2$. Many studies have reported its use for enrichment of phosphoproteins and phosphopeptides and the retention mechanism is considered to be “mixed-mode” ion exchange, being largely dependent upon pH and buffer concentration [92]. In 2010, Krenkova *et al.* fabricated a polymer monolith in a capillary format which incorporated encapsulated hydroxyapaptite nanorods (50 nm X 150 nm) [93]. This was achieved by admixing the nanorods into a monomer mixture of hydroxyethyl methacrylate and ethylenedimethacrylate prior to polymerization within the fused silica capillary housing. A balance was struck between the amount of nanorods which could be added to the monolith and the resulting monolith permeability. SEM and EDX characterization allowed the authors to visualize the nanorod distribution throughout the monolithic structure and to obtain semi-quantitative information about the hydroxyapatite content as shown in Figure 2.3. Using a phosphate gradient, a 6 minute separation of selected proteins was possible, and the authors also demonstrated the use of the monolith for the selective enrichment of phosphopeptides from a β-casein tryptic digest prior to matrix assisted laser desorption ionisation mass spectrometry (MALDI-MS).

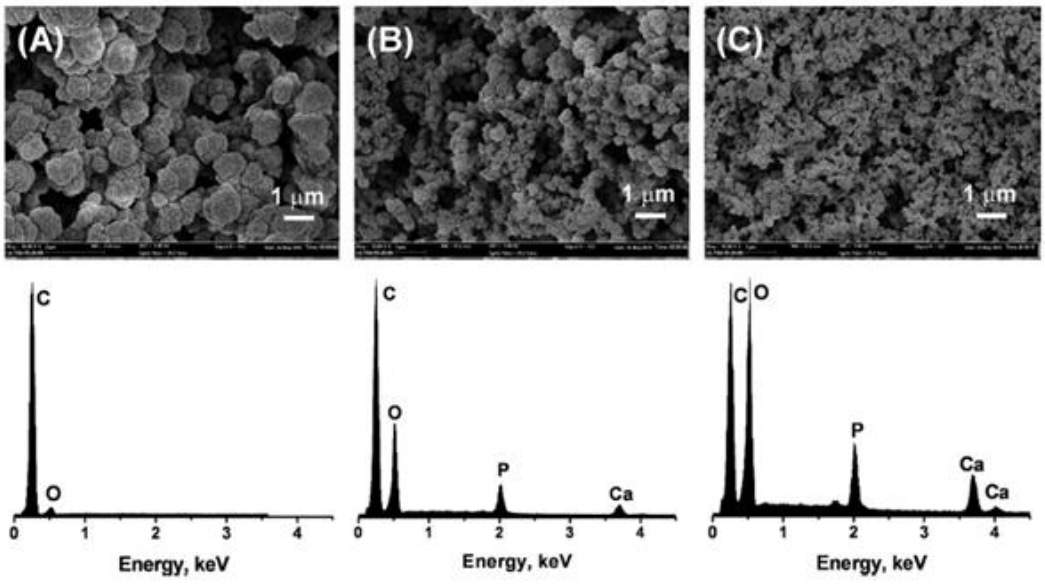

Figure 2.3: *SEM images and EDX spectra for polymer monoliths with different mass loadings of hydroxyapatite nano-rods. (A): nano-rod/monomer ratio 0/50, (B): 30/50, (C): 60/50. Reproduced with permission from [94].*

More recently, Krenkova *et al.* prepared polymer monoliths within pipette-tip housings for the off-line enrichment of phosphopeptides prior to analysis by MALDI-MS[95]. Similar to their previous work above, hydroxyapatite nanoparticles were simply admixed into the monomer mixture before the mixture was then aspirated into the pipette-tip and polymerised *in-situ*.

1.2.2 Nickel-cobalt nano-particles

Tobal *et al.* encapsulated 10 nm-sized Ni-Co nano-particles into a polymer monolith for the enrichment of β-casein tryptic peptides prior to MS characterisation [96]. Up to 10 % by weight of nano-particles could be included in the monomer mixture prior to polymerisation in 75 µm i.d. fused silica capillary without any negative effects upon monolith permeability. A protein digest (10 pmol) was loaded on the monolith which was washed with acidified water to elute non-phosphorylated biomolecules and then eluted with a *water/acetonitrile (60/40 1% formic acid) step gradient.*

1.2.3 Titanium dioxide/zirconium dioxide nano-particles.

Hsieh *et al.* [97] prepared an ethylene dimethacrylate monolith in a pipette-tip format in which 20 nm titanium dioxide (TiO_2) nanoparticles were encapsulated by inclusion in the monomer mixture prior to *in-situ* polymerisation. Phosphorylated peptides were isolated from non-phosphopeptides by the embedded TiO_2 nanoparticles and eluted by 100 m*M* ammonium phosphate (pH 8.5), rendering it compatible with 2,5-dihydroxybenzoic acid (DHB)/ 1 % phosphoric acid matrix and allowing for direct analysis of the elution fraction by matrix-assisted laser desorption/ionisation mass spectrometry (MALDI-MS) without the necessity of desalting pre-treatment. A mixture of tryptic digested (α-casein and β-casein) spiked into bovine serum albumin (BSA) and non-phosphorylated peptides were selectivity assessed using the TiO_2 tips. A wash buffer of 50 m*M* ammonium hydrogen carbonate (pH 8) in 50 % acetonitrile was used to reduce non-specific binding of non-phosphorylated peptides. Almost all phosphorylated peptides were detected by

MALDI-MS analysis. The lowest detectable amount of phosphopeptide was estimated at low femtomole level.

A similar report was later published by Rainer *et al.,* who prepared a poly(divinylbenzene) (DVB) monolith with encapsulated TiO_2 nano-particles (<100 nm) or TiO_2/ZrO_2 mixed nano-particles, within pipette-tip housing [98].Approximately 20 phosphopeptides could be retained from an α-casein tryptic digest and the use of a robotic sample handling system allowed the sample to be repeatedly passed back and forth across the bed thus significantly improving recovery.

1.2.4 Iron oxide nanoparticles

Iron oxide nanoparticles typically in size between 1 – 100 nm in diameter and are divided into three main forms, maghemite (γ-Fe_2O_3), haematite (α-Fe_2O_3) and magnetite (Fe_3O_4) [99]. Recently, iron oxides such as α-Fe_2O_3 particles [100] and Fe_3O_4 nanoparticles [99] have been demonstrated for phosphopeptide enrichment in a batch mode. In a recent study, Krenkova and Foret immobilised 20 nm citrate stabilised Fe_3O_4 nanoparticles via multivalent electrostatic attachment onto a quaternary ammonium functionalised glycidyl methacrylate monolith in a capillary format [101]. Stable attachment of the nano-particles directly to the monolith surface was achieved via multivalent electrostatic interactions, which is an obvious advance over encapsulation techniques. The dynamic binding capacity was measured for adenosine-5'-phosphate and found to be 86 μmol/mL column volume. The monolith was used for the selective extraction of phosphopeptides from a tryptic digest of α-casein and β-casein prior to MALDI-MS characterisation (as shown in Figure 2.4) and the selectivity was directly compared with a commercial TiO_2 extraction tip.

More recently in 2013, the same authors prepared a similar monolith in a pipette-tip housing in which the monolith was a 2-hydroxyethyl methacrylate-*co*-ethylene dimethacrylate monolith which had been functionalised with quaternary ammonium functional groups to facilitate the electrostatic attachment of negatively charged citrate stabilised iron oxide nanoparticles. Again the monolith was directly compared with a commercial titanium dioxide extraction tip for the enrichment of α-casein and β-casein tryptic digests prior to MALDI-MS analysis [102].

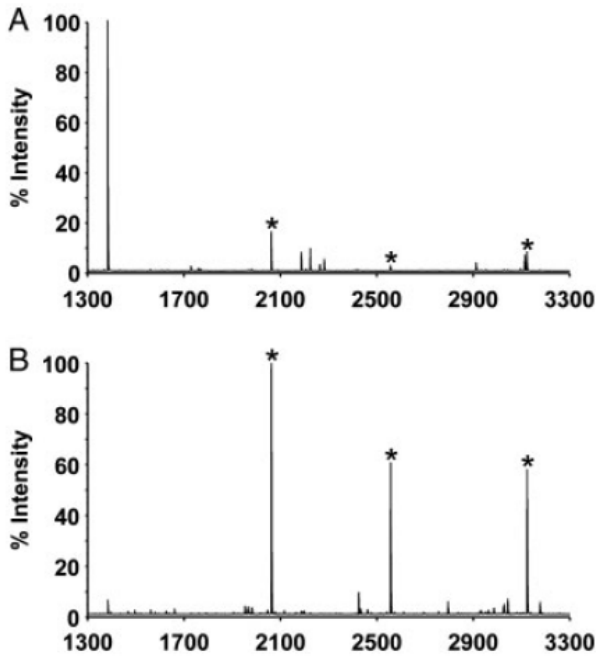

Figure 2.4: *MALDI-MS spectrum of a β-casein tryptic digest before (A) and after (B) enrichment on an iron oxide nanoparticle modified polymer monolith. Reproduced from [101].*

1.3 Overarching aims of this chapter.

The aim of this chapter is to fabricate polymer monoliths in capillary formats and to use two-step photografting methods to modify the surface chemistry such that iron oxide nanoparticles can be immobilised in a dense homogeneous layer. Scanning C^4D characterisation will be used as a quality control technique to evaluate the monoliths at separate stages throughout the modification protocol and to verify the homogeneity of nanoparticle coverage along the monolith length. The application of the monolith for the separation of small phosphorylated compounds (nucleotides) will also be demonstrated.

2.2. Experimental.

2.2.1 Reagents and materials.

Iron (II) chloride heptahydrate (≥99.0%), iron (III) chloride hexahydrate (puriss), citric acid (99+%), ammonium hydroxide, diethylamine, iodoethane, nitromethane, sodium hydroxide, monobasic and dibasic sodium phosphate, hydrochloric acid, acetone, HPLC grade acetonitrile, methanol, butyl methacrylate

(BuMA),glycidyl methacrylate(GMA),ethylene dimethacrylate (EDMA), 1-decanol, 2,2-dimethoxy-2-phenylacetophenone (DAP), 3-(trimethoxysilyl)propyl methacrylate, benzophenone, adenosine, adenosine monophosphate, adenosine diphosphate, adenosine-5-triphosphate, and potassium phosphate were purchased from Sigma Aldrich (Dublin, Ireland). Teflon coated UV-transparent fused silica capillary (100 µm i.d.) was obtained from Composite Metal Services (Shipley, West Yorkshire, UK). Deionised water was provided by a MilliQ Direct Q5 water purification system from Millipore (Millipore Bedford, MA, USA).

2.2.2 Instrumentation

Photo-polymerisation and photo-grafting were carried out using a Spectrolinker XL-1000 UV Crosslinker at 254 nm (Spectronics Corp., Westbury, NY, USA). A KD Scientific syringe pump (KDS-100-CE, KD Scientific Inc, Holliston, MA, USA) was used for all washing and functionalisation of monoliths. Model K120 Knauer pump (Knauer, Berlin, Germany) was used for the immobilisation of iron oxide nanoparticles. The balance used was a Sartorius Extend (Sartorius, Goettingen, Germany). The sonication bath used was from Branson Ultrasonics Corporation (Danbury, CT, USA). The centrifuge used was a Sartorius Sigma 1-14 Microcentrifuge (Sartorius Stedim UK Ltd., Epson, Surrey, UK.). Dynamic light scattering (DLS) measurements were conducted on a Zetasizer Nano instrument (Malvern, Worcestershire, UK) at 25 °C. Field emission scanning electron microscopy (FESEM) was performed using a Hitachi S-70 3400N instrument (Hitachi, Maidenhead, UK). TEM images were obtained using a JEOL 2000 FX TEM scan (at an accelerating voltage of 80 kV) for samples deposited on carbon-coated (400 mesh) copper grids. The preparation of samples involved depositing 15 µL of the diluted dispersion in heptane onto the grid and allowing the solvent to evaporate prior to imaging. A TraceDec scanning capacitively coupled contactless conductivity detection (sC4D) detector (Innovative Sensor Technologies, GmbH, Innsbruck, Austria) was used in scanning mode for monolith characterisation with settings of -6 dB, 50% gain and 0 offset. Chromatography was performed using a Dionex Ultimate 3000 Capillary LC system (Dionex, Sunnyvale, CA, USA) at a flow rate of 2 µL/min. The injection volume was 100 nL, with detection by UV at 214 nm using a 3 nLflow-cell. Mobile phase A was 20:80 acetonitrile/water and mobile phase B 20:80

acetonitrile/500 m*M* phosphate buffer. The gradient conditions were as follows: 0-1.6 mins 5-20% B, 1.61-5.00 mins 50 B %, 5.1-10 mins 5 % B.

2.2.3 Silanisation of teflon coated fused silica capillary

All flow rates used during this procedure were 2 µL/min. Teflon coated fused silica capillary (100 µm i.d.) was flushed with 200 m*M* NaOH for 30 minutes followed by deionised water for 10 minutes, 200 m*M* HCl for 30 minutes and deionised water for 10 minutes. Acetone was then flushed through the capillary for 10 minutes and the capillary purged with nitrogen gas for 10 minutes to remove any acetone in the capillary. The capillary was then flushed with 50 % 3-(trimethoxysilyl)propyl methacrylate in acetone for 30 minutes, sealed at both ends with rubber septa and placed in a water bath at 60° C for 20 hours. The fused silica capillary was subsequently washed with acetone for 30 minutes and finally purged with nitrogen gas for 10 minutes.

2.2.4 Preparation of polymer monoliths in capillary formats.

A monomer mixture consisting of 24% BUMA, 16% EDMA, 60 % 1- decanol and 1 % DAP (w.r.t. total monomer concentration) was prepared and deoxygenated for 10 minutes with a stream of nitrogen gas. The deoxygenated mixture was filled by capillary action into silanised fused silica (above) and the capillary sealed at both ends and irradiated with 2 J/cm^2 of UV energy (254 nm). The resulting monolith was flushed with methanol at 2 µL/min for 2 hours to remove unreacted monomers and porogen. Two poly(BuMA-*co*-EDMA) columns were prepared in this work and labelled as Monolith A and Monolith B, which were 8 cm and 7 cm respectively.

2.2.5 Surface modification of polymer monoliths with quaternary ammonium groups.

A deoxygenated solution of 5 % benzophenone in MeOH was flushed through the monolith for 30 minutes at 1 µL/min using a syringe pump. The monolith was sealed with rubber septa and irradiated with 1 J/cm^2 of UV energy (254 nm). The monolith was then washed with methanol for 60 minutes using a syringe pump to remove excess benzophenone. A deoxygenated solution of 15 % GMA in MeOH was then flushed through the monolith for 30 minutes at 1 µL/min using a syringe pump. The monolith was again sealed with rubber septa and irradiated with 1 J/cm^2

of UV energy (254 nm). The monolith was washed with methanol for 60 minutes using a syringe pump removing any excess GMA. Following this, a solution of 1 *M* diethylamine was flushed through the monolith for 60 minutes at 1 µL/min. The monolith was sealed with rubber septa and placed in a water bath at 70°C for 24 hours. The monolith was washed by flushing with water until the column effluent pH was ~ 7.0. The monolith was subsequently flushed with a 1:1 v/v iodoethane/nitromethane for 60 minutes at 1 µL/min. The monolith was sealed and placed in a water bath at 80°C for 5 hours. Finally, the monolith was washed with ethanol using a syringe pump for 3 hours at 1 µL/min followed by an overnight water wash.

2.2.6 Synthesis of citrate stabilised iron oxide nanoparticles

Citrate stabilised nanoparticles were prepared by co-precipitation of iron salts. In a typical synthesis a mixture of $FeCl_3.6H_2O$ and $FeCl_2.4H_2O$ in a 2:1 molar ratio was added to 40 mL deoxygenated water, in a three-necked round bottomed flask. The solution was purged with nitrogen for 15 minutes before heating to 80 ˚C with stirring under a constant flow of N_2 in an oil bath. Once the solution had reached the required temperature, 5 mL of NH_4OH was introduced drop wise into the reaction vessel, resulting in the formation of a black precipitate. A further 30 minutes heating at this temperature was observed, before the addition of 2 mL of citric acid solution (2.6 M) into the nanoparticle suspension. The temperature was then raised to 95 ˚C and an additional 90 minutes heating under magnetic agitation was observed. The nanoparticle suspension was then allowed to cool and was introduced into a dialysis membrane to remove any excess unbound citric acid for a period of 72 hours. Following dialysis, nanoparticle suspensions were centrifuged for 30 minutes at 13,200 rpm to remove any large aggregates.

2.2.7 Immobilisation of iron oxide nanoparticles on modified polymer monoliths

A suspension of iron oxide nanoparticles prepared by co-precipitation was filled into a 300 µL PEEK loop which was connected at one end to a Knaeur pump and at the other end to a quaternerised capillary monolith. The monolith was coated with nanoparticles at 1 µL/min until the colour of the white monolith turned a homogeneous light brown colour along the entire length of the monolith. Coating was

repeated by reversing the direction of the capillary monolith (1 µL/min for 60 minutes) to ensure a homogeneous coating of nanoparticles along the length of the monolith.

2.2.8 Scanning contactless conductivity characterisation of capillary polymer monoliths.

While constantly pumping water at 1 µL/min through the monolith, a C^4D detector cell was carefully moved at discrete intervals (either of 1 mm or 5 mm) along the column length using a ruler as a guide. The detector response (which was proportional to surface charge on the stationary phase) was recorded at each interval which permitted a plot of detector response versus detector position along the monolith (in mm) to be constructed. Each "scan" of the monolith was repeated in triplicate and results for each detector location averaged for reporting purposes.

3. Results and Discussion

3.1 Characterisation of Fe_3O_4 nanoparticles

Negatively charged citrate-stabilised Fe_3O_4 nanoparticles were prepared using a coprecipitation method described by Sahoo *et al.*[103] in which ferrous and ferric salts were oxidised under alkaline conditions as showed below.

$$2Fe^{3+} + Fe^{2+} + OH^- \rightarrow Fe_3O_4 + 4H_2O$$

Subsequent characterisation of the nanoparticle suspension by transmission electron microscopy showed roughly spherical particles as shown in Figure 2.5. Although the population of particles appears to have quite a broad size distribution in Figure 2.5, this was not considered to be detrimental for our purposes, since the ultimate fate of the nanoparticles was dense immobilisation upon a flow-through monolithic surface. Nevertheless, particle size analysis and zeta potential measurements were also made to confirm that the average size of the particles was 15.8 nm with a polydispersity index of 0.179 as shown in Figure 2.6. The zeta potential of the nanoparticles was -23.4 mV, clearly illustrating that the nanoparticle surface was capped with citrate anions. Krenkova *et al.* [101] investigated the effect of citrate concentration on the stability of iron oxide nanoparticles prepared using the co-precipitation method. They concluded that an absence of citrate anions resulted in

nanoparticles with poor colloidal stability leading to rapid aggregation whereas a citrate concentration of 1.5 %w/v proved to be more stable giving the nanoparticles a negative charge.

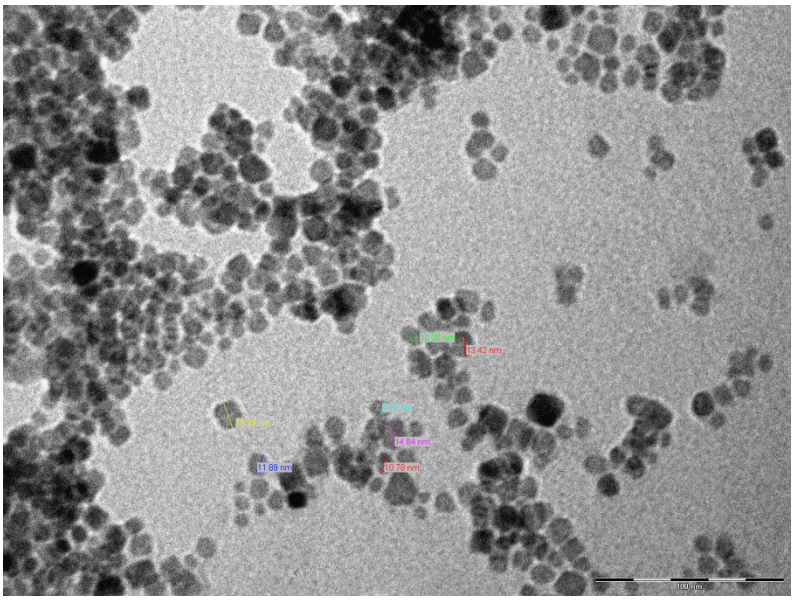

Figure 2.5: *TEM image of prepared iron oxide nanoparticles. Scale bar (bottom right) is divided into five 20 nm segments.*

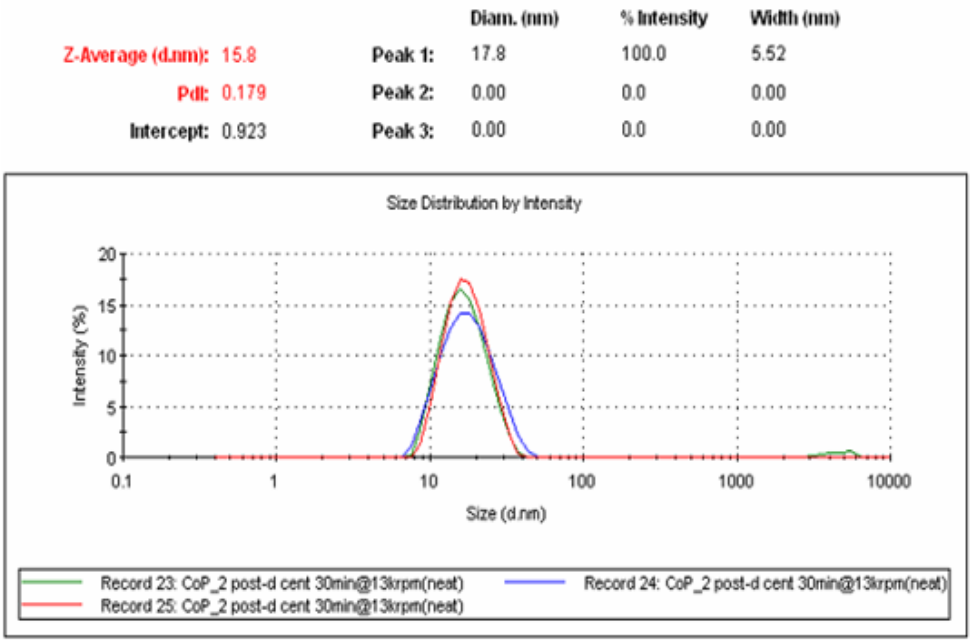

Figure 2.6: *Dynamic light scattering data for determination of size distribution of prepared iron oxide nanoparticles.*

The resulting repulsive interactions between neighbouring nanoparticles ensured that particle aggregation did not occur. During the course of this work, nanoparticle suspensions were stable for several months at room temperature.

3.2 Characterisation of nanoparticle-modified monoliths using backpressure measurements.

In order to electrostatically attach iron oxide nanoparticles to a polymer monolith, the monolith first required a chemical modification to render it positively charged. Two strategies were considered in this work. The first strategy involved preparation of a monolith with reactive functional groups (GMA-*co*-EDMA) which can subsequently be chemically modified via amination of the epoxy groups. The disadvantage of this method (as described in Section 1.6.2) is that most of the reactive epoxy groups are buried deep within the monolith globules rather than being presented at the surface, which places a limit upon the total ion-exchange capacity of the resulting monolith after chemical modification. For this reason, this strategy, although initially considered, was not adopted in this work.

An alternative strategy (adopted in this work) involved grafting poly(GMA) onto a prepared BuMA-*co*-EDMA monolith such that the grafted chains (each emanating from a single graft point on the surface) would bear multiple pendant epoxy groups available for reaction in a subsequent chemical modification step. A two-step grafting protocol was used in which a free-radical initiator (benzophenone) was covalently anchored to the monolith surface in the first step [104],[105], [106],[107],[108]. This was achieved using UV irradiation which facilitated hydrogen abstraction from the polymer surface such that a monolayer of benzophenone was covalently attached and resistant to removal during any subsequent solvent flushes. The second step involved filling the monolith pore volume with the graftable monomer (in this case GMA) in the absence of initiator. During the subsequent irradiation cycle, the benzophenone immobilised at the surface resulted in grafting of poly(GMA) chains directly from the pore surface at a multitude of attachment sites. The absence of initiator in the bulk pore volume resulted in little or no formation of an unwanted gel of poly(GMA) which otherwise would have blocked the pore volume leading to unacceptably high backpressures as described by Rohr *et al.* [106]. A schematic representation of the grafting process is shown in Figure 2.7.

After grafting of the monolith surface with poly(GMA), the pendant epoxy groups on the polymer grafts were first reacted with diethylamine in order to produce 1-(N,N-diethylamino)-2-hydroxypropyl functionalities. The final step involved alkylation of these tertiary amine groups with iodoethane resulting in a monolith with a strong anion exchange character and an anticipated high surface density of positively charged attachment sites for subsequent immobilisation of the negatively charged nanoparticles [101]. The amination mechanism is also shown in Figure 2.7. Conveniently, monoliths turned colour from white to brown after coating with nanoparticles and so a crude evaluation of the stability of nanoparticle immobilisation was possible by verifying that the monolith retained its brown colour over prolonged use. A more comprehensive evaluation of nanoparticle coating homogeneity along the column length was performed using scanning contactless conductivity detection and is discussed in more detail in Section 3.3.

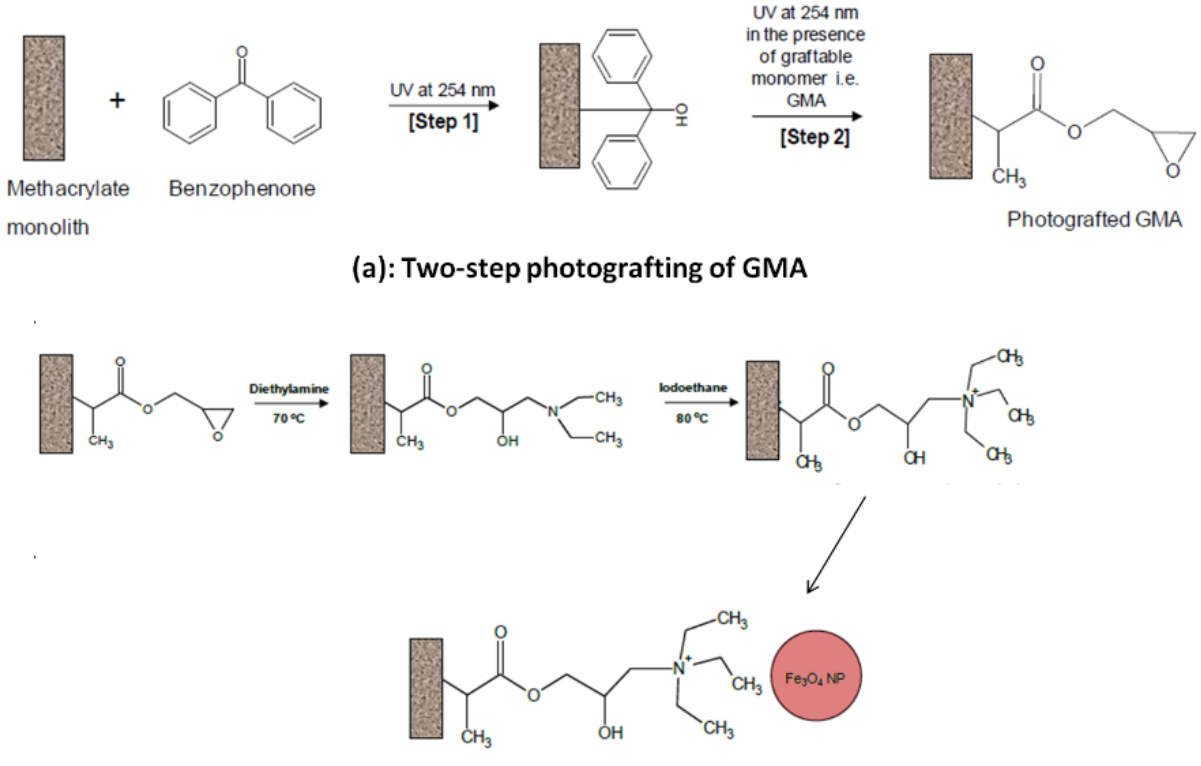

Figure 2.7: *Schematic diagram of (a) two-step photografting of GMA to a methacrylate monolith and (b) amination of poly(GMA) grafts and subsequent iron oxide nanoparticle attachment.*

The monoliths prepared in this study were subjected to back-pressure measurements at different stages throughout the modification process. Backpressure measurement is a facile method for monolith characterisation, providing important information on monolith-to-monolith reproducibility. Monolith back-pressure is a function of column dimensions, solvent viscosity and temperature however during this work all of these parameters were held constant (i.e. the capillary monoliths were all 100 µm i.d. and the back-pressure solvent was water at room temperature (22 ^{o}C) in all cases. However, more importantly monolith backpressure is also a function of monolith density which itself is related to pore size. For example, a monolith with large pores (low density monolith) will typically result in lower operating pressures than a monolith with smaller pores (higher density monolith).

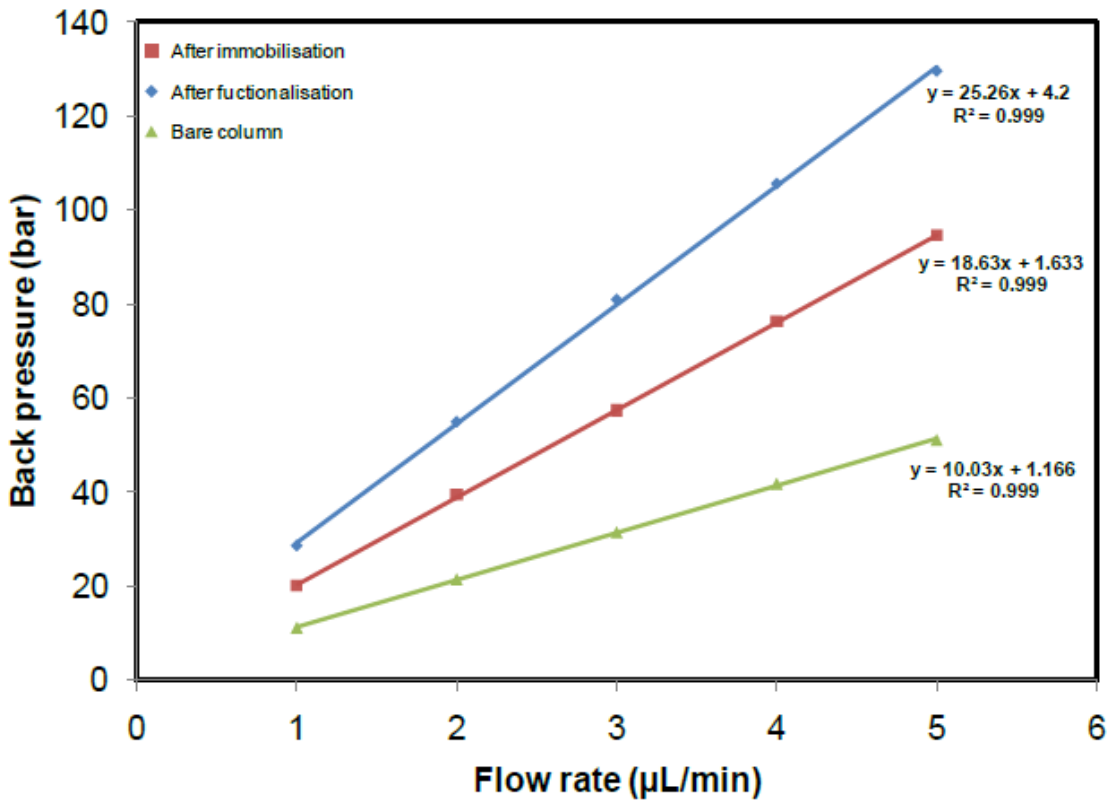

Figure 2.8: *Backpressure measurements for Monolith A before grafting/amination (green plot), after amination (blue plot) and after immobilisation of iron oxide nanoparticles (red plot).*

Measuring monolith backpressure can also reveal if the pore volume is blocked or partially blocked, both of which instances result in increased

backpressure. Therefore, monolith backpressure was measured before and after the grafting/amination protocol and also after the subsequent attachment of the iron oxide nanoparticles. Figure 2.8 shows a plot of backpressure (bar) versus flow rate (µL/min) of Monolith A before and after amination. A clear increase in column backpressure was observed for Monolith A after the grafting/amination protocol, with backpressure increasing from 51 bar at 5 µL/min before amination to 130 bar at 5 µL/min after grafting/amination, representing a 155 % increase in back-pressure. After subsequent immobilisation of iron oxide nanoparticles there was a significant decrease in backpressure to 95 bar at 5 µL/min, corresponding to a 27 % decrease.

The same backpressure study was performed with Monolith B and results are shown in Figure 2.9 below. Again an increase in column backpressure was observed after the grafting/amination, this time increasing from 52 bar at 5 µL/min to 114 bar at 5 µL/min after grafting/amination, representing an increase of 119 %. Immobilisation of nanoparticles upon the aminated monolith resulted in a decreased backpressure of 99 bar at 5 µL/min, which calculates as a 13 % decrease.

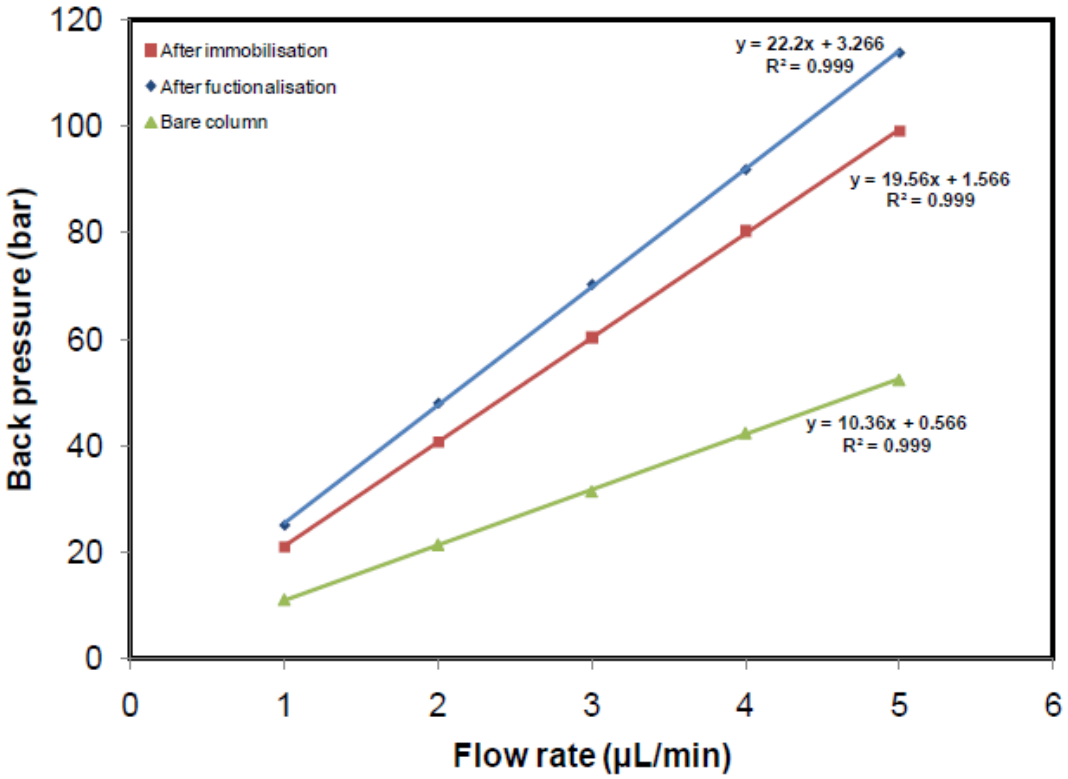

Figure 2.9: *Backpressure measurements for Monolith B before grafting/amination (green plot), after amination (blue plot) and after immobilisation of iron oxide nanoparticles (red plot).*

By comparing the results of backpressure measurements for Monolith A and Monolith B it is clear that the backpressure profiles were linear (R^2 = 0.999) across the entire study range which illustrates that monolith swelling due to solvent effects did not occur. In addition, the linear profiles demonstrate that both monoliths had a suitable level of mechanical rigidity and were resistant to physical compression under the chosen operating conditions. Furthermore, the backpressure of Monolith A and Monolith B before the grafting/amination step was very similar at 51 bar and 52 bar respectively which demonstrates the reproducibility of the monolith fabrication protocol given that both monoliths were prepared from separate monomer mixtures on different days. The increase in column backpressure after the grafting amination step is consistent with observations by Connolly *et al.* [109] who grafted a GMA-*co*-EDMA monolith with a monomer bearing a quaternary ammonium functional group namely: [2(methacryloyloxy)ethyl] trimethylammonium chloride. In that work the authors observed “electrolyte responsive flow permeability” which manifested as increased backpressure when pumping water through the grafted monolith relative to 2 m*M* sodium benzoate.

The authors reported that pumping 100 % water resulted in expansion of grafted chains into the pore volume of the monolith due to electrostatic repulsion between adjacent positively charged grafted chains. This expansion of the polymer chains resulted in a lower “effective pore volume” which resulted in higher backpressures at a given flow rate.

In the work described in this chapter a similar observation can be made for both monoliths. Although in this work the grafted monomer (GMA) does not bear a charged functional group, subsequent amination via reaction of the epoxy group as shown in Figure 2.7 renders the grafted chains highly positive which resulted in charge repulsion and a reduction in the effective pore volume as illustrated in Figure 2.10. Figure 2.10b shows that the pore volume is reduced which explains the significant increase in column backpressure relative to the ungrafted monolith. Since the initial operating backpressure of both ungrafted monoliths was broadly similar, it is reasonable to expect that both monoliths would have macropores of similar dimensions, but not necessarily the same population of smaller mesopores and micropores which are known to contribute most significantly to monolith surface area. It is possible therefore that differences in mesopore/micropore populations

between the two different monoliths would lead to differences in surface area, resulting in different backpressure increases of different magnitudes after grafting.

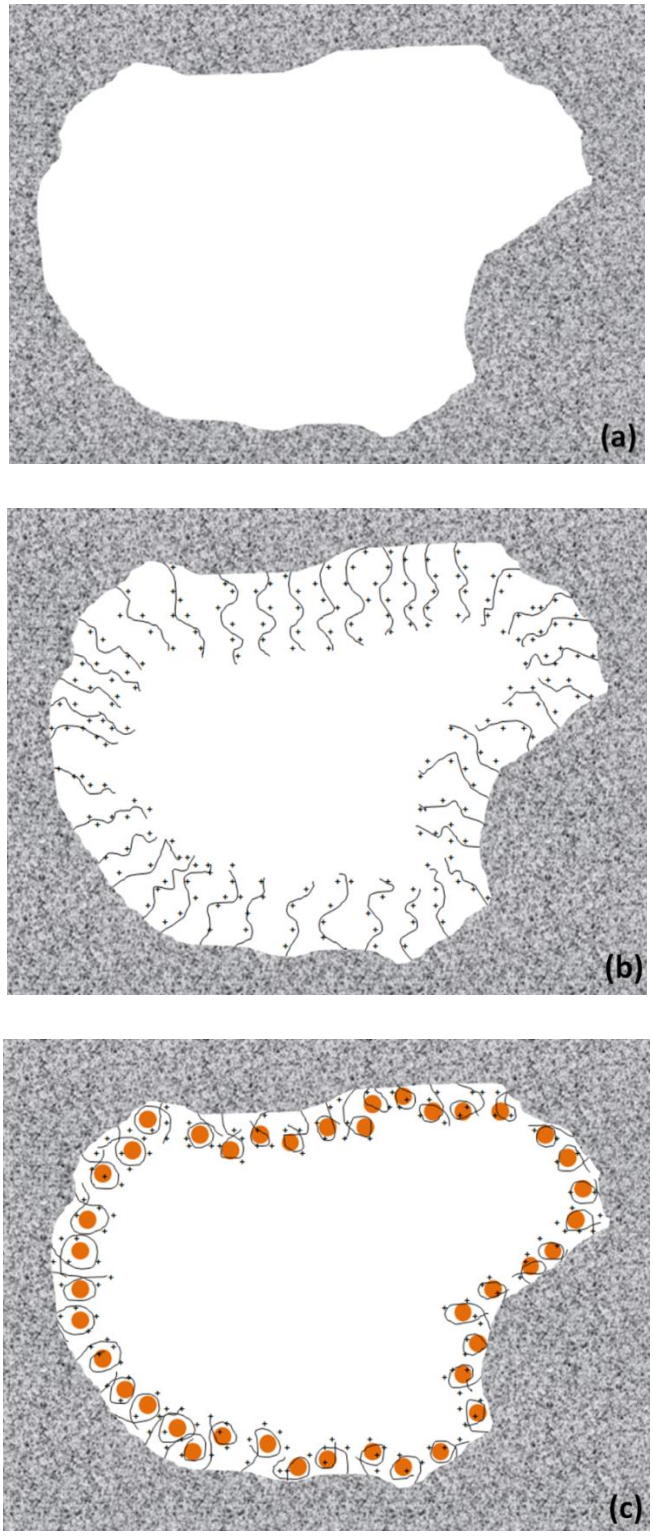

Figure 2.10: *Schematic diagram of a monolith pore (a) before grafting, (b) after grafting and amination and (c) after subsequent immobilisation of iron oxide nanoparticles.*

This was indeed the case since the reported actual % backpressure increase was 155 % for Monolith A and 119 % for Monolith B. Although this increase shows a difference, it must be remembered that the grafting/amination protocol described in this work comprised eight discrete steps, any one of which could be subject to error[1]. Therefore, the difference between the backpressure increase for both monoliths should be viewed in this context.

After immobilisation of iron oxide nanoparticles on both monoliths a significant decrease in backpressure was observed. The nature of the interaction between iron oxide nanoparticles and grafted polymer chains is electrostatic in nature, and it is proposed here that the nature of the nanoparticle attachment is similar to that observed by Dionex Corporation (now Thermo) with their Dionex Propac IMAC-10 stationary phase [110]. The Propac IMAC-10 material is a 10 µm hydrophilic polymer bead to which isolated poly(iminodiacetic acid) grafts are covalently attached. These polymer grafts bearing pendant chelating functional groups extend away from the surface until the stationary phase is charged with metal cations (such as copper). When this occurs, chelation reactions along the polymer graft causes intramolecular chain collapse which results in the polymer chains folding upon themselves to form a bound-metal/polymer “nanoparticle”. This phenomenon is illustrated in Figure 2.11 below. It is proposed that in the work reported in this chapter the positively charged polymer chains are subject to intramolecular chain collapse when the negatively charged iron oxide nanoparticles are introduced into the monolith. The positively charged polymer chains which initially extended out into the pore volume adopt a coiled configuration around the oppositely charged nanoparticles, effectively increasing the pore volume as shown above in Figure 2.10, albeit not to the same extent as in the ungrafted monolith.

[1](1): Immobilisation of benzophenone, (2): washing to remove excess benzophenone, (3): grafting of GMA, (4): washing ungrafted GMA from the monolith, (5): reaction of epoxy groups with diethylamine at 70 ^{o}C,(6): washing to remove unreacted diethylamine, (7): reaction with iodoethane at 80 ^{o}C, (8): washing to remove excess iodoethane.

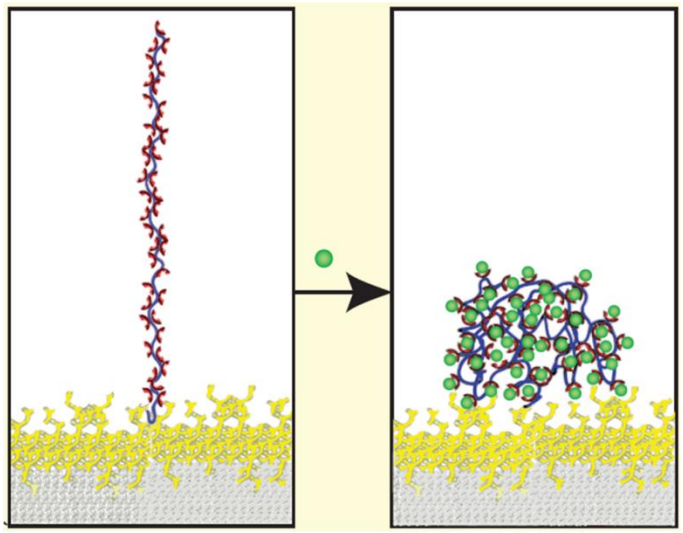

Figure 2.11: *Schematic representation of intramolecular chain collapse of chelating polymer grafts when a Dionex Propac IMAC-10 column is flushed with copper cations (displayed as green circles). Reproduced from [110].*

3.3 Characterisation of nanoparticle-modified monoliths using scanning contactless conductivity measurements

Scanning capacitively coupled contactless conductivity detection (sC^{4}D) was used here as a complementary characterisation technique for the monoliths at specific milestones during their modification with iron oxide nanoparticles. Clearly, backpressure measurements alone are not sufficient for the full characterisation of nanoparticle monoliths. Backpressure measurements only reveals the *total backpressure* of the monolithic column across its entire length. If partial or total blockage of pores had occurred within the column, the only way to verify the axial location of such a blockage would be to measure backpressure and then incrementally cut the monolith shorter and repeat. Obviously this strategy would result in a monolith that could not subsequently be used for chromatographic separations. There exists a reasonable possibility of localised blockages occurring during the various stages of modification (mainly confined to photografting steps or nanoparticle coating steps) and so an alternative characterisation tool was required to evaluate the monoliths. Scanning C^{4}D is ideal in that it offers a completely non-destructive, non-invasive method of characterising a number of monolith quality criteria such as:

- The axial homogeneity of monolith density
- The axial homogeneity of charged bonded functional groups (post-grafting)
- The relative increase/decrease in charge density (before/after grafting)
- The axial homogeneity/distribution of nanoparticles along the monolith length.

Therefore, at the three previously identified stages in monolith fabrication/modification, scanning C^4D profiles were collected in triplicate by threading the capillary monolith through the cell of a commercial C^4D detector head and establishing a continuous flow of water at a nominal flow rate of 1 µL/min. The monolith and connecting tubing was secured to the table alongside a ruler which was used to calibrate the exact axial location of the detector head along the column length. The detector head, being mobile, could readily be manually moved or "scanned" along the column length at millimetre increments and the conductive response of the stationary phase was recorded at each millimetre location for the purposes of plotting the data. The conductive response itself is actually a function of a number of parameters. Firstly, the conductivity of the buffer flowing through the monolith contributes to the overall response and so water was selected instead of a buffer in order to minimise this contribution (and thus maximise the conductive contribution of other monolith parameters). It should be noted that in this work, a buffer was also not necessary since the polymer monolith, once modified with quaternary ammonium groups bears a positive charge across the entire working pH range. The second contribution is from the size of the "virtual electrode area" [111] which itself is function of the capillary diameter (constant in this work at 100 µm) and the monolith pore volume. As described in Chapter 1Section 1.7.2, localised non homogeneity in monolith density result in higher response for less dense regions of the monolith (i.e: larger pore size) and a lower response for more dense regions of the monolith (i.e: smaller pore size). The final contribution to the detector response is the presence of charged functional groups on the polymer monolith, either semi-permanently coated [78] or covalently attached functional groups as in this work.

Figure 2.12 shows an overlay of scanning C^4D profiles (each collected in triplicate) of Monolith A at the three key stages in monolith fabrication. Figure 2.12a shows the conductive response after fabrication of the base monolith (before grafting/amination steps). The average response was 80 mV and the straight line

response clearly shows that the monolith density (and thus average pore size) was homogeneous along the entire monolith length. There was no indication of localised gross voids or specific regions of higher monolith density which would have manifested as increases or decreases in response at the particular fault site respectively. Profile (b) is the conductive response of the monolith after the grafting/amination process and shows a clear increase in average conductive response to 1240 mV.

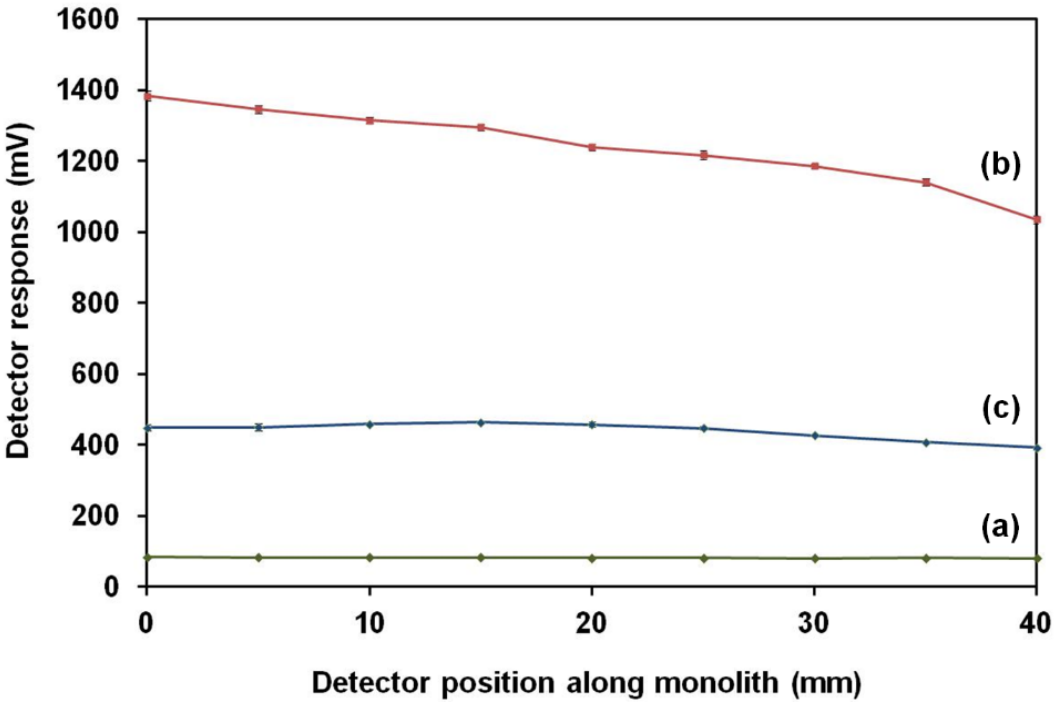

Figure 2.12: *Overlay of scanning C^4D profiles of Monolith A before grafting/amination (a), after grafting/amination (b) and after nanoparticle immobilisation (c).*

An increase in conductive response is entirely expected since the base monolith bears no ionisable functional groups whereas the functionalised monolith bears strong anion exchange functional groups. Interestingly there is a noticeable gradient of conductive response along the column length from 1384 mV at one end (left) to 1035 mV at the other end (right), which represents a 25 % decrease in response. Gradients of conductive response have been reported before by Currivan *et al.* [112] and were the product of intentional bias in incident UV energy during photografting steps across different regions of the column. In this work, since each

C^4D profile was measured in triplicate (error bars are included, but are too small to see), one can be reasonably confident that the drop-off in response is real and permanent along the column length. The advantage of scanning C^4D is clear in identifying exact locations along the column length where graft density (and thus ion-exchange capacity) differs from the remainder of the column, without the necessity to cut the column for elemental analysis or otherwise damage the column.

After immobilisation of iron oxide nanoparticles via electrostatic attraction, the overall conductive response fell along the column length and is shown as Profile (c) in Figure 2.12. It is presumed that the measured conductive response decreased due to interactions of the relatively large negatively charged nanoparticles with multiple positively charged polymer grafts in order to maintain charge balance at the stationary phase surface.

The scanning C^4D experiment was repeated for Monolith B and the results are shown in Figure 2.13. The conductive response increased from an average of 86 mV (Profile a) to 1549 mV (Profile b) as expected.

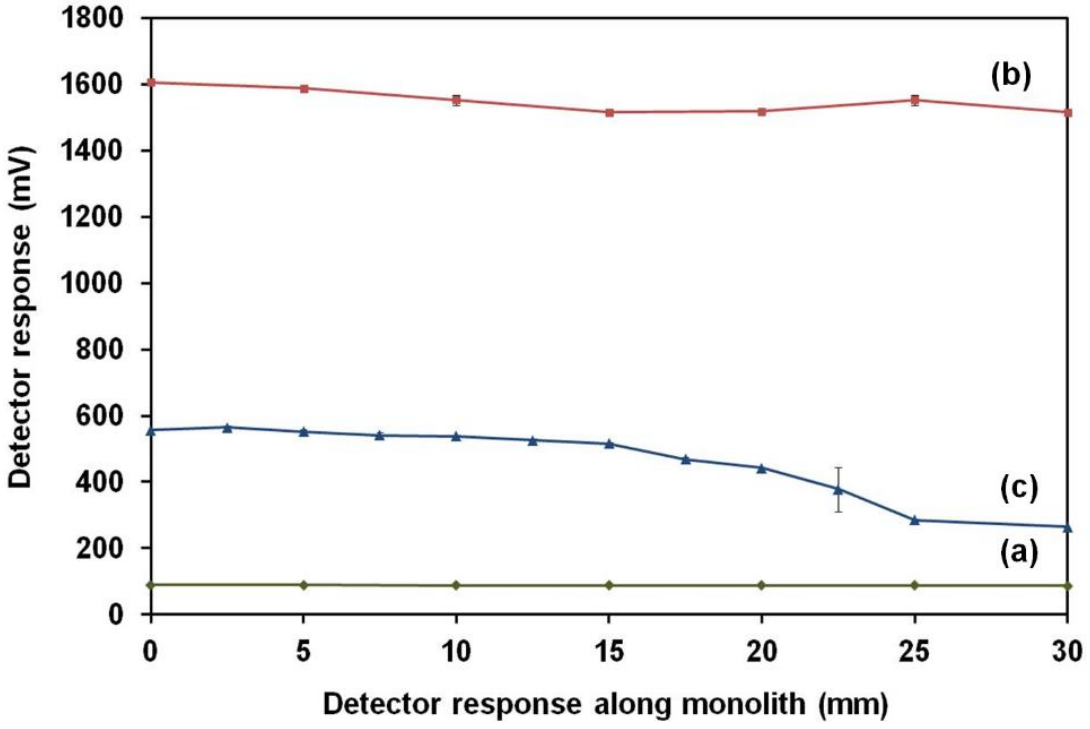

Figure 2.13: *Overlay of scanning C^4D profiles of Monolith B before grafting/amination (a), after grafting/amination (b) and after nanoparticle immobilisation (c).*

Again, the conductive response decreased upon immobilisation of iron oxide nanoparticles (Profile c). In this case however, the homogeneity of nanoparticle coverage appears to be different for Monolith B relative to Monolith A as evidenced by the drop-off in response in the final third of the column length. Since nanoparticle immobilisation lead directly to a decrease in conductive response, it follows that nanoparticle density at the surface may be higher on the second half of the column relative to the first half of the column. While this would require further future studies to validate, the preliminary results here are nevertheless in broad agreement with observations recently published by Currivan *et al.*[113] who recently used scanning C^4D to evaluate the coverage of gold nanoparticles upon polymer monoliths. They reported a consistent decrease in conductive response upon an aminated monolith in regions of the monolith where citrate-stabilised gold nanoparticles were subsequently immobilised.

For the sake of further clarity, the backpressure profile and scanning C^4D profiles are grouped together in Figure 2.14 below, illustrating the increase in backpressure and conductive response for both monoliths upon grafting/amination (green arrows) and the subsequent decrease in backpressure and conductive response after immobilisation of nanoparticles (red arrows).

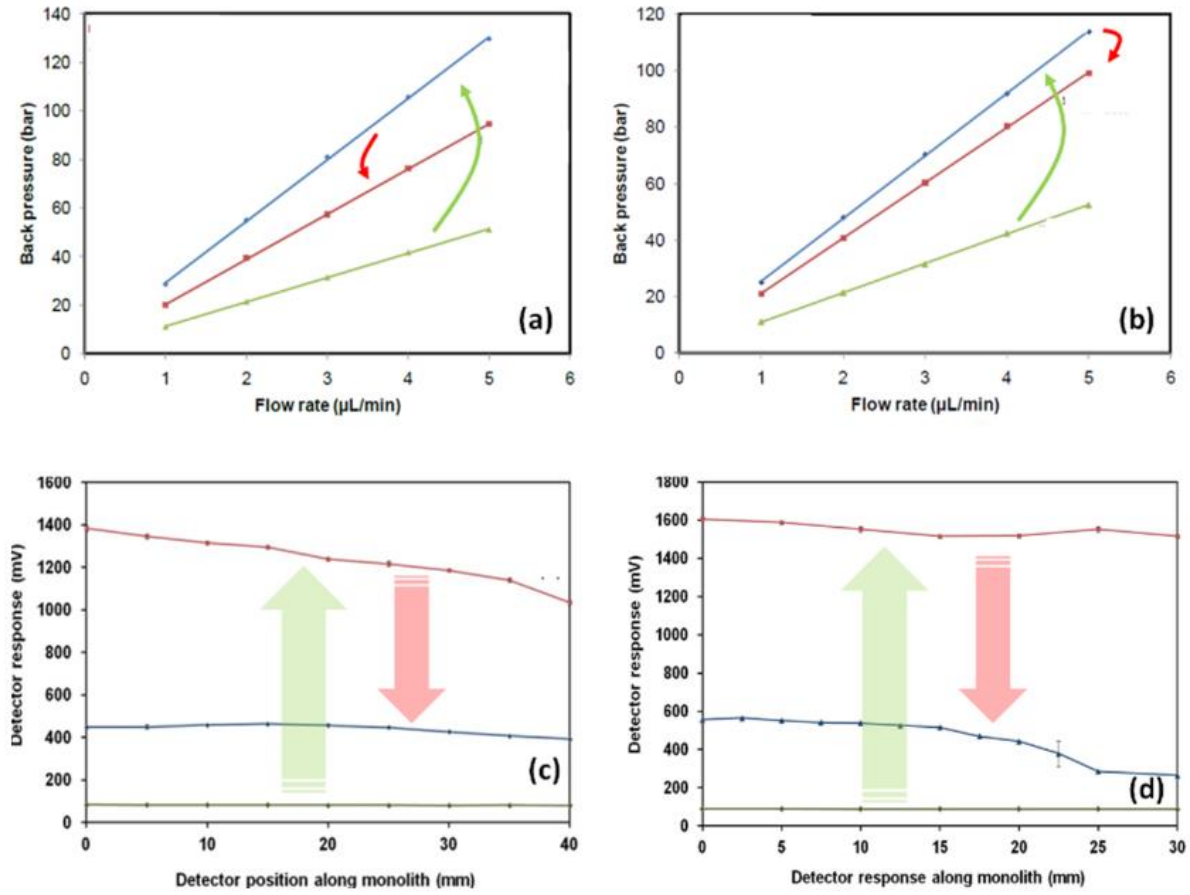

Figure 2.14: *Backpressure profiles and scanning C^4D profiles for Monolith A (a,c) and Monolith B (b,d).*

3.4 Characterisation of nanoparticle-modified monoliths using field emission scanning electron microscopy.

The monoliths characterised in Section 3.2 and 3.3 above were further subjected to Fe-SEM analysis in order to visualise the distribution of nanoparticles across the surface of the monolith. The resulting Fe-SEM images are presented in Figure 2.15 below. Figure 2.15 (a) and (b) show a blank monolith which was not modified with nanoparticles. The monolith completely filled the capillary with no obvious signs of gross voids being present and with the monolith securely attached to the inner capillary walls. The monolith globules in Figure 2.15(b) have a characteristically smooth surface typical of polymer monoliths which are known to have a low surface area.

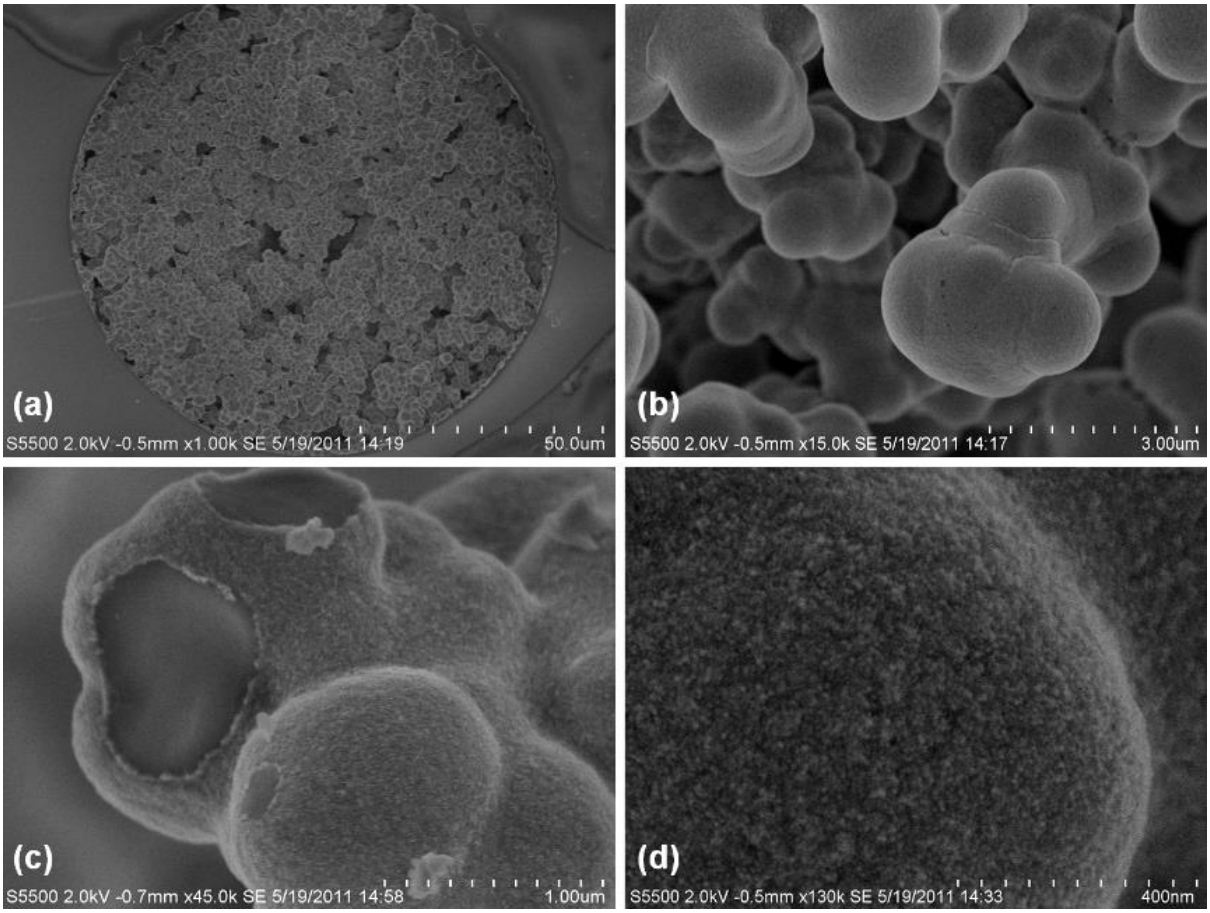

Figure 2.15: *Fe-SEM images of the base monolith at 1,000 and 15,000 magnification (a,b) and the same monolith after nanoparticle attachment at 45,000 and 130,000 magnification (c,d).*

In contrast, Figure 2.15 (c-d) shows the significantly roughened surface of a monolith coated with iron oxide nanoparticles. Figure 2.15(c) in particular shows a region of monolith which has been damaged during sample preparation (which involves cross-sectioning of the monolith) in which a monolith globule has been sheared off, revealing a the cut face which illustrates the nature of the homogeneous surface coating of nanoparticles relative to the bare sliced region of monolith. Figure 2.15 (d) shows a magnified region of monolith in which the nanoparticle coating is readily identifiable as a homogeneous layer of individual nanoparticle clusters which appear as white features against a dark background. Figure 2.16 (a) and (b) also show the same monolith at similar magnification which further demonstrates the dense coverage of nanoparticles which can tentatively be identified as individual closely spaced particles (Figure 2.16b). Again, this region of monolith was

specifically selected for presentation since fortuitously a small region of nanoparticle coating has been removed during the sample preparation process, revealing the underlying (uncoated) monolith which appears as a black area in the centre of each image.

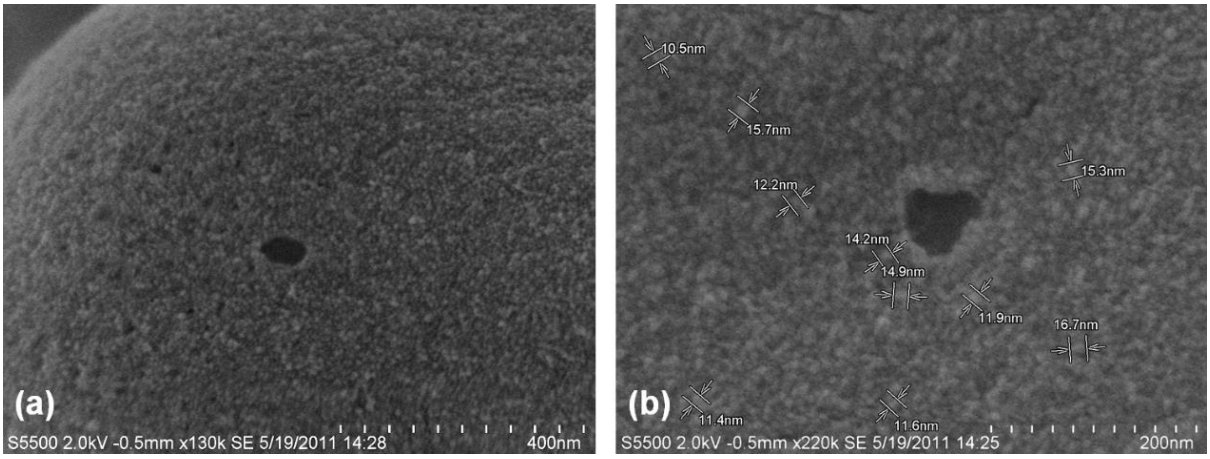

Figure 2.16: *Fe-SEM images illustrating the dense coverage of iron oxide nanoparticles.*

3.5 Separation of phosphorylated compounds (nucleotides) on an iron oxide nanoparticle modified polymer monolith.

Finally, a selected iron oxide modified monolith (Monolith B) was investigated for the separation of a mixture of nucleotides using a phosphate buffer gradient. As previously stated, it is known that phosphorylated compounds interact strongly with iron oxide surfaces via Lewis acid/base interactions which can be disrupted using a phosphate buffer due to mass action effects. It was therefore anticipated that selected nucleotides would elute in order of increasing phosphorylation using a mobile phase gradient of increasing phosphate buffer. Adenosine monophosphate (AMP), adenosine diphosphate (ADP) and adenosine triphosphate (ATP) were selected as test nucleotides and adenosine was also included in the test mix to verify the nature of the retention mechanism. Using a constant concentration of acetonitrile (20 %) in both mobile phase A and B, a phosphate gradient up to 200 mM was ran at 2 µL/min as shown in Figure 2.17. As expected, adenosine eluted first since it is not phosphorylated and is expected to have the weakest retention on the modified stationary phase. The peak shape of adenosine is quite broad relative to the other

peaks in the chromatogram. This is due to the fact that adenosine is not phosphorylated and so is retained only due to hydrophobic interactions (presumably the underlying monolith retains some of its hydrophobic character despite all of the subsequent grafting/nanoparticle attachment steps). Since the acetonitrile content in mobile phase A and mobile phase B is constant at 20 % v/v, then during the "gradient", the adenosine is eluted isocratically by a reversed phase mechanism. Isocratic elution of small molecules on polymer monoliths is known to result in relatively poor chromatographic efficiency. Conversely, the nucleotides eluted in order of AMP, ADP and ATP due to the increasing strength of interaction with the stationary phase. (Note: all three nucleotides eluted within 5 minutes and so the gradient from 5 minutes to 10 minutes was used to restore the original gradient conditions). Although this separation represents a preliminary chromatographic characterisation of this novel stationary phase, it nevertheless demonstrates that a polymer monolith can readily be modified with iron oxide nanoparticles for applications in capillary metal oxide affinity chromatography"

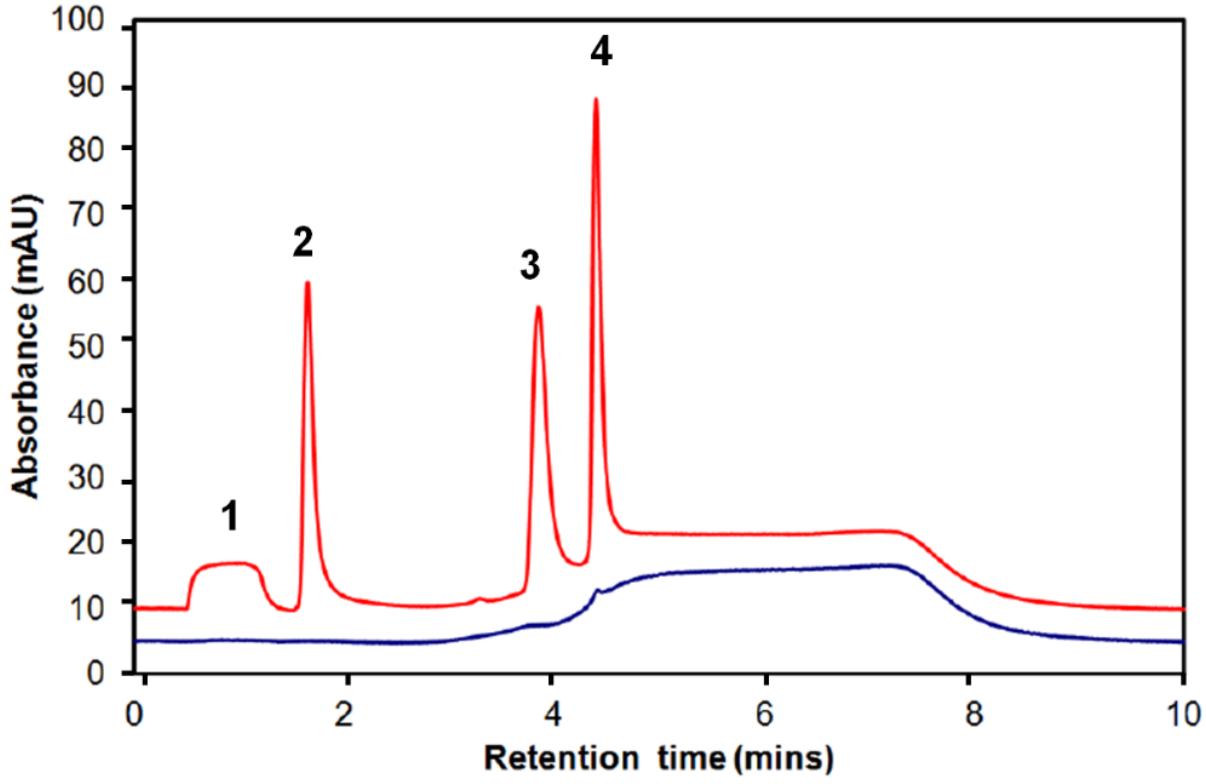

Figure 2.17: *Gradient separation of nucleotides on an iron oxide nanoparticle modified monolith. Gradient: Mobile phase A: 20 % CH_3CN/ 80 % water and Mobile phase B: 20 % CH_3CN/ 80 % 500 mM K_3PO_4 buffer, 0-1.6 mins 5-20% B, 1.61-5.00*

mins 50 B %, 5.1-10 mins 5 % B, Flow rate 2 µl/min. Detection at 214 nm. Injection volume: 100 nL. Peak assignments: (1): adenosine, (2): AMP, (3): ADP, (4): ATP.

4. Conclusions

In this chapter we have successfully demonstrated the fabrication of porous polymer monoliths in fused silica capillary and functionalised the polymer surface with quaternary ammonium functional groups using a two-step grafting protocol. Iron oxide nanoparticles prepared using a co-precipitation of iron salts were readily immobilised via electrostatic interactions. In this work, there was no evidence of nanoparticle detachment from the surface over time which is presumably due to the very stable nature of their attachement via multi-point interactions with the surface. Backpressure measurements revealed an increase in backpressure after grafting which subsequently decreased upon immobilisation of the nanoparticles which clearly indicates that the nanoparticles were attached via interactions with the grafted polymer chains on the monolith surface. Scanning C^4D characterisation also corroborated these findings since an increase in conductive response was observed after aminating the surface, which subsequently decreased upon attachment of nanoparticles. Although the coverage of nanoparticles could be easily visualised along the column length when using transparent fused silica capillary housings (the stationary phase turned pale brown along the column length), only scanning C^4D methods would be able to evaluate the axial coverage of nanoparticles if a non-transparent column housing had been used (such as polyimide coated capillary or PEEK). Finally, this work represents the first time that a high efficiency chromatographic separation has been achieved on a iron oxide nanoparticle-modified monolith for *small molecules*, using metal oxide affinity retention mechanisms.

Chapter 3: Development of an iron-oxide nanoparticle modified silica monolith in spin column format for enrichment of phosphorylated compounds.

1. Introduction

Silica monoliths are characterised by a bimodal pore structure comprising of macropores (1-2 µm) and mesopores (~13 nm). The macropores allow fluid flow through the monolith at significantly lower backpressures relative to a packed bed whereas the mesopores contribute to the high surface area (typically up to 300 m^2/g) that silica monoliths are known for. Silica monoliths can be chemically modified with organosilanes resulting in a wide range of selectivities (reversed phase, HILIC, chiral) depending on the nature of the silane reagent.

Several reports have however appeared in the literature describing alternative methods for modification of silica monoliths, namely with selected nanoparticles. The first report of a nanoparticle-modified silica monolith was in 2006 when Hutchinson *et al.* immobilised 70 nm quaternary ammonium anion-exchange latex nanoparticles upon a silica monolith in fused silica capillary by electrostatic attractive forces [114]. The capacity of a 50 µm diameter 25 cm latex-coated monolith was found to be 0.342 nanoequivalents and 80,000 plates per column could be achieved for the separation of weakly retained anions using capillary electrochromatography. Later in 2007, Glenn *et al.* coated a bare silica monolith (4.6 mm X 100 mm) with Dionex AS9-HC latex nanoparticles and examined the resulting nano-structured monolith for the anion-exchange separation of common inorganic anions [115].Again the nanoparticles were immobilised by simple electrostatic interactions and the selectivity, efficiency and stability of the stationary phase was directly compared with a monolith semi-permanently coated with didodecyldimethylammonium bromide. The latex-coated monolith was demonstrated to exhibit 50% higher efficiency relative to the surfactant-coated monolith, with retention decreasing by only 1 % over several months of periodic use.

Ibrahim *et al.* used a quaternary ammonium latex-coated silica monolith in HILIC mode for the separation of benzoates, nucleotides and amino acids [116]. Using an elevated flow rate of 10 mL/min on the 100 x 4.6 mm monolith, a separation of naphthalene, uracil and cytosine was possible within only 15 seconds

with a mobile phase containing up to 85 % acetonitrile. More recently in 2012 the same research group demonstrated the separation of small organic and inorganic ions via a mixed mode HILIC/anion exchange mechanism on a silica monolith coated with either Dionex AS9-SC, Dionex AS12A or Dionex DNA pac latex [117]. The authors proposed that the introduction of the latex on the silica surface increased the thickness of the water layer on the monolith by 8-10 times enabling retention when high percentages of acetonitrile were used as mobile phase. To our knowledge, the only report of a metal oxide nanoparticle immobilised upon a silica monolith was published by Sun *et al.* in 2012 [118]. The authors integrated cerium oxide nanoparticles into a silica monolith for the selective removal of arsenic from water in a flow through reactor. This was achieved by impregnating silica monoliths with a cerium nitrate solution and then drying at 60 ^{o}C for 12 hours followed by calcination at 450 ^{o}C. Figure 3.1 illustrates the coverage of nanoparticles that was possible using this method.

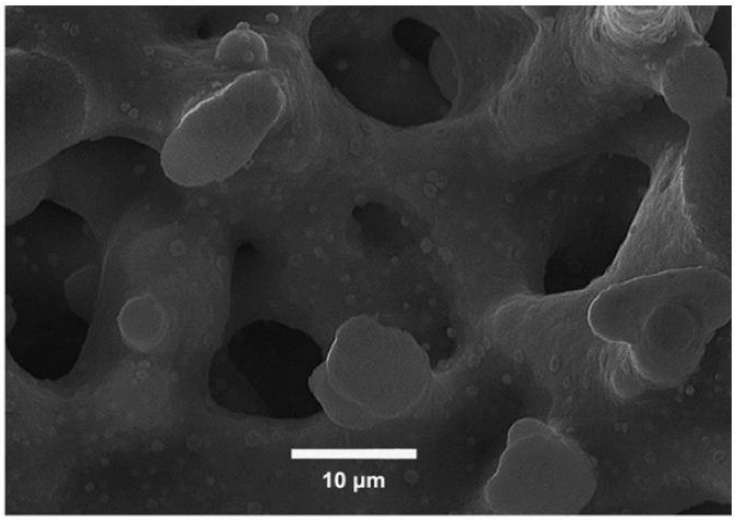

Figure 3.1: *Silica monolith modified by cerium oxide nanoparticles. Reproduced from [118].*

This chapter describes the immobilisation of iron oxide nanoparticles upon a commercial silica monolith in a centrifugal spin column format. The coverage of the nanoparticles is optimised using a layer-by-layer approach and scanning electron microscopy and EDX is used to evaluate the coverage achieved. Finally, the application of the monolith for the extraction of phosphorylated compounds is demonstrated.

2. Experimental.

2.1 Reagents and materials.

Iron (II) chloride heptahydrate (≥ 99.0 %), iron (III) chloride hexahydrate, citric acid (99 %), ammonium hydroxide (28 % NH_3 in water, ≥ 99.99 %), sodium hydroxide, monobasic sodium phosphate, dibasic sodium phosphate, hydrochloric acid, acetone, poly(diallyldimethylammonium) chloride solution (10 wt% in H_2O, PDAMAC), tetrabutylammonium phosphate monobasic solution (TBAP), α-casein from bovine milk, trypsin from bovine pancreas, urea, ammonium bicarbonate, dithiothreitol (DTT), trifluoroacetic acid (TFA), iodoacetamide, formic acid, potassium chloride, adenosine, adenosine monophosphate (AMP), adenosine diphosphate (ADP), adenosine-5-triphosphate (ATP) and potassium phosphate were purchased from Sigma Aldrich (Gillingham, UK). HPLC grade acetonitrile and methanol were purchased from Labscan (Stillorgan, Dublin, Ireland). Deionised water was provided by a MilliQ Direct Q5 water purification system from Millipore (Millipore, Bedford, MA, USA).MonoSpin NH_2 spin columns were supplied by Carl Stuart Limited (Carl Stuart Limited, Tallaght, Dublin, Ireland)

2.2 Instrumentation.

All instrumentation was used as described in Chapter 2 with the following additions. HPLC was performed using an Agilent 1200 Series LC system (Agilent Technologies, Santa Clara, CA, USA). For the separation of nucleotides, the column used was a 4.6 mm × 75 mm Waters Symmetry C_{18}, 3.5 µm particle size, 100 Å pore size. For the separation of nucleotides, mobile phase A was 5 m*M* TBAP (pH 7.0) in 5 % ACN and mobile phase B was 5 mM TBAP (pH 7.0) in 80 % ACN. The gradient programme was as follows: 0-5 mins: 0 % B, 5-15 mins: 0-50 % B, 15-20 mins: 50 % B, 20.0-20.5 mins: 50-0 % B and 20.5-30 mins: 0 % B. The flow rate used was 0.4 mL/min, column temperature was 40 ^{o}C, detection wavelength was 254 nm and the injection volume was 40 µL. For the separation of peptides, the column used was a 3.0 mm x 100 mm Phenomenex Onyx monolithic C_{18} silica column. Mobile phase A was 0.01 % TFA in water and mobile phase B was 0.08 % TFA in ACN. The gradient programme was as follows: 0-45 mins: 5 % to 100 % B, 45-45.1 mins: 100-5 % B, 45.1-55 mins: 5 % B. The flow rate used was 0.4 mL/min, column temperature was 40 ^{o}C, detection wavelength was 214 nm and the injection volume was 10 µL. Stock

standards of adenosine, AMP, ADP and ATP were prepared in water and diluted as appropriate.

2.3 Immobilisation of Fe_3O_4 nanoparticles on SPE silica monoliths

Fe_3O_4 nanoparticles prepared as described in Chapter 2, Section 2.2.6were diluted fivefold in deionised water which had been filtered using a 0.5 µm syringe filter. A volume of 1 mL of Fe_3O_4nanoparticles was flushed through a MonoSpin column for 4 minutes at 6000 rpm using a centrifuge followed by a water wash. This process was repeated with further 1 mL aliquots until the colour of the monolith turned brown and effluent was the same colour as the original suspension, indicating saturation of the monolith with nanoparticles. Alternatively, a layer-by-layer approach was adopted in which 1 mL of nanoparticle suspension was passed through the monolith followed by a water rinse followed by 1 mL of 0.2 m*M* PDAMAC. The Fe_3O_4 nanoparticle/PDAMAC flushing sequence was repeated a further three times, resulting in a total of four layers of nanoparticles upon the silica surface.

2.4 Preparation of tryptic digests

1,000 µL of α-casein (10 mg/mL) prepared in 6 *M* urea/100 m*M* ammonium bicarbonate was incubated with 50 µL of 1 *M* DTT (in 100 m*M* ammonium bicarbonate) at 56 ºC for 60 minutes using a water bath. Iodoacetamide (200 µL, 55 m*M*) was added and the mixture vortexed and incubated at room temperature in darkness for 1 hour. DTT was added (200 µL) to consume any unreacted iodoacetamide and the solution stored in darkness at room temperature for 30 minutes followed by dilution with 7.75 mL of 100 m*M* ammonium bicarbonate. Trypsin was prepared at 1 mg/mL in 1 m*M* HCl, 200 m*M* $CaCl_2$ and 20 µL added and the mixture vortexed and incubated at 37 ºC overnight. The reaction was stopped by adjusting the pH to pH 2.5 using 10 % TFA.

3. Results and discussion.

3.1 Immobilisation of Fe_3O_4 nanoparticles on aminated monolithic spin columns.

MonoSpin products marketed by GL Sciences [119] are centrifugal spin columns for sample preparation which can be operated in any commercial bench-top

centrifuge. Figure 3.2 illustrates a commercially available MonoSpin cartridge housing and a schematic of the monolithic silica bed within.

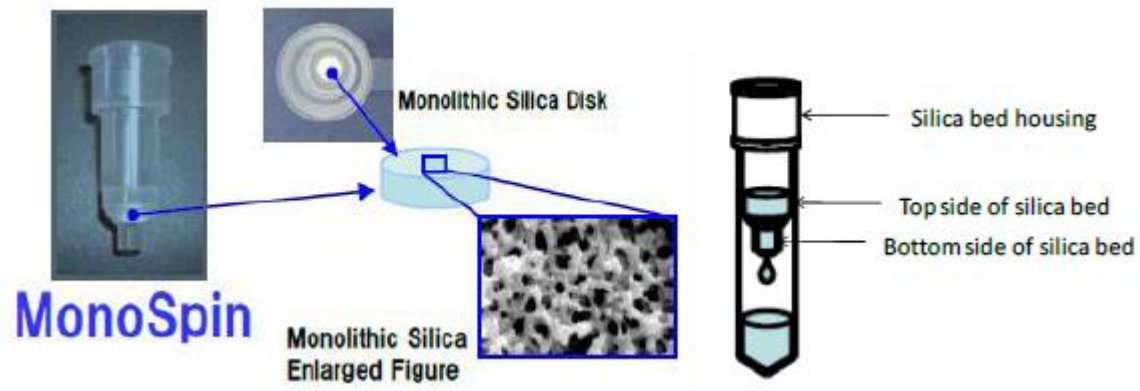

Figure 3.2: *Schematic diagram of a MonoSpin cartridge assembly [119].*

The cartridge comprises a monolithic disk (modified with various chemistries) which is located at the bottom of a ~1,000 µL well into which samples are loaded. In common with all silica monoliths, the monolith is characterised by large macropores (approx 2 µm to 5 µm) through which liquids can readily flow when a pressure (in this case centrifugal) is applied. The monolith also has mesopores (2 nm to 50 nm) which contribute to the high surface areas of the monolith and thus the high binding capacity. The entire device (equipped with a snap-cap lid) is inserted into a second centrifugation tube for recovery of wash buffers or eluted analyte as appropriate. Both tubes, once assembled are then placed in a bench-top centrifuge and spun at 5,000 to 10,000 rpm. Regardless of the specific application, a common conditioning, sample loading and elution protocol is usually followed as shown in Figure 3.3.

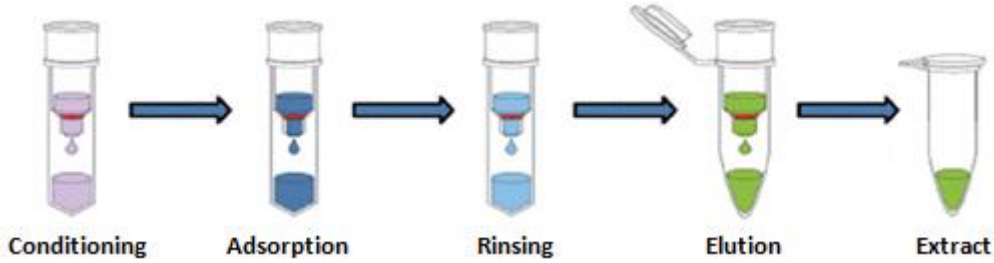

Figure 3.3: *Typical solid phase extraction operating protocol for MonoSpin columns [119].*

MonoSpin columns are commercially available in a wide range of selectivities which include C_{18}, amide, strong and weak anion exchange, strong and weak cation

exchange, phenylboronic acid (for extraction of compounds with cis-diol groups) and titanium dioxide (for extraction of phosphorylated compounds). MonoSpin columns with immobilised Protein A or Protein G are also available for extraction of immunoglobulins and MonoSpin columns with immobilised trypsin are available for rapid centrifugal enzymatic digestion [119].

In the work presented in this chapter, iron oxide nanoparticles were immobilised upon MonoSpin cartridges in an effort to offer alternative selectivity relative to titanium dioxide (TiO_2) MonoSpin cartridges for the extraction of selected phosphorylated compounds. Two alternative strategies were trialled in this work for the immobilisation and compared directly in terms of the surface density of the resulting nanoparticles. The first and simplest strategy involved direct attachment to the monolith surface. It is known that negatively charged citrate-stabilised Fe_3O_4 nanoparticles can be electrostatically attached to surfaces which bear amino groups and therefore in this work, aminated MonoSpin cartridges were employed. A schematic diagram of this protocol is shown in Figure 3.4 below.

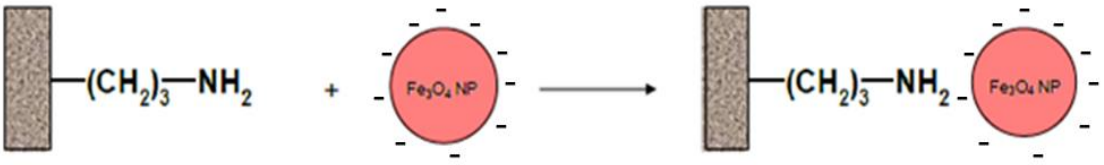

Figure 3.4: *Schematic diagram of direct electrostatic attachment of Fe_3O_4 nanoparticles to an aminated silica monolith.*

By flushing a 1:5 dilution of the prepared nanoparticles through the monolith (in multiple consecutive 1,000 µL aliquots) the progress of the immobilisation could be readily monitored by observing a gradual colour change of the silica monolith bed from white to tan as shown in Figure 3.5.

Figure 3.5: *Digital photograph (looking down the sample well) of a blank (left) and an aminated silica monolith after coating with citrate-stabilised Fe_3O_4 nanoparticles (right).*

In addition, the effluent emerged as a colourless solution, clearly indicating the retention of the nanoparticles upon the monolith. Therefore, nanoparticle flushing steps were discontinued at the point where the colour of the effluent matched that of the original diluted nanoparticle suspension. Coverage of the nanoparticles upon the monolith was evaluated by carefully removing the monolith from its housing and subjecting to FE-SEM analysis. Figure 3.6 shows images of the monolith before (a,b) and after (c,d) immobilisation of nanoparticles. Figure 3.6 (a) shows the blank monolith at relatively low magnification, clearly illustrating the large flow-through macropores which appear to range in size from 2 µm to 6 µm, whereas Figure 3.6 (b) shows the same blank monolith magnified 100,000 times which allows the mesoporous structure to be easily visualised. After immobilisation of the nanoparticles, the permeability of the monolith was not impaired in any way as evidenced by Figure 3.6 (c), showing that the macroporous structure remained intact and that no gross macropore blockages were evident. Finally, Figure 3.6 (d) shows that at high magnification (200,000x) a homogeneous coverage of nanoparticles is clearly visible. The interparticle spacing is presumably due to electrostatic repulsive effects between adjacent negatively charged nanoparticles, placing a finite limit upon the density of coverage that could be achieved.

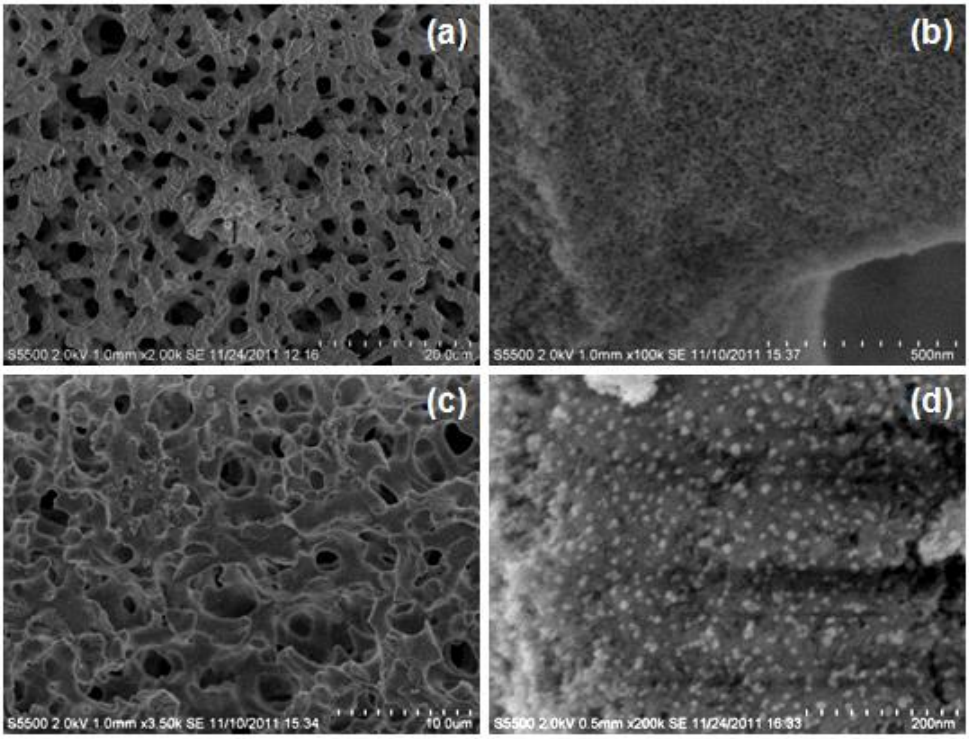

Figure 3.6: *FE-SEM images of an aminated silica MonoSpin with immobilised Fe_3O_4 nanoparticles. (a): blank monolith at 2,000x magnification, (b): blank monolith at 100,000x magnification, (c): Fe_3O_4 nanoparticle-modified monolith at 3,500x magnification and (d): Fe_3O_4 nanoparticle-modified monolith at 200,000x magnification.*

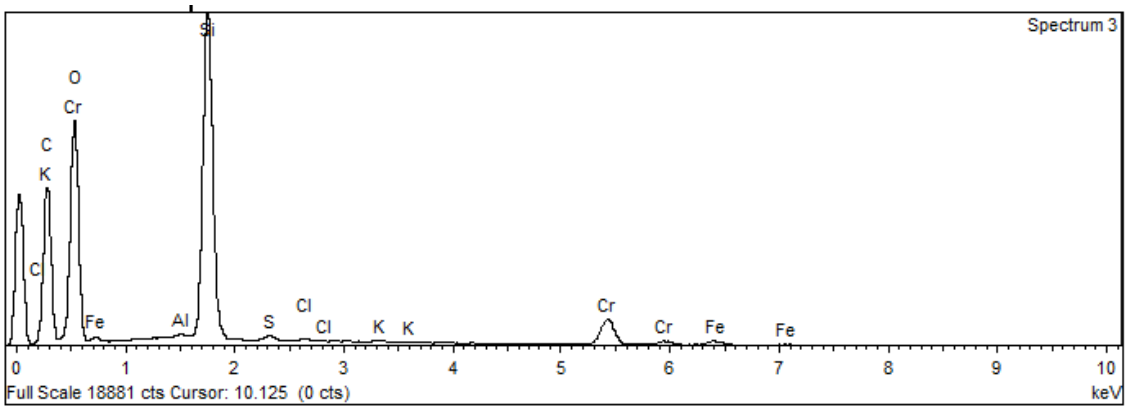

Figure 3.7: *EDX spectrum of an aminated silica MonoSpin with immobilised Fe_3O_4 nanoparticles (single layer coating).*

In order to further verify the presence of Fe_3O_4 nanoparticles, EDX analysis was performed on the sample shown in Figure 3.6 (d) and the results are illustrated in Figure 3.7.A peak for iron is clearly visible at ~ 6.4 keV and ~ 7.1 keV. Additional

signals for silicon (1.7 keV) and oxygen (0.5 keV) are expected due to the nature of the underlying SiO_2 monolithic substrate. Signals for carbon are possibly due to the carbon atoms of the aminopropyl bonded phase, whereas the chromium signal is due to the 30 nm chromium sputter coating used for sample preparation prior to EDX analysis. Mean values (n = 3) for the iron present in the sample was 0.43 +/- 0.30 wt%. Typically, under the operating conditions used in this EDX experiment the penetration depth of the electron beam (approximately 2 µm) was expected to exceed the thickness of a given section of the monolith skeleton, possibly penetrating an underlying macropore due to the non-planar, highly porous nature of the sample as shown in Figure 3.8. Since the nanoparticles were immobilised right at the surface of the monolith skeleton, they are anticipated to contribute relatively weakly to the overall detectable signal and therefore these EDX results should be viewed as semi-quantitative (relative to other elements present) at best.

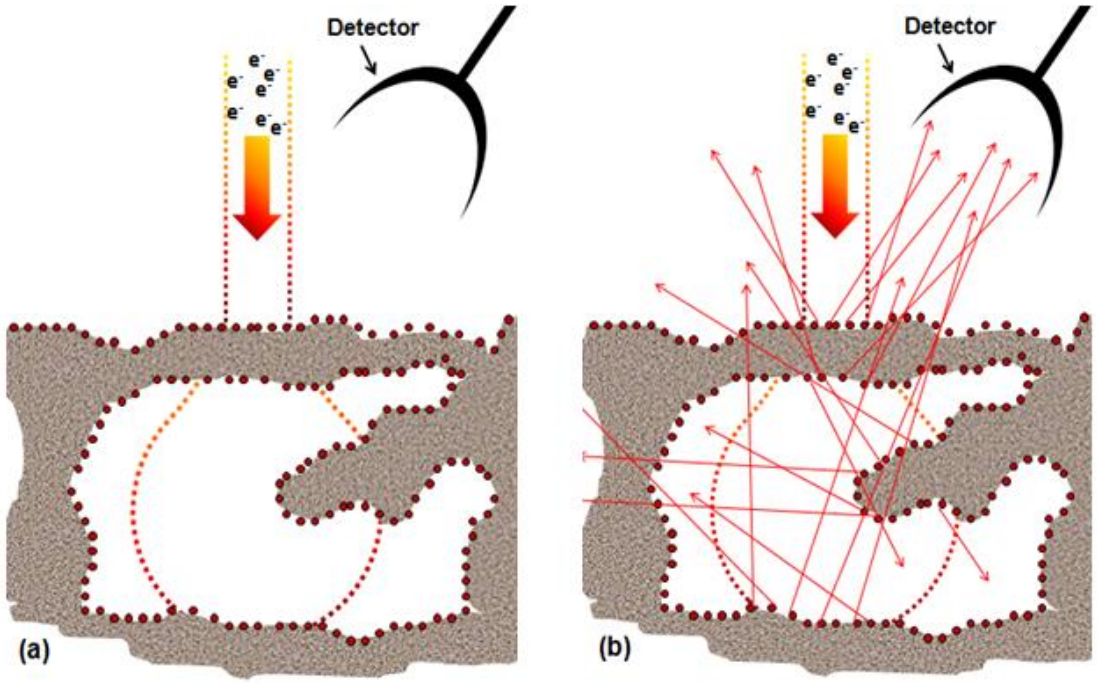

Figure 3.8: *(a) Schematic diagram of proposed penetration depth of electron beam in EDX. Not all immobilised nanoparticles are irradiated by the beam. (b) Not all emitted X-rays reach detector due to due random emission vectors leading to reduced accuracy.*

After characterisation of the above monolith, a second protocol was investigated for comparative purposes involving the use of layer-by-layer methods in an effort to increase nanoparticle coverage as discussed below.

3.2 Immobilisation of Fe_3O_4 nanoparticles on monolithic spin columns using layer-by-layer methods.

Layer-by-Layer (LbL) assembly methods are frequently employed to develop films, coatings and three-dimensional arrays of nanoparticles [120],[121],[122],[123]. In this work, the cationic polyelectrolyte poly(diallyldimethylammonium) chloride was selected based upon its good water solubility and permanent positive charge as shown in Figure 3.9. The protocol involved first depositing a layer of negatively charged Fe_3O_4 nanoparticles upon an aminated monolith as previous discussed in Section 2.3. A solution of poly(diallyldimethylammonium) chloride in water was then flushed through the monolith to coat the surface via electrostatic interactions with the immobilised nanoparticles. This facilitated the immobilisation of a second layer of nanoparticles upon the first, via the intermediate coating of positively charged polymer. As shown schematically in Figure 3.9, up to four layers of nanoparticles could be immobilised in this manner before the monolith appeared to be saturated (as evidenced by brown nanoparticle breakthrough upon subsequent coating attempts).

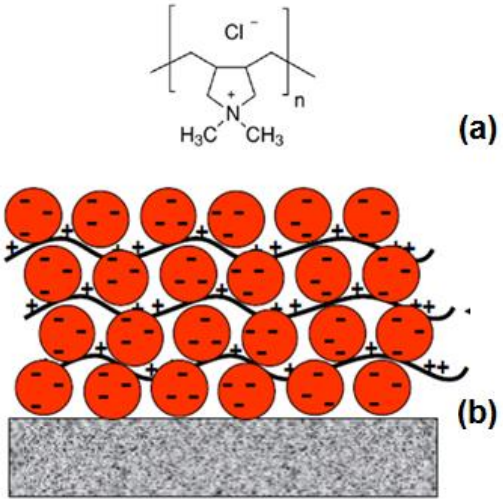

Figure 3.9: *(a): Molecular structure of poly(diallyldimethylammonium) chloride. (b): Schematic representation of layer-by-layer assembly of negatively charged nanoparticles using a positively charged linear polymer.*

The first indication that significantly higher nanoparticle loadings were achieved using the layer-by-layer approach was that much larger volumes (by at least a factor of three) were required to be flushed through the monolith before breakthrough was observed. Subsequent Fe-SEM analysis also indicated a significant increase in nanoparticle loading. A visual comparison of Figure 3.6 and Figure 3.10 (below) reveals that coverage of nanoparticles is very dense and homogeneous relative to the single-layer nanoparticle coating method previously discussed in Section 2.3.

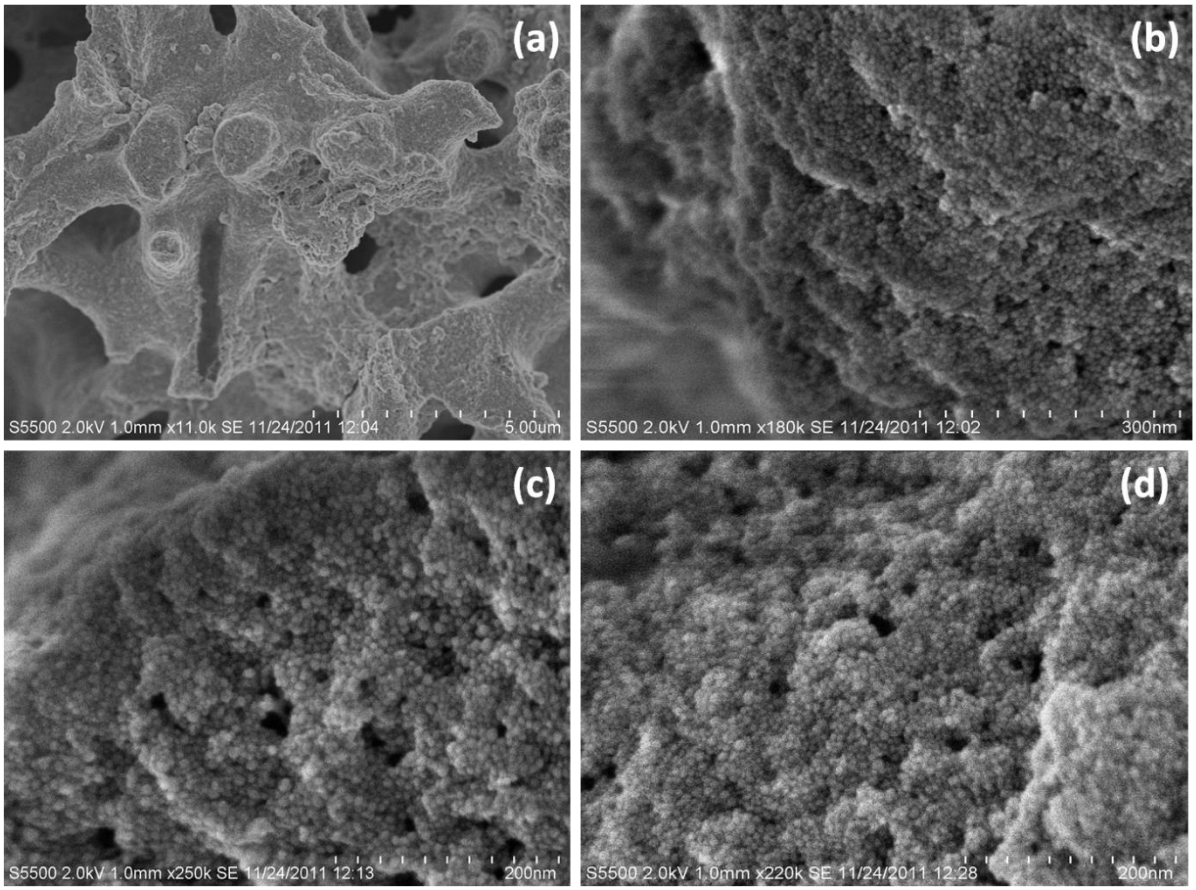

Figure 3.10: *FE-SEM images of a silica monolith modified with Fe_3O_4 nanoparticles using a layer-by-layer approach.(a) 11,000 x magnification, (a) 180,000 x magnification, (a) 250,000 x magnification, (a) 220,000 x magnification.*

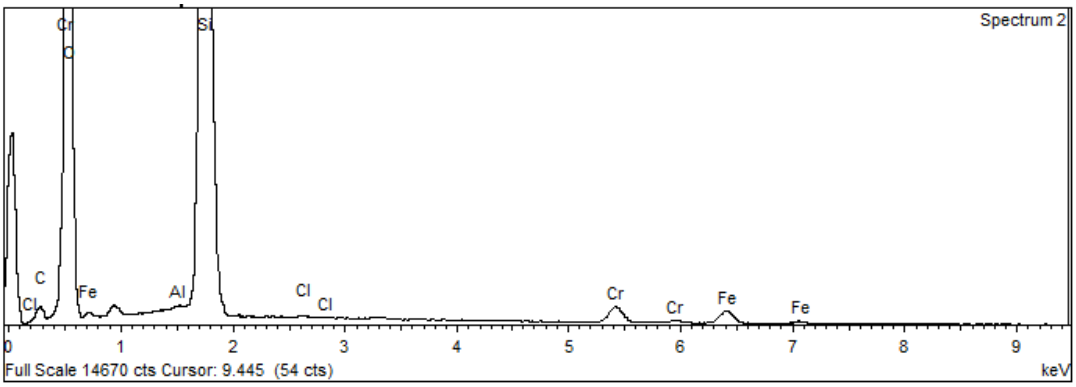

Figure 3.11: *EDX spectrum of an aminated silica MonoSpin with 4 layers of immobilised Fe_3O_4 nanoparticles (layer-by-layer coating).*

Individual nanoparticles are readily identifiable as discrete spheres which appear to cover the entire available surface of the monolith with no underlying silica immediately visible. EDX analysis on the monolith shown in Figure 3.10 was performed and results are shown in Figure 3.11. Again a peak for iron can be seen at ~ 6.4 keV and ~ 7.1 keV, but with this monolith the mean amount of iron (n = 3) was 2.49 ± 0.53 wt %. This increase in iron content represents almost a six fold increase for the layer-by-layer monolith relative to the monolith coated with only a single layer of nanoparticles. The monolith modified using the layer-by-layer approach was chosen for further solid phase extraction applications described below.

3.3 Chromatographic method development and method validation for LC separation of selected nucleotides.

In order to evaluate the selectivity of the nano-structured monolith for phosphorylated compounds, a range of nucleotides, namely adenosine, AMP, ADP and ATP were selected for study. It was anticipated that adenosine would display little or no selectivity for the iron oxide surface during a solid phase extraction protocol since it bears no phosphate groups. Therefore, a liquid chromatographic ion-pair assay was developed for the separation of adenosine, AMP, ADP and ATP using tetrabutylammonium phosphate as ion-pair reagent and a Waters Symmetry C_{18} column. A gradient method was developed, the conditions of which are listed in the Experimental, Section 2.2. Column temperature was also evaluated between 20 ^{o}C and 45 ^{o}C and no change in selectivity or significant change in resolution was

observed. For example, at a column temperature of 20 ^{o}C, resolution between ADP and ATP was 11.8 whereas at 45 ^{o}C resolution had decreased by only 5 % to 11.2. Nevertheless, in an effort to minimise column backpressure, the column temperature was set to 45 ^{o}C for the remainder of this work. The optimised separation of a 5 µ*M* standard of adenosine and the three nucleotides is shown in Figure 3.12.

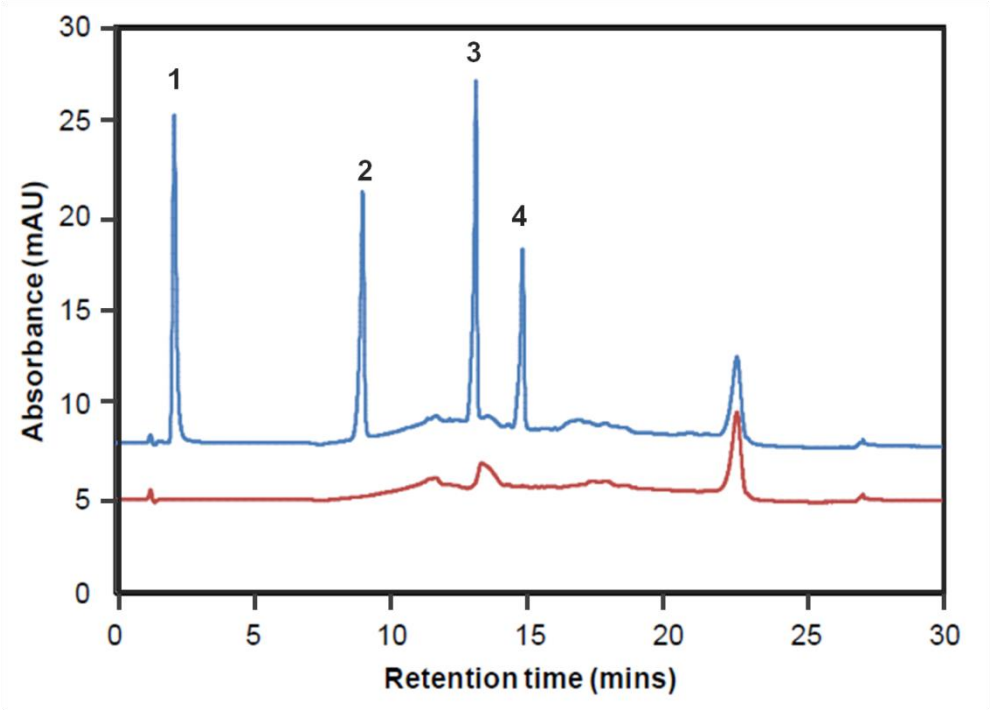

Figure 3.12: *Optimised separation of a 5 µM standard of adenosine, AMP, ADP and ATP overlaid with a blank injection. Chromatographic conditions: Column: 4.6 mm x 75 mm Waters Symmetry C_{18}, 3.5 um, mobile phase A: 5 mM TBAP (pH 7.0) in 5 % ACN, mobile phase B: 5 mM TBAP (pH 7.0) in 80 % ACN. Gradient programme: 0-5 mins: 0 % B, 5-15 mins: 0-50 % B, 15-20 mins: 50 % B, 20.0-20.5 mins: 50-0 % B and 20.5-30 mins: 0 % B. Flow rate: 0.4 mL/min, injection volume: 40 µL, column temperature: 40 ^{o}C, detection wavelength: 254 nm.*

Linearity of the method was determined by injecting (in triplicate) adenosine, AMP, ADP and ATP standards ranging in concentration from 100 n*M* to 250 µ*M* and plotting peak area versus concentration as shown in Figure 3.13 below. The method was linear for all analytes across the concentration range under investigation with R^2 values ≥0.9980.

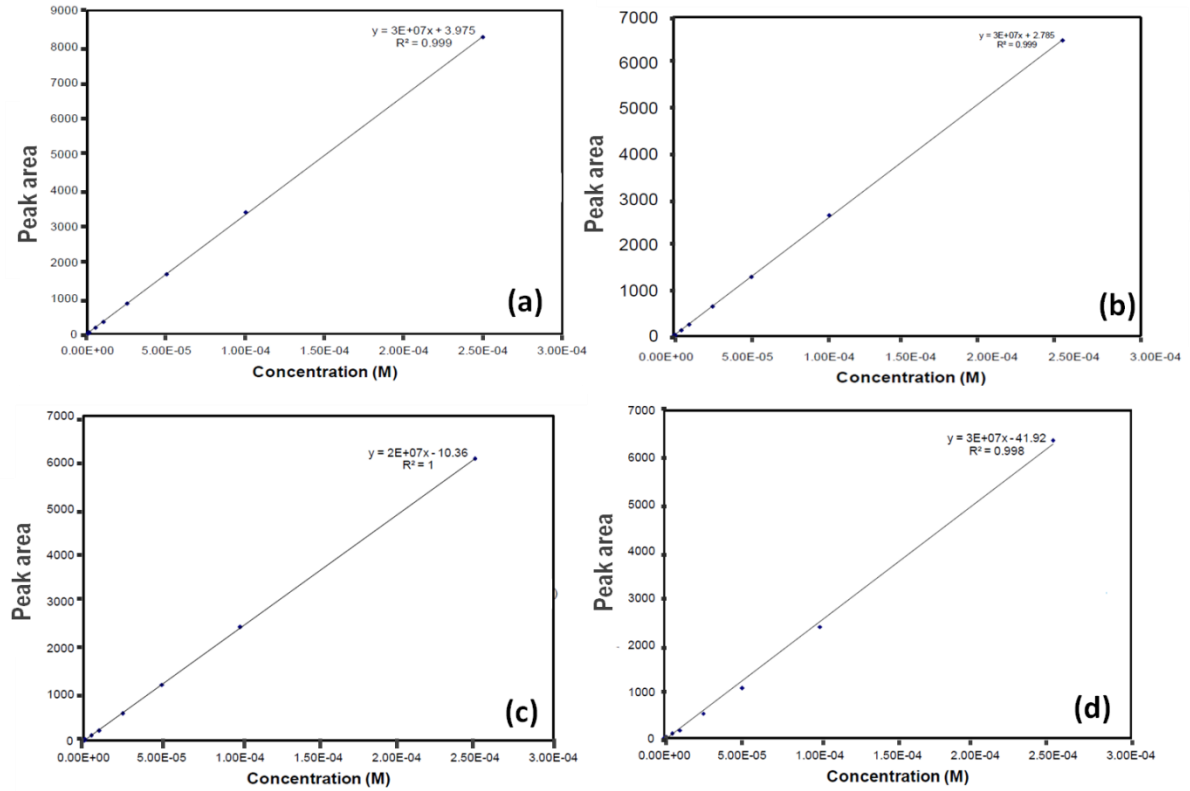

Figure 3.13: *Linearity plots for (a) adenosine, (b) AMP, (c) ADP and (d) ATP. Chromatographic conditions as given in Figure 3.12. Standard concentrations: 100 nM, 250 nM, 500 nM, 1 µM, 5 µM, 10 µM, 25 µM, 50 µM, 100 µM, and 250 µM.*

Concentrations of nucleotides at the low, mid-level and high end of the linear range were used for a precision study; namely 100 n*M*, 1 µ*M* and 50 µ*M*. Six consecutive injections of each standard were made and %RSD was ≤ 0.4 % for retention time and ≤ 0.4 % for peak area at each concentration level (except at 100 n*M*, which was ≤ 3.9 %). Sensitivity (limit of detection, LOD) of the method was taken as the concentration of each analyte which gave a signal to noise ratio of 3, and determined to be 10 n*M* for each analyte. The limit of quantitation (LOQ) was 100 n*M*.

3.4. Trap and release of nucleotides using a MonoSpin cartridge modified with Fe_3O_4 nanoparticles using the layer by layer approach.

After optimisation of the chromatographic conditions, 5 µ*M* mixture of adenosine, AMP, ADP and ATP was used to evaluate the MonoSpin cartridge immobilised with Fe_3O_4 nanoparticles via the LbL approach. The extraction protocol is shown schematically in Figure 3.3 and involved four discrete steps. After conditioning of the monolith with water, 800 µL of standard was passed through the

monolith by centrifugation at 6,000 r.p.m and the eluate("flow-through") retained for analysis. The monolith was then washed with 800 µL of 50 % acetonitrile followed by 800 µL water. Finally, the retained nucleotides were eluted with 800 µL of 25 m*M* phosphate buffer (pH 6.86) and the collected fraction retained for analysis. The extraction protocol was also repeated on a blank monolith which had not been modified with Fe_3O_4 nanoparticles for comparative purposes. Figure 3.14 shows an overlay of the "flow-through" fraction from a blank MonoSpin and a Fe_3O_4 nanoparticle-modified MonoSpin.

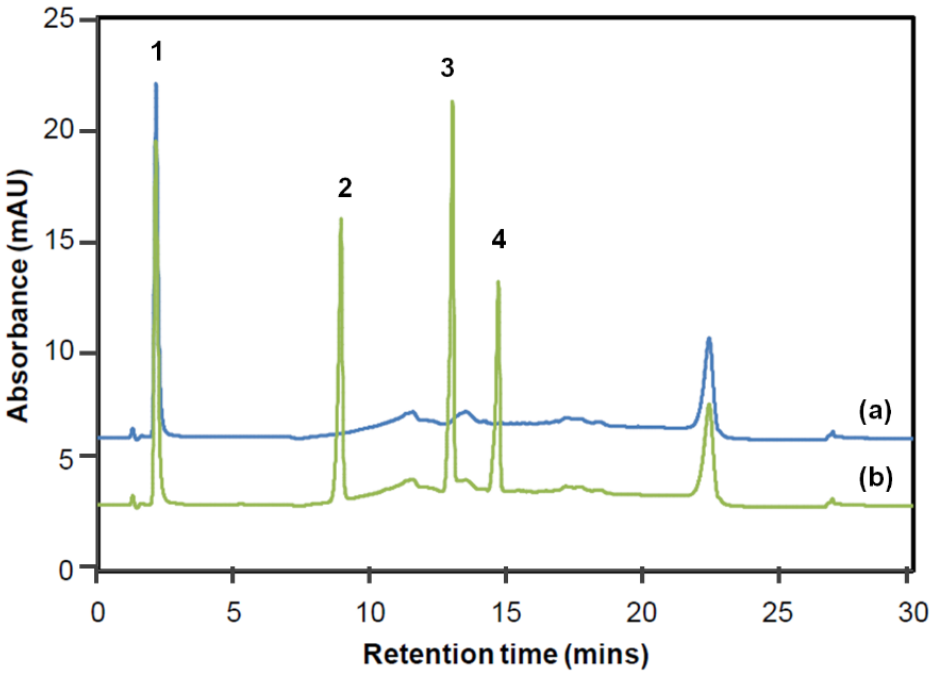

Figure 3.14: *HPLC analysis of the flow-through fraction from a Fe_3O_4 nanoparticle modified MonoSpin (a) and a blank MonoSpin (b) Chromatographic conditions and peak assignments as in Figure 3.12.*

By comparison of peak area with a 5 µ*M* standard (shown in Figure 3.12) it is clear from Figure 3.14 above that the blank MonoSpin as expected, did not retain any of the compounds, with recoveries of 97.2 % for adenosine, 98.8 % for AMP, 97.7 % for ADP and 97.9 % for ATP. Conversely, the Fe_3O_4 nanoparticle modified MonoSpin retained all three phosphorylated nucleotides but did not retain adenosine due to its lack of a phosphate group. A subsequent water rinse of both monoliths showed no evidence of unwanted elution of the retained nucleotides (Figure 3.15) with the exception of a small peak for AMP.

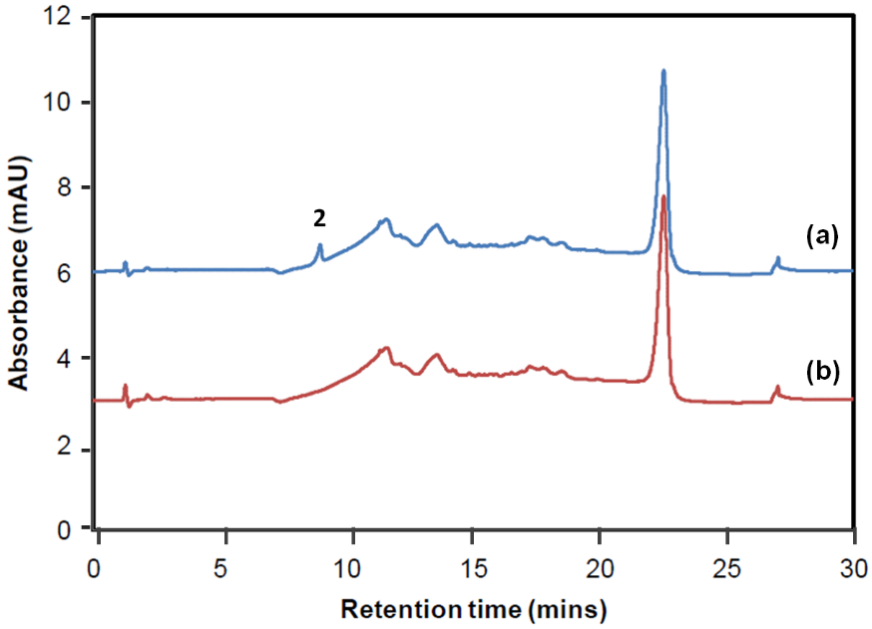

Figure 3.15: *HPLC analysis of the water rinse fraction from a Fe_3O_4 nanoparticle modified MonoSpin (a) and a blank MonoSpin (b). Chromatographic conditions and peak assignments as in Figure 3.12.*

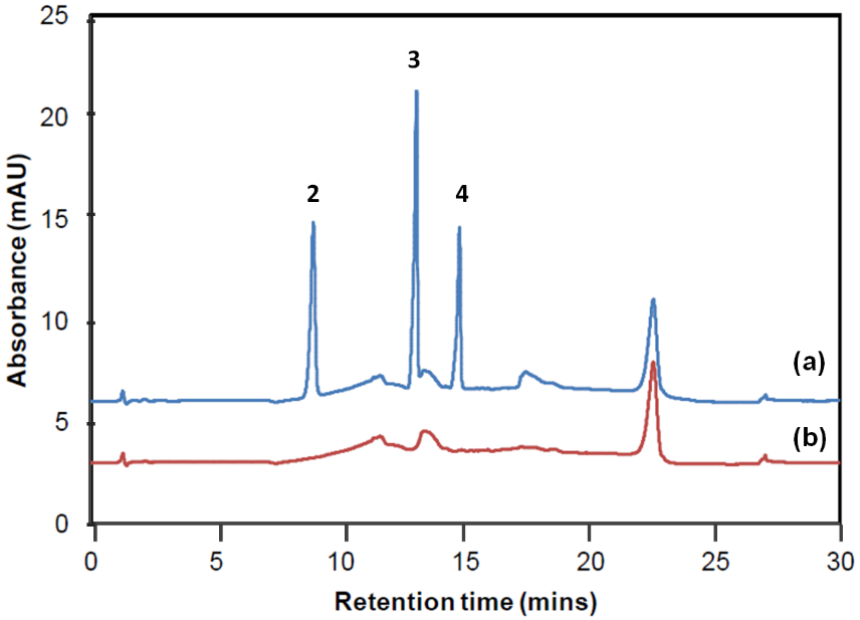

Figure 3.16: *HPLC analysis of the eluted fraction phosphate buffer from a Fe_3O_4 nanoparticle modified MonoSpin (a) and a blank MonoSpin (b). Chromatographic conditions and peak assignments as in Figure 3.12.*

Finally, both monoliths were flushed with 800 µL of 25 m*M* phosphate buffer and the eluate analysed by HPLC. Figure 3.16 illustrates that no nucleotides were recovered

from the blank monolith (having not been initially retained) whereas AMP, ADP and ATP were recovered from the Fe_3O_4 nanoparticle modified MonoSpin. Recovery values relative to a 5 µ*M* standard mixture were 80 % for AMP, 86 % for ADP and 82 % for ATP.

A preliminary examination of pre-concentration factors for the nucleotides was carried out in which the 800 µL of 5 µ*M* standard was loaded, and recovered in 200 µL of phosphate buffer. Comparison to a 5 µ*M* standard revealed that preconcentration factors of 115 % for AMP, 373 % for ADP and 243 % for ATP were achieved.

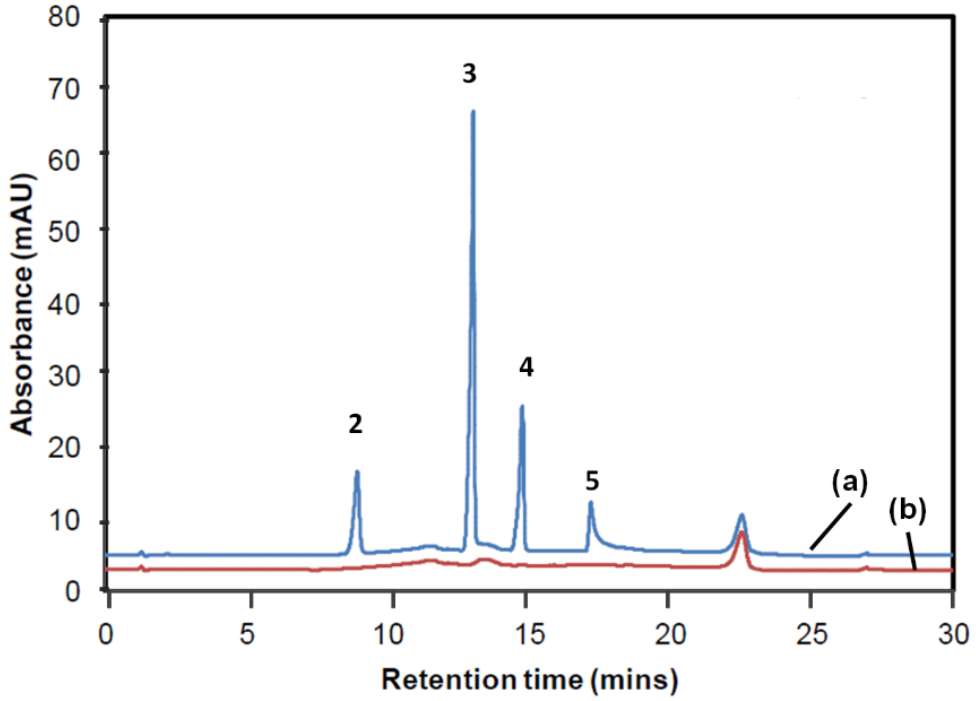

Figure 3.17: *HPLC analysis of the eluted fraction from a Fe_3O_4 nanoparticle modified MonoSpin showing pre-concentration factors up to 373 % (a) and a blank MonoSpin (b) Chromatographic conditions and peak assignments as in Figure 3.12.*

It is proposed that these values fall short of the expected 400 % due to possible overloading of the Fe_3O_4 nanoparticle modified MonoSpin. Interestingly, preconcentration factors for nucleotides with multiple phosphate groups (ADP and ATP) were higher than AMP, indicating that the Fe_3O_4 surface was more selective for highly phosphorylated species. Building upon this observation therefore, the Fe_3O_4

nanoparticle modified MonoSpins in this work were applied to the extraction of glycopeptides from a tryptic digest as described in the next section.

3.5. Development of chromatographic separation of α-casein tryptic peptides.

Alpha casein (α-casein) is a 214 amino-acid protein found in mammalian milk. It has an important role in the capacity of milk to transport calcium phosphate. Phosphoproteins in eurkaryotes tend to be phosphorylated at serine, threonine or tyrosine residues. In the case of α-casein it is phosphorylated at specific serine residues as indicated with red arrows in Figure 3.18. Other serine residues which are not phosphorylated are presumably present on the interior of the protein structure and are not sterically accessible to phosphorylation.

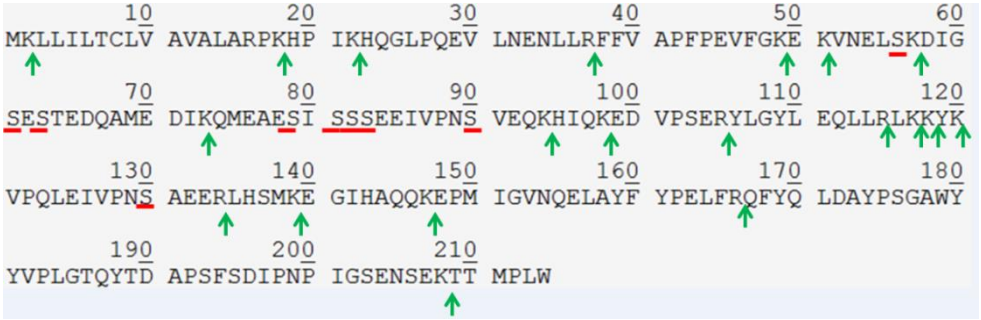

Figure 3.18: *Amino acid sequence of α-casein showing the sites of phosphorylation [124].*

Trypsin is a proteolytic enzyme which cleaves peptides after arginine (R) residues and lysine (K) residues except when either amino acid is directly followed by proline (K). Figure 3.18shows all of the theoretical cleavage sites (green arrows) on α-casein when using trypsin as proteolytic enzyme. Typical trypsin digestion protocols involve dissolving the substrate protein in urea to unfold the higher levels of protein structure (secondary, tertiary etc) and thus maximise the exposure of all potential cleavage sites as indicated in Figure 3.18. Additionally, dithiothreitol is used to reduce disulphide linkages between cysteine residues, and iodoacetamide is used to acetylate the resulting thiol groups thus preventing reformation of the disulphide bridges in subsequent steps. The tryptic digest is performed at a pH and ionic strength at which the activity of trypsin is maximised; usually when urea is used to denature the substrate, the concentration of urea is diluted to a safe level before addition of trypsin to avoid denaturation of the enzyme itself. Autolysis is usually

minimised by using a substrate/enzyme ratio of 50:1. Figure 3.19 shows all possible tryptic peptides of α-casein (totalling 21) of which four are expected to be phosphorylated. Therefore, a tryptic digest of α-casein comprises a mixture of phosphopeptides and non-phosphorylated peptides and was therefore considered to be a suitable candidate sample for examining the specificity of the Fe_3O_4 nanoparticle modified monoliths for extraction of phosphopeptides in the presence of other peptides.

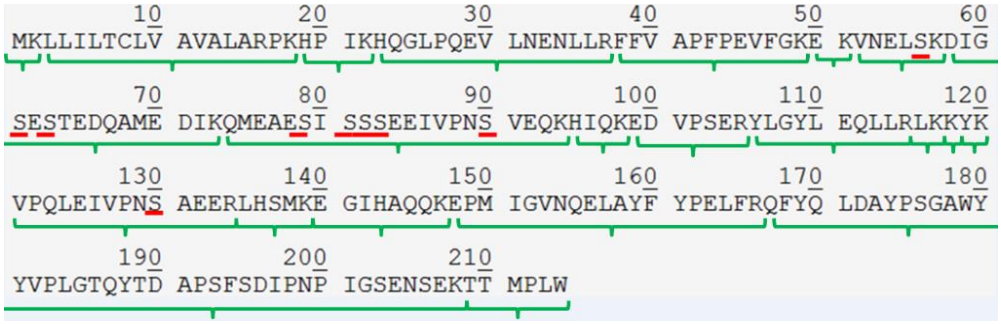

Figure 3.19: *Amino acid sequence of α-casein showing all possible tryptic peptides. Phosphopeptides have a red bar at the phosphorylation site [124].*

A chromatographic method was developed for the separation of the a-casein tryptic digest, the object of which was to maximise the number of peptides resolved without regard for minimising the total runtime. Therefore a C_{18} silica monolith was used with an acetonitrile gradient using trifluoroacetic acid as an ion-pair reagent in both mobile phase A and mobile phase B in order to maximise retention of the peptides. A preliminary gradient programme of 5 % mobile phase B (0.08 % TFA in ACN) to 100 % mobile phase B over 45 minutes was adopted and the effect of flow-rate was investigated from 0.4 mL/min to 0.8 mL/min. Figure 3.20 shows an overlay of the resulting chromatograms which are truncated for clarity, showing the region of the chromatogram across which the peptides eluted. The optimised flow rate was selected as 0.8 mL/min based upon the separation achieved between the peptides indicated with arrows in Figure 3.20.

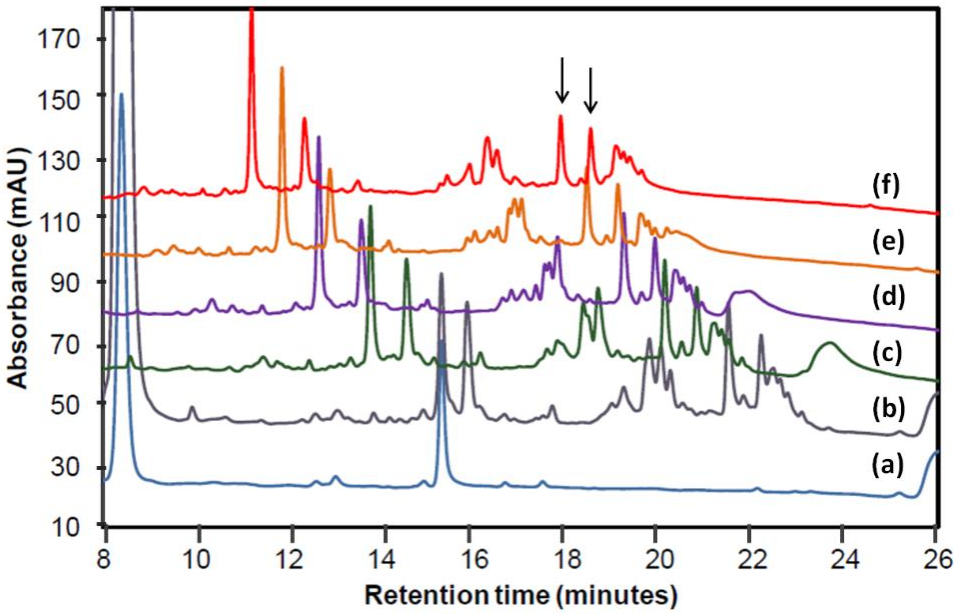

Figure 3.20: *Effect of flow rate upon separation of α-casein tryptic peptides. (a) blank at 0.4 mL/min, (b): peptide mix at 0.4 mL/min, (c): 0.5 mL/min, (d): 0.6 mL/min, (e): 0.7 mL/min, (f): 0.8 mL/min. Chromatographic conditions: Column: 3.0 mm x 100 mm Phenomenex Onyx monolithic C_{18} silica column, Mobile phase A: 0.1 % TFA in water, Mobile phase B: 0.08 % TFA in ACN. Gradient programme: 0-45 mins: 5 % to 100 % B, 45-45.1 mins: 100-5 % B, 45.1-55 mins: 5 % B. Injection volume: 25 µL, column temperature: 40 ^{o}C, detection wavelength: 214 nm.*

Using this flow rate, the gradient programme was then optimised by reducing the gradient slope (from 5 %B – 100 % B to 5 %B -60 % B over the same time period of 45 minutes). Figure 3.21 shows an overlay of the resulting chromatograms in which the gradient programme changes from 5 % to 90 % B (chromatogram b) to 5 % - 60 % B (chromatogram e). Clearly the shallower gradient programme (Gradient Programme (e)) resulted in better separation, particularly of the peaks indicated with (*), albeit with a longer separation time.

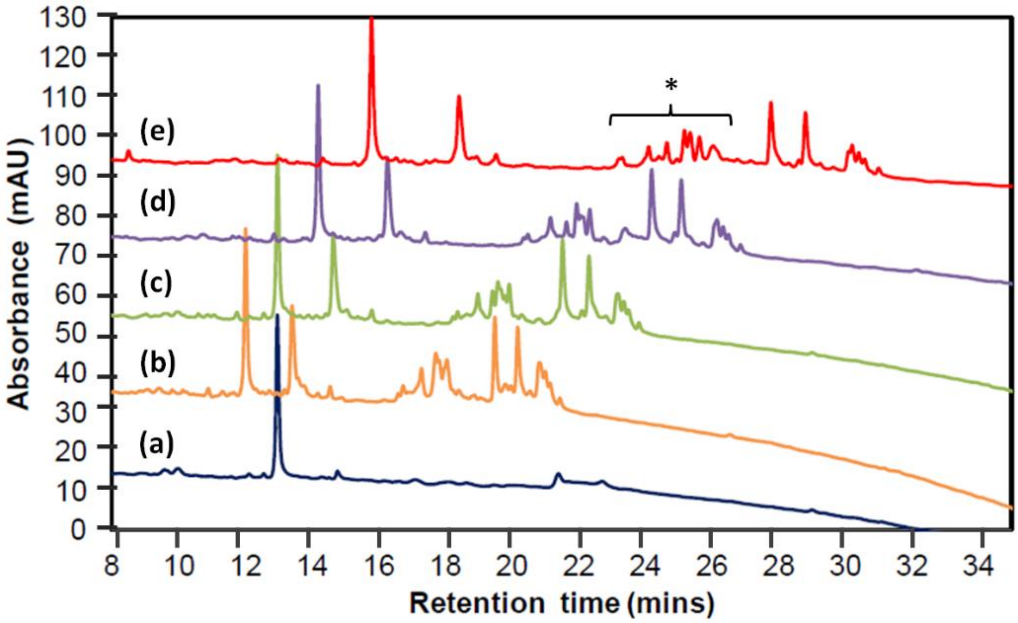

Figure 3.21: *Effect of gradient slope upon separation of α-casein tryptic peptides. (a) blank at 5 % B to 80 % B over 45 minutes, (b): peptide mix at 5 % B to 90 % B, (c) peptide mix at 5 % B to 80 % B, (d) peptide mix at 5 % B to 70 % B, (e) peptide mix at 5 % B to 60 % B. Flow rate: 0.8 mL/min. All other chromatographic conditions are as shown in Figure 3.20.*

The optimised separation is shown in Figure 3.22 overlaid with a blank injection. In an effort to maximise sensitivity for low abundance peptides, an injection volume of 50 µL was used in the displayed separation and all subsequent separations. The peak at ~ 16 minutes appeared in every subsequent blank injection and also every injection of peptide standard and was therefore disregarded. Early eluting peaks which also appeared in the blank between 0 minutes and 6 minutes were due to other non-peptide components of the tryptic digest mixture such as urea, dithiothreitol and iodoacetamide which exhibited poor retention under the optimum conditions but significant detector response at the selected detector wavelength of 214 nm. For the sake of clarity, all subsequent chromatograms are displayed in expanded form from ~ 8 minutes to ~ 32 minutes.

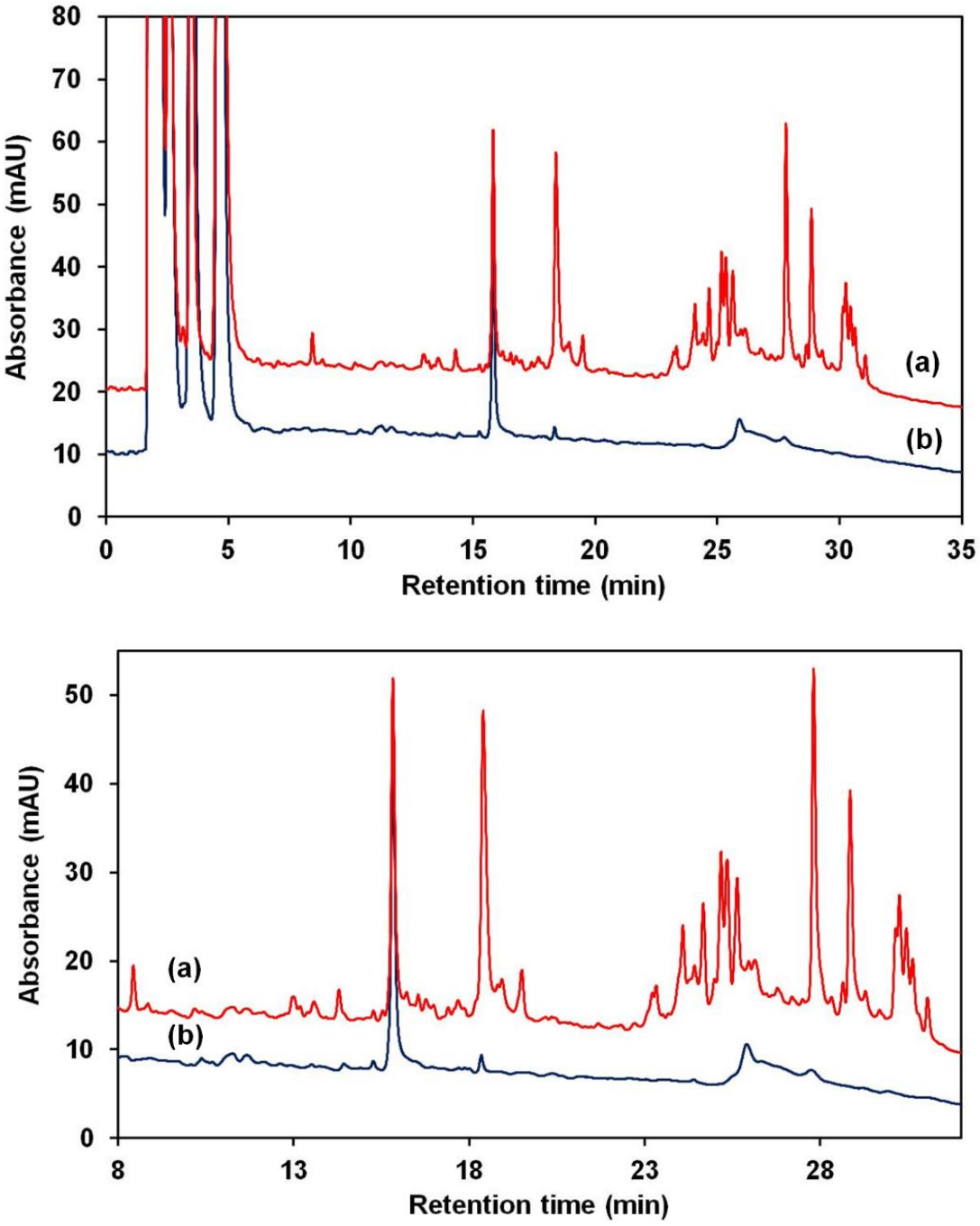

Figure 3.22: *Optimised separation of α-casein tryptic peptides (a) overlaid with a blank (b). Upper chromatogram pair shown at full scale. Lower chromatogram pair shown at expanded scale. Chromatographic conditions: Column: 3.0 mm x 100 mm Phenomenex Onyx monolithic C_{18} silica column, Mobile phase A: 0.1 % TFA in water, Mobile phase B: 0.08 % TFA in ACN. Gradient programme: 0-45 mins: 5 % to 60 % B, 45-45.1 mins: 60-5 % B, 45.1-55 mins: 5 % B. Injection volume: 50 µL, column temperature: 40 ^{o}C, detection wavelength: 214 nm.*

The selectivity of the nano-structured MonoSpin columns was evaluated using the following protocol which was adapted from on suggested by GL Sciences for use with their TiO_2MonoSpin products, which in this work were used for comparative analysis for phosphopeptide enrichment [119]. Firstly, the monolith was conditioned with 200 m*M* phosphate buffer, followed by equilibrating with 0.1 % formic acid in 50 % ACN. The peptide mixture was then loaded in 0.1 % TFA and the collected effluent referred to as the “flow-through” fraction. The monolith was then rinsed with 0.1 % formic acid, 0.1 M KCl in 50 % ACN. Elution was achieved by flushing the monolith with 1 % NH_2OH.

Four monoliths in total were subjected to this protocol and the developed separation used to evaluate phosphopeptide enrichment. The first monolith was a blank aminated MonoSpin which contained no immobilised nanoparticles. The second monolith was one which incorporated a layer of nanoparticles without using a layer-by-layer approach (shown in Figure 3.6). The third monolith had 4 layers of nanoparticles using the layer-by-layer approach (shown in Figure 3.10). The fourth and final monolith was the commercially available TiO_2 monolith.

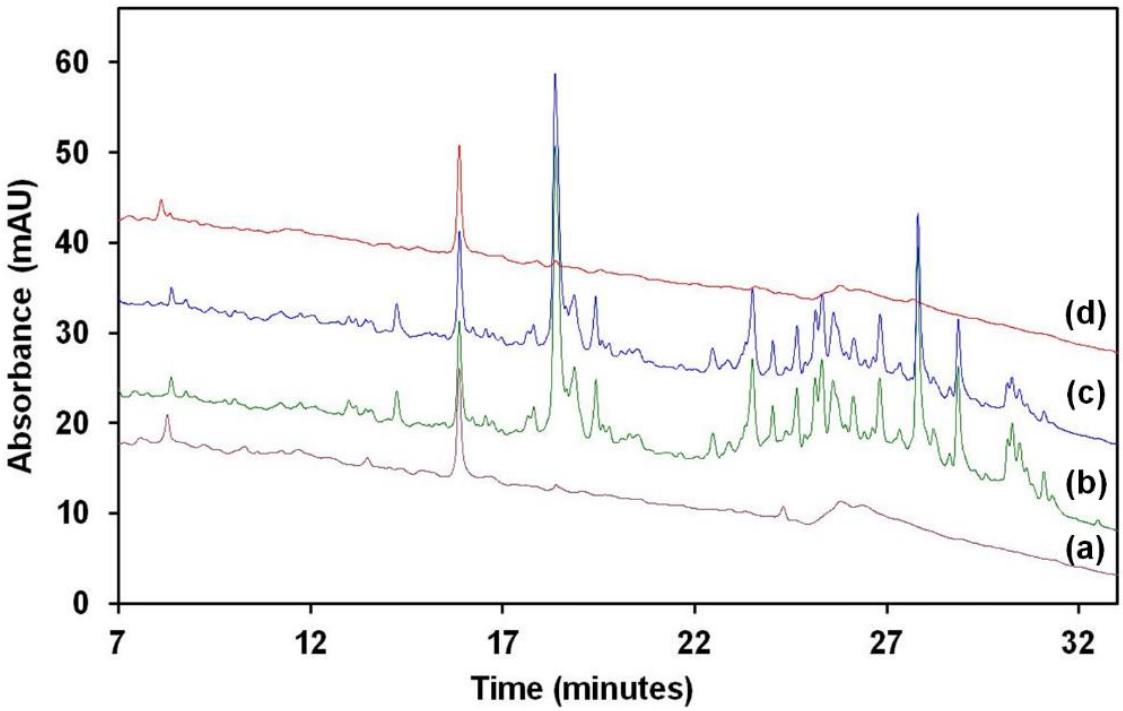

Figure 3.23: *Overlay of (a) blank, (b) peptide standard, (c) flow-through fraction and (d) 1 % NH_2OH elution fraction for a Blank Aminated MonoSpin. Chromatographic conditions as in Figure 3.22.*

Figure 3.23 shows an overlay of relevant chromatograms for the evaluation of a Blank Aminated MonoSpin for phosphopeptide enrichment. As expected, the peptide peak profile for the flow-through fraction (c) is identical to that of the peptide standard (b), clearly indicating that no peptides (phosphorylated or otherwise) were retained upon this monolith.

In contrast, the monolith modified with Fe_3O_4 nanoparticles (without intermediate polyelectrolyte layers) as shown in Figure 3.24 below exhibited some clear differences between the flow-through fraction (c) and the peptide standard (b). As expected, the peptide peak profile remained largely unchanged after passage through the monolith with the exception of three peak groupings indicated with (*) which either decreased in size or were completely eliminated (and therefore retained on the iron oxide surface). Preliminary efforts to elute the bound phosphoproteins were only partially successful (chromatogram d, 31 minutes) and further work is required to optimise the elution step of the protocol. Nevertheless, the selectivity of the Fe_3O_4 nanoparticle modified monolith for phosphoproteins over other non-phosphorylated proteins is clear.

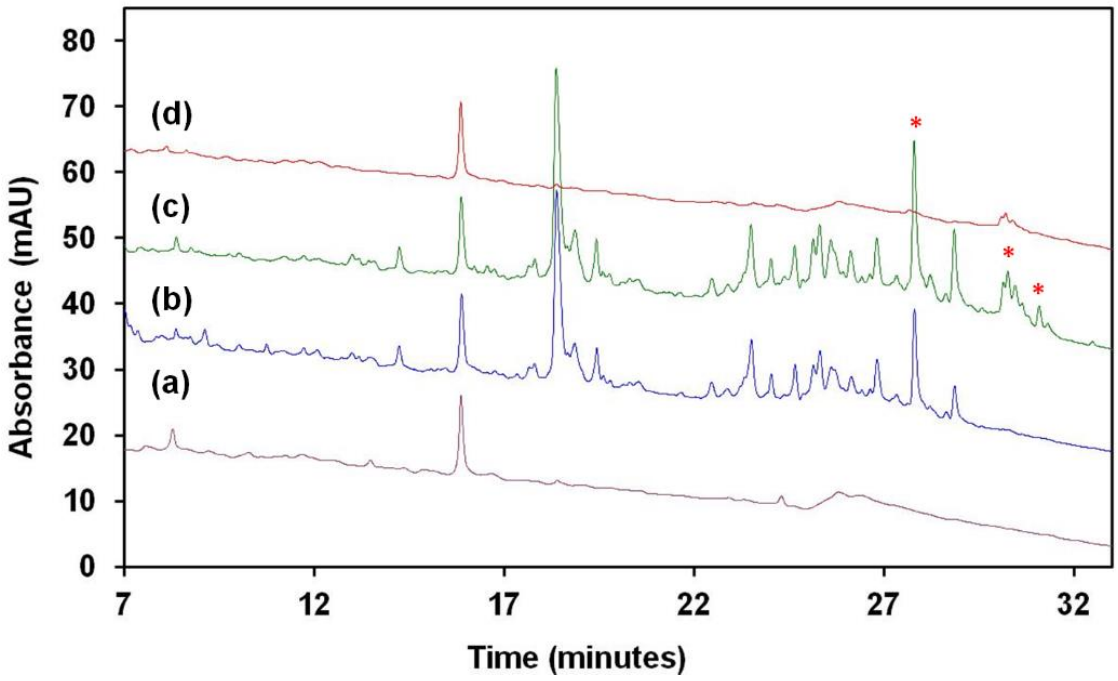

Figure 3.24: *Overlay of (a) blank, (b) flow-through fraction, (c) peptide standard and (d) 1 % NH_2OH elution fraction for a Fe_3O_4 nanoparticle single-layer modified MonoSpin. Chromatographic conditions as in Figure 3.22.*

Interestingly, when the MonoSpin modified with Fe_3O_4 nanoparticles using the layer-by-layer approach (i.e. four layers of nanoparticles) was subjected to the same peptide enrichment protocol, a slightly different peptide peak profile was obtained as shown in Figure 3.25. When one compares the flow through fraction for each monolith type (Chromatogram c in both Figure 3.24 and Figure 3.25) it is clear that the layer-by-layer Fe_3O_4 nanoparticle monolith has a different capacity for phosphopeptides, possibly due to the presence of the positively charged polyelectrolyte which may have resulted in electrostatic repulsion of positively charged peptides during sample loading steps.

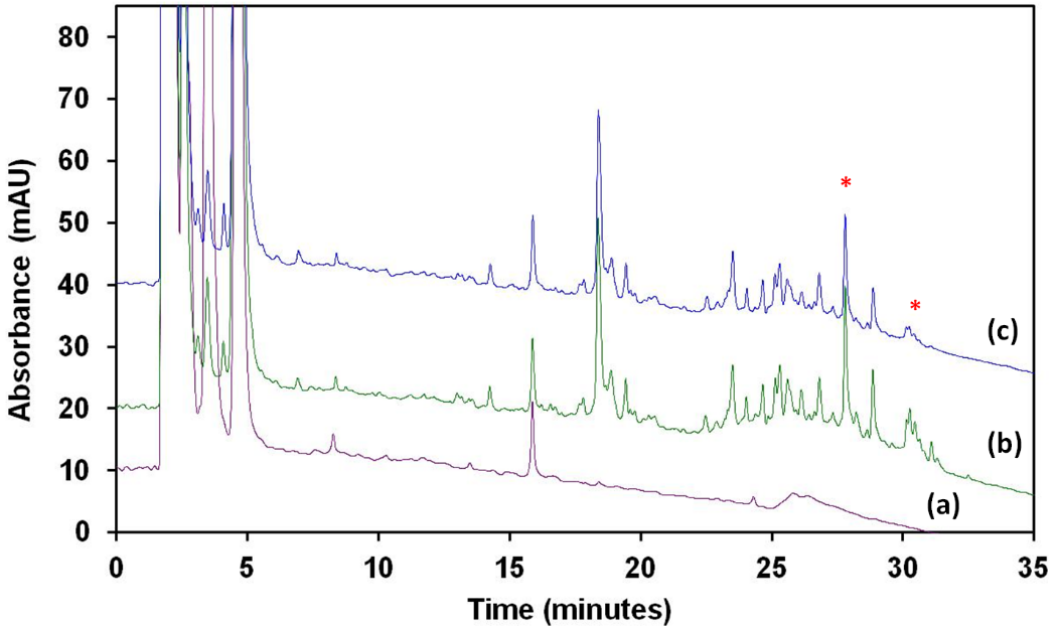

Figure 3.25: *Overlay of (a) blank, (b) peptide standard and (c) flow-through fraction for a Fe_3O_4 nanoparticle modified MonoSpin using a layer-by-layer approach. Chromatographic conditions as in Figure 3.22.*

Finally, for comparative purposes a commercially available TiO_2MonoSpin was subjected to the peptide extraction protocol. A significantly different extraction selectivity was observed for this monolith as shown in Figure 3.26, particularly for the peptide at ~ 18 minutes which was significantly reduced in size after passage through the monolith. This was in contrast to previous results on the Fe_3O_4 monoliths, neither of which appeared to demonstrate any appreciable selectivity for this particular peptide. Other peptides between 28 minutes and 30 minutes were

extracted as expected, further validating the selectivity of the iron oxide monoliths for phosphopeptides over non-phosphorylated peptides.

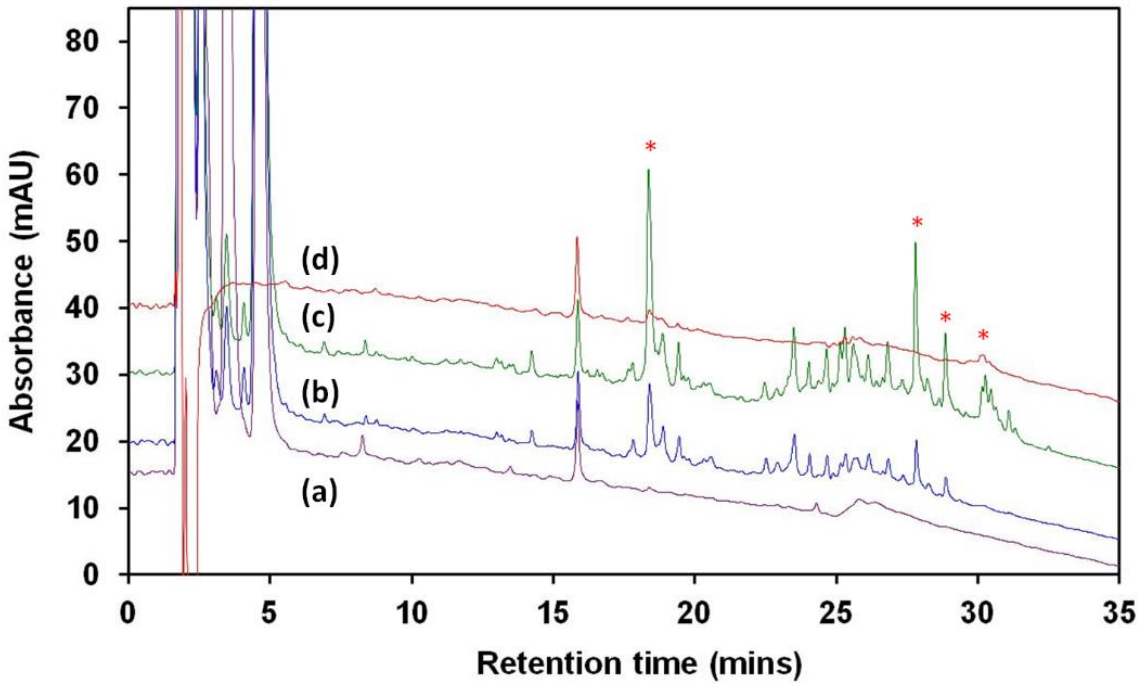

Figure 3.26: *Overlay of (a) blank, (b) flow-through fraction (c) peptide standard and (d) 1 % NH_2OH elution fraction for a TiO_2 MonoSpin column. Chromatographic conditions as in Figure 3.22.*

4. Conclusion

Commercially available centrifugally driven solid-phase extraction silica monoliths were immobilised with 15.8 nm citrate stabilised iron oxide nanoparticles with a dense coverage without detrimental blockage of the flow-through macropores. The Fe_3O_4 nanoparticles were synthesised via co-precipitation and particle size distribution and zeta potential measured using DLS. Fe_3O_4 nanoparticles had an average particle size distribution of 15.8 nm with a zeta potential of -23.4 mV. Negatively charged citrate stabilised Fe_3O_4 nanoparticles were synthesised and immobilised on a silica monolith bearing amine moieties on the surface using Layer-by-Layer approach.TEM was also used to measure particle size distribution and demonstrated no aggregation of Fe_3O_4 nanoparticles. FE-SEM was used to verify and visualise a highly dense coverage of iron oxide nanoparticles electrostatically immobilised on the porous silica monolith. Since Fe_3O_4 is known to form reversible complexes with phosphorylated species, the silica monoliths were subsequently

used for the enrichment of selected nucleotides and phosphorylated peptides. The ability to enhance the chemistry of SPE cartridge allowed the development of novel nano-agglomerated monolithic stationary phases. In this chapter, we enhanced and applied a commercially available solid phase extraction silica monolith immobilised with novel iron oxide nanoparticles for the successful trap and release of simple and complex phosphorylated compounds. Furthermore, this novel MonoSpin cartridge was also used to preconcentrate a mixture of AMP, ADP and ATP.As a concept, Metal oxide affinity chromatography (MOAC) is interesting and has huge potential. Even though, TiO_2 is widely used, our Fe_3O_4 nanoparticles column could be used as a potential tool for the separation of simple and more complex phosphorylated species.

References

[1] H. H. Strain and J. Sherma, *J. Chem. Educ*, 44 (4), **(1967)**, p 235
[2] F. Svec, *Journal of Chromatography* B. 841, **(2006)**, 52
[3] G. Guiochon, *Journal of Chromatography* A. 1168, **(2007)**, 103
[4] F. Svec, *J. Sep. Sci.*, 27, **(2004)**, 747
[5] M.S. Tsvett, Ber. Deut. Botan. Gessel. 24, **(1906)**, 322
[6] F. Svec, *Journal of Chromatography* A. 1217, **(2010)**, 904
[7] N. Tanaka, T. Ikegami, *Current Opinion in Chemical Biology*. 8, **(2004)**, 528
[8] Nakanishi, K., Kobayasji, *Chem. Mater*. 16, **(2004)**, 3652
[9] A. Nguyen, N Dinh, Q. Cam, T. Sparrman, K. Igrum, *J Sep Sci.* 32, **(2010)**, 2608.
[10] M. Rainer, H. Sonderegger, R. Bakry, C. W. Huck, S. Morandell, L. A. Huber, D. T. Gjerde and G. K. Bonn, *Proteomics*, 8, **(2008)**, 4593
[11] M. Vázquez, B. Paull, *Anal. Chim. Acta*, 668, **(2010)**, 100
[12] S. Eeltink, E. Hilder, F. Svec, W. T. Kok, *Journal of Sep. Science*. 30, **(2007)**, 407
[13] J. Giddings, *Dynamic of Chromatography*. M, Dekker, New York, NY, **1965**
[14] A. Duan, S. Xie, L. Yuan. *Trends in Analytical Chemistry*. 30, **(2011)**, No.3
[15] D. T. T. Nguyan, D. Guillarme, S. Rudaz, J. L. Veuthey, *J. Sep. Sci.,*29, **(2006)**, 1836.

[16] H. Kobayashi, D. Tokuda, J. Ilchimaru, T. Ikegami, K. Miyabe, N. Tanaka. *Journal of Chromatography* A. 1109, **(2006)**, 2.
[17] K. Nakanishi, H. Minakuchi, N. Soga, N. Tanaka, *Journal of Sol Gel Sci and Techn,* 8, **(1997)**, 547.
[18]A. Siouffi, F. Ziarelli, S. Caldarelli, *J. Chromatogr. A*, 1109, **(2006)**, 26
[19] K.K. Unger, *Porous silica*, Elsevier, Amsterdam. **(1979)**, Chapter 2
[20]K. Nakanishi, N. Soga, *J. Am. Ceram. Soc*. 74, **(1991)**, 2518
[21] http://www.phenomenex.com/Products/HPLCDetail/Onyx/Monolithic%20C18
[22]Merck Chromolith™ Information Sheet: General Information and Applications, **(2002)**.

[23]http://www.glsciencesinc.com/ProductInfo/Proteomics/Documents/TiO2/MonoTipTiOmanual_061009.pdf
[24] http://www.glsciences.com/products/monolithic_products/mono_spin.pdf
[25]http://www.hichrom.co.uk/assets/Products/GLS/MonoTips/GLSMonoTip_TiO_Coated-Hi.pdf
[26] J. M. J. Frechet, F. Svec, T. B. Stachowiak, *Chem Mater*. 18, **(2006)**, 5952
[27] B. Paull, D. Connolly, B. Twamley. *Chem Commun.*, 46, **(2010)**, 2110
[28]S. Hjerten, J. L. Liao, R. Zhang. *Journal of Chromatography*. 473, **(1989)**, 273
[29] F. Svec, J.M. Frechet, *Analytical Chemistry*. 64, **(1992)**, 820
[30] G. Han, M. Ye, H. Zou. *The Analyst, Critical review.* 133, **(2008)**, 1128-1138
[31] Q. Wang, F. Svec, J. M. J Frechet. *Journal of Chromatography* A. 669, **(1994)**, 230-235
[32] C.Viklund, F. Svec, J.M.J. Frechet, K. Irgum, *Chem. Mater*. 8, **(1996)**, 744
[33]F. Svec, T.B. Tennikova, Z. Deyl. *Monolithic Materials, Preparation, Properties and Application,* Elsevier, Amsterdam, **(2003)**
[34] S. Eeltink, E. Hilder, F. Svec, W. T. Kok, *Journal of Sep. Science*. 30, **(2007)**, 409
[35] A.I. Copper, W.P. Hems, A.B. Holmes. *Macromolecules*. 32, **(1999)**, 2156
[36] S. Hjerten, J. L. Liao, R. Zhang. *Journal of Chromatography*. 473, **(1989)**, 273
[37] C. Viklund, E. Ponten, B. Glad, K. Ingum, P. Horsted, F. Svec, *Chem. Mater*. 9, **(1997)**, 463

[38] M. Kumakura, I. Kaetsu, K. Asami, S. Suzuki, *Journal of Material Science*. 24, **(1989)**, 1809
[39] T.B. Tennikova, F.Svec, B.G. Belenkii. *Journal of Liquid chromatography*. 13, **(1990)**, 63
[40] F. Svec, J.M.J. Frechet, *Macromolecules*, 28, **(1995)**, 7580
[41] J. Krenkova, N. Lacher, F. Svec, *J. Chromatogr. A,* 1216, **(2009)**, 3252.
[42] F. Plieva, B. Bober, M. Dainiak, I. Galaev, B. Mattiasson, *J. Mol. Recognit.,*19, **(2006)**, 305.

[43] C. Bisjak, R. Bakry, C. Huck, G. Bonn, *Chromatographia*, 62, **(2005)**, S31.
[44] E. G. Vlakh, T. B. Tennikova, *J .Sep. Sci*., 30, **(2007)**, 2801.
[45] Y. Ueki, T. Umemura, T. Odake, K. Tsunoda, Anal. Chem., 76, **(2004)**, 7007

[46] O. G. Potter, M. C. Breadmore, E. F. Hilder, *Analyst*, 131, **(2006)**, 1094.
[47] S. M. Heilmann, J. K. Rasmussen, L. R. Krepski, *Chemistry and Technology of 2-Alkenyl Azlactones*, **(2001)**
[48] S. Xie, F. Svec, J. Frechet, *J. Polym. Sci. Part A: Polym. Chem*., 35, **(1997)**, 1013.

[49] D. Connolly, B. Twamley, B. Paull, *Chem Comm,* **(2010)**
[50] B. Ranby, International Journal of Adhesion & Adhesives. 19, **(1999)**, 337-343
[51] Sigma Aldrich, *Application: Free radical initiators*. Accessed in January **2012**
[52] B. Ranby, *Current trends in polymer photochemistry*. 38, **(1998)**, 1229
[53] B. Zhang, B. Ranby. *Journal of Applied polymer science*. 43, **(1991)**, 621
[54] S. Eeltink, W. T. Kok, F. Svec, *Journal of Separation Science*. 30, **(2007)**, 410
[55] T. B. Stachowiak, F. Svec, J.M.J. Frechet. *Chem. Mater.*18, **(2006)**, 5950
[56] T. Rohr, E. Hilder, J. Donovan, F. Svec, J.M.J. Frechet. *Macromolecules.* 36, **(2003)**, 1679
[57] D. Sykora, , V. Kasicka, P. Matejka, V. Kral, *J. Sep. Sci.*, 33, **(2010)**, 1–16.

[58] Hilder, E.F., Svec, F., Frechet, J.M.J., *J. Chromatogr. A,* **(2004)**, *1053*, 101-106
[59] Hutchinson J.P., Hilder, E.F., Shellie, R.A., Smith, J.A., Haddad, P.R.,*Analyst,* **(2006)**, 131, 215–221
[60] Hilder, E.F., Svec, F., Frechet, J.M.J., J. Chromatogr. A **(2004)**, 1053, 101-106
[61] Li, Y., Chen, Y., Xiang, R., Ciuparu, D., Pfefferle, L.D., Horvath, C., Wilkins, J.A., *Anal. Chem*. **(2005)**, *77*, 1398-1406
[62] Chambers, S.D., Svec, F., Frechet, J.M.J., *J. Chromatogr. A,***(2011)**, *1218*, 2546-2552
[63] Chambers, S.D., Holcombe, T.W., Svec, F., Frechet, J.M.J., *Anal. Chem*. **(2011)**, *83*, 9478-9484.
[64] Wang, M-M., Yan, X-P.,*Anal. Chem*. **(2012)**, *84*, 39-44
[65] Xu, Y., Cao, Q., Svec, F., Frechet, J.M.J., *Anal. Chem.***(2010)**, *82*, 3352-3358
[66] Cao, Q., Xu, Y., Liu, F., Svec, F., Frechet, J.M.J., *Anal. Chem.***(2010)**, *82*, 7416-7421
[67] Lv, Y., Alejandro, F.M., Frechet, J.M.J., Svec, F., *J. Chromatogr.A*., 1261, **(2012),** 121
[68] Alwael, H., Connolly, D., Clarke, P., Thompson, R., Twamley, B., O'Connor, B., Paull, B., *Analyst ,* **(2011)**, *136*, 2619-2628
[69] Zeemann, A.J., Schnell, E., Volgger, D., Bonn, G.K., Anal. Chem., **(1998)**, 70, 563.
[70] Fracassi da Silva, J.A., do Lago, C.L., Anal. Chem. **(1998)**, 70, 4339.
[71] Kuban, P., Hauser, P.C., Electrophoresis **(2004)**, 25, 3387.
[72] Brito-Neto, J. G.A., da Silva, J.A.F., Blanes, L., do Lago, C.L., Electroanalysis, **(2005)**, 17, 1198.

[74] D. Connolly, P. Floris, P.N. Nesterenko, B. Paull, Trends in Analytical Chemistry, 29, **(2010)**, 870
[75] K. Nesterenko, O, Yavorska, M. Macka, A. Yavorskyy, B. Paull. *Anal. Methods*. 3, **(2011)**, 539
[76] D. Connolly, L.P. Barron, E. Gillespie, B. Paull, Chromatographia, 70, **(2009),** 915
[77] Z. Walsh, P.A. Levkin, V. Jain, B. Paull, F. Svec, M. Macka, J. Sep. 788 Sci. 33, **(2010)**, 61.
[78] E. Gillespie, M. Macka, D. Connolly, B. Paull, Analyst, 131, **(2006)**, 886.
[79] L. Negroni, S. Claverol, J. Rosenbaum, E. Chevet, M. Bonneu, J.M. Schmitter. *Journal of Chromatography B*, 891– 892, **(2012),** 109– 112

[80] F.Wolschin, W. Weckwerth. *Plant Methods- Bio-Med Central,***(2005)**, 1-9
[81] T. E. Thingholm, O. N. Jensen, M. R. Larsen, *Proteomics*. 9, **(2009)**, 1451-1468
[82] G. Han, M. Ye, H. Zou. *The Analyst, Critical review.* 133, **(2008)**, 1128-1138
[83] I. L. Batalha, C. R. Lowe, A. C.A. Roque, Trends in Biotechnology, Vol. 30, (February **2012**), No. 2
[84] J. Porath, J. Carlsson, I. Olsson, G. Belfrage, *Nature*. 258, **(1975)**, 598-599
[85] T. S. Nuhse, A. Stensballe, O. N. Jensen, S. C. Peck, *Mol. Cell Proteomics*. 2, **(2003)**, 1234–1243

[86] E.K. Ueda, P.W. Gout, L. Morganti. *J. Chromatogr.A*. 988, **(2003)**, 1-23
[87] J. Nawrocki, C. Dunlap, A. McCormick, P. Carr, *J. Chromatogr.A.* 1028, **(2004)** 1
[88] H. J. Zhou, R. J. Tian, and M. L. Ye, S. Y. Xu, S. Feng, C. S. Pan, X. G. Jiang, X. Li, H. F. Zou, 28, **(2007)**, 2201-2215.
[89] P.A. Connor, A.J. McQuillan, *Langmuir,* 15, **(1999)**, 2916
[90] K. Tani, T. Sumizawa, M. Watanabe, M. Tachibana, H. Koizumi, T. Kiba, *Chromatographia,* 55, **(2002)**, 33.

[91] A. Leitner, *Trends Anal. Chem.* 29, **(2010)**, 177-185
[92] Mamone, G., Picariello, G., Ferranti, P., Addeo, F., *Proteomics* ,**(2010)**, 10, 380-393.
[93] Krenkova, J., Lacher, N., Svec, F., *Anal. Chem.***(2010)**, *82*, 8335-8341
[94] Y. Li, Y. Chen, R. Xiang, D. Cinparu, L.D. Pfefferle, C. Horvath, J.A. Wilkins, Anal. Chem. 77, **(2005)**, 1398.

[95] J. Krenkova, F. Foret, F. Svec, Anal. and Bioanl. Chem., 405 (2013) 2175
[96] Tobal, K., Guerre, O., Rolando, C., Le Gac, S., *Molecular Cell. Proteomics,***(2006)**, *5*, S278-S278
[97] H.C. Hsieh, C. Sheu, F.K. Shi, D.T. Li, *J. Chromatogr. A.,* 1165, **(2007)**, 128.
[98] Rainer, M., Sonderegger, H., Bakry, R., Huck, C.W., Morandell, S., Huber, L.A., Gjerde, D.T., Bonn, G.K., *Proteomics,***(2008)**, *8*, 4593-4602
[99] A. Lee, H. J. Yang, E.S. Lim, J. Kim, Y. Kim, *Rapid Commun. Mass Spectrom*. 22, **(2008)**, 2561.

[100] L. Han, Z. Shan, B. Tu, D. Zhao, *J. Colloid Interface Sci.*, 318, **(2008)**, 315–321.
[101] J. Krenkova, F. Foret, J. Sep. Sci., 34, **(2011)**, 2106–2112
[102] J. Krenkova, F. Foret, J. Anal and Bioanalytical Chem, 405, **(2013)**, 2175
[103] Sahoo Y., Goodarzi A., Swihart M. T., Kaur N., Furlani E.P., Prasad P.N., J. Phys. Chem. B, **(2005)**, 109, 3879-3885

[104] E.F. Hilder, F. Svec, J.M. Frechet, *Anal. Chem.* 76, **(2004)**, 3887
[105] V. Pucci, M.A. Raggi, F. Svec, J.M. Frechet, *J. Sep. Sci*. 27, **(2004)**, 779
[106] T. Rohr, E.F. Hilder, J.J. Donovan, F. Svec, J.M.J. Frechet, *Macromolecules*, 36, **(2003)**, 1677

[107] B. Ranby, W. T. Yang and O. Tretinnikov, Nucl*. Instrum. Methods Phys. Res*., Sect. B, 151, **(1999)**, 301

[108] T. B. Stachowiak, F. Svec and J. M. J. Fre´chet, *Chem. Mater*., 18, **(2006),** 5950.
[109] D. Connolly, B. Paull, J. Sep. Sci., 32, **(2009)**, 2653
[110] *Thermo Scientific ProPac IMAC 10 Product Manual, 065090, Revision 05, July **2012***
[111] Connolly D, O'Shea V, Clarke P, O'Connor B, Paull B J Sep Sci., 30 **(2007)**3060
[112] S. Currivan, D. Connolly, E. Gillespie and B. Paull, J. sep. Sci., 33 **(2010)** 1
[113] S. Currivan, D. Connolly, B. Paull, Microchemical Journal, **2012**, *in press,* DOI: http://dx.doi.org/10.1016/j.microc.2012.08.007
[114] J.P. Hutchinson, E.F. Hilder, M. Macka, N. Avdalovic, P.R. Haddad, J. Chromatogr. A., 1109 **(2006)** 10
[115] K.M. Glenn, C.A. Lucy, J. Chromatogr. A., 1155 **(2007)** 8
[116] M.O.A. Ibrahim, T. Zhou, C.A. Lucy, J. Sep. Sci., 33 **(2010)** 773
[117] M.O.A. Ibrahim, C.A. Lucy, Talanta, 100 **(2012)** 313
[118] W. Sun, Qi Li, S. Gao, J.K. Shang, Chemical Engineering Journal, 185-186 **(2012)** 136-143
[119] www.glsciences.com/c-product/sample/solid/monospin-series/
[120] J.P. Chapel, J.F. Berret, Current Opinion in Colloid and Interface Science, 17 **(2012)** 97
[121] H.I. Labouta, M. Schneider, International Journal of Pharmaceutics, 395 **(2010)** 236
[122] S. Srivastava, N.A. Kotov, Accounts of Chemical Research, 41 **(2008)** 1831
[123] Y. Wang, A.S. Angelatos, F. Caruso, Chemistry of Materials, 20 **(2008)** 848
[124] *www.uniprot.org*